Comparison of the HadGEM2 climate-chemistry model against in-situ and SCIAMACHY atmospheric methane data

G. D. Hayman et al.

We thank the reviewers for their comments and are very pleased that both reviewers recommend publication. Our responses to the review comments are given below.

NOTE: All references to page, line or Section numbers in the Main Paper and Supplement are based on the revised version of the paper and Supplement and not the difference between the revised version and the discussion paper (i.e. track change version).

Anonymous Referee #1

This study has evaluated wetland CH4 emission estimates from the UK community land model JULES by comparing model simulations with in-situ and satellite observations of atmospheric CH4 concentrations. Their results highlight the large uncertainties in the current estimates for wetland CH4 emissions, as well as the potential for using space-based observations of atmospheric CH4 columns to evaluate land surface models. This paper is well written, and very informative. It should be accepted for publication in ACP after some minor changes.

Major comments:

1. The authors have shown that the HadGEM2 CH4 simulations have a much steeper fall-off in the upper troposphere and stratosphere than the (ACE/HALOE) observations, resulting in a model underestimation of XCH4 columns by about 50ppb when compared to SCIAMACHY retrievals. However, it is interesting to know the comparisons of the annual growth rates (as well as the annual cycles) derived from their un-constrained and constrained HadGEM2 XCH4 simulations, so that we can further understand how the issues with model CH4 simulations in the upper troposphere and stratosphere will affect the comparisons of model simulations with space-borne observations.

Response:

Figure 10 in the paper shows a comparison of time series and annual cycles of the observed atmospheric methane columns (XCH4) from SCIAMACHY and those derived from the HadGEM2 runs, constrained with the HALOE/ACE-assimilated TOMCAT output. We will include in the Supplement an equivalent comparison for the same runs using the unconstrained model results, make reference to it in either Section 3.2.1 or 3.2.2 and expand the discussion in Section 4.1 (see also response to 2 below).

Manuscript Changes:

A paragraph (Supplement, page 29) and a new figure has been added to the Supplement (as Figure 20, page 31). The figure shows a comparison of time series and annual cycles of the observed atmospheric methane columns (XCH4) from SCIAMACHY and those derived from the unconstrained HadGEM2 runs.

This is referenced in the main paper in Section 3.2.2 (starting at line 678 on page 7) and discussed in Section 3.3.1 on page 8 (starting at line 726).

2. While the HadGEM2 run using JULES-GIEMS wetland emissions shows better agreement with in-situ observations, simulations forced by the FUNG emission inventory seem to score much higher in the comparisons against SCIAMACHY over Northern Hemisphere. Here, more detailed explanations are needed: for example, whether it is related to the transport model errors, or it is caused by the use of constrained HadGEM2 simulations.

Response:

This is linked to the previous comment comparing the HadGEM2 outputs using the constrained and unconstrained outputs. The following figures show a comparison of the time series of the observed and modelled atmospheric methane columns for the constrained (Panel a of Figure 10 in the paper) and the unconstrained model outputs.

XCH4 - HadGEM2 constrained with HALOE/ACE assimilated TOMCAT

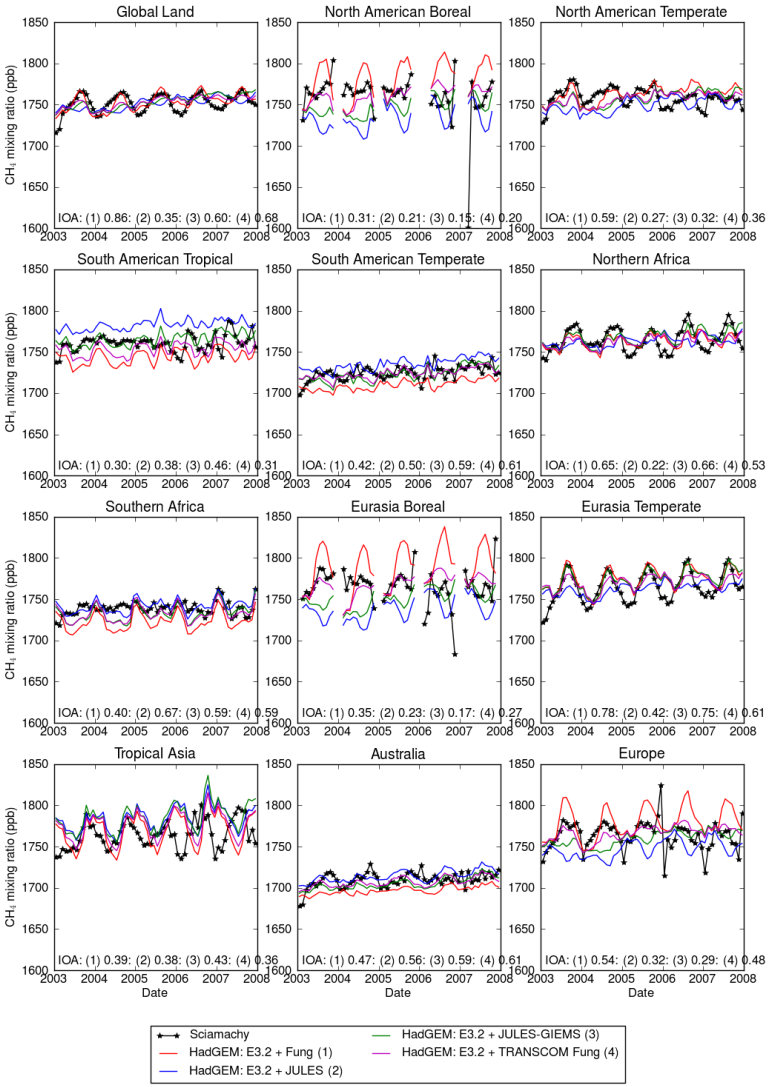

XCH4 - HadGEM2 unconstrained

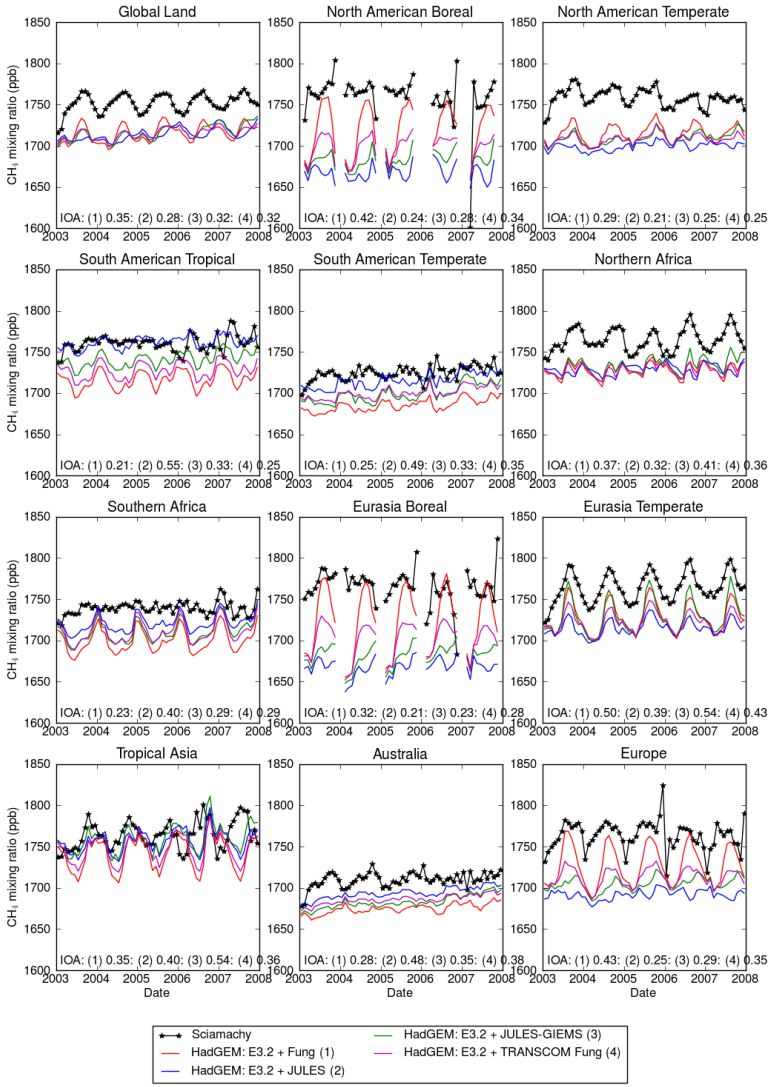

We will expand the discussion in Section 4.1 to show that the tendencies in the metrics used are similar for the constrained and unconstrained outputs, suggesting that the different wetland emission inventories largely explain the performance against the atmospheric column measurements.

In our response to the other Reviewer (see below), we have since undertaken a run using the FUNG inventory prepared for the TRANSCOM methane model intercomparison (cited paper by Patra et al., 2011), scaled to give an annual emission estimate of 181 Tg per annum. This has lower boreal emissions than our FUNG inventory and this may explain the 'apparent' good performance against the SCIAMACHY atmospheric column measurements. The following figures also include this new model run. We will include the output of this run in the revised paper and discuss it where appropriate.

We will also include some discussion on the consistency of the comparisons with the surface atmospheric methane concentrations and the atmospheric column methane measurements.

Manuscript Changes:

See also response to Reviewer 2 about the HadGEM2 run using the TRANSCOM FUNG wetland inventory.

The specific point is discussed in Section 3.3.1 (starting at line 726 on page 8).

Minor comments:
1. Line 16, Page 11: 'The WFM-DOAS algorithm is one of : : :'. Some introductions on the quality of the WFMFv2.3 XCH4 retrievals (such as the biases at different latitude bands) will be helpful.

Response:

The validation of the WFM-DOAS v2.3 XCH4 dataset has been published in Dils et al. (2014). The biases at all individual TCCON stations are listed in Table 7 of the paper. The relative accuracy, which is the relevant quantity to measure the variability of the regional biases, is 7.8 ppb for WFMD. We will amend Section 2.2.2 (page 12977), where the SCIAMACHY XCH4 product is described.

"The WFM-DOAS algorithm is one of the algorithms currently being compared in the ESA project: Greenhouse Gases Climate Change Initiative (GHG-CCI; Buchwitz et al., 2013). **The SCIAMACHY dataset has been validated and its relative accuracy, a quality measure quantifying regional biases, is 7.8 ppb (Dils et al., 2014)**."

We will add the paper to the References:

> Dils, B., Buchwitz, M., Reuter, M., Schneising, O., Boesch, H., Parker, R., Guerlet, S., Aben, I., Blumenstock, T., Burrows, J. P., Butz, A., Deutscher, N. M., Frankenberg, C., Hase, F., Hasekamp, O. P., Heymann, J., De Mazière, M., Notholt, J., Sussmann, R., Warneke, T., Griffith, D., Sherlock, V., and Wunch, D.: The Greenhouse Gas Climate Change Initiative (GHG-CCI): comparative validation of GHG-CCI SCIAMACHY/ENVISAT and TANSO-FTS/GOSAT CO2 and CH4 retrieval algorithm products with measurements from the TCCON, Atmos. Meas. Tech., 7, 1723-1744, doi:10.5194/amt-7-1723-2014, 2014.

Manuscript Changes:

The sentence, "The SCIAMACHY dataset has been validated and its relative accuracy, a quality measure quantifying regional biases, is 7.8 ppb (Dils et al., 2014)", added to Section 2.2.2 (line 327 on page 4).

2. Figure 3: I am not sure why sin(latitude) instead of latitude is chosen as x-axis. Also, it would be easier for the reader to see if the dots are connected with (coloured) dashed lines.

Response:

Figure 3 uses sin(latitude) for the x-axis as this weights by area and emphasises the tropical regions. We will replace the figure using latitude for the x axis (this makes no real difference to the plots) and we will add dotted lines.

Manuscript Changes:

The plot in Figure 3 now uses latitude for the x-axis. Dotted lines have been added between the data points. As noted above, output from the additional HadGEM2 run using the TRANSCOM Fung wetland inventory have also been included in this figure.

3. Line 24, Page 15: 'suggesting the annual pattern of non-wetland methane emissions may not be correct : : :', It will help the reader to understand if the authors can present the contributions from different emission categories to the observed CH4 concentrations over one or two selected sites.

Response:

The HadGEM2 model configuration used in this work is not set-up to give tracers, which tag or colour specific methane emission sectors. We have therefore selected a number of surface atmospheric methane sites (e.g., Barrow and Plateau Assy in Figure 6) and derived the contribution of the different methane source sectors to the overall emissions. This will be included in the revised paper.

Manuscript Changes:

Paragraph added to Section 3.1 (starting at line 502 on page 6) and a new table added to the Supplement (Table 4, pages 12 and 13) providing information on the contribution of the different methane emission sources at 2 locations.

Anonymous Referee #2

A study by G. Hayman and co-authors makes an attempt to use Sciamachy observations of atmospheric methane as a tool for evaluating the JULES model simulated methane emissions from wetlands. The use of the satellite data to get the information about fluxes in areas remote from the observations has been tried before in the frame work of inverse modeling, but this study use the observations directly to compared with transport model simulated fields. This makes a step towards wider use of the remote sensing data from Sciamachy and other missions for validation the ESM-estimated CH4 fields, reducing the space for uncertainties of the simulated fluxes in the tropical and subtropical regions where the wetland emissions are high. Authors showed good amount of effort and creativity dealing with difficult problem of simulating stratospheric CH4 content. There are some weaker points in the study design, such as the choice of the FUNG emission scenario, which doesn't seem optimal in high latitudes, as better results were reported with other datasets, notably by Patra, et al, (2011) Overall the paper is well written and provided a valuable contribution. I recommend to publish it after minor corrections.

Response:

As indicated in the paper, we used an implementation of the Fung wetland methane inventory for consistency with other work (as reported subsequently in O'Connor et al., Geoscientific Model Development, 2014, doi:10.5194/gmd-7-41-2014). O'Connor et al. (pages 63-64) found that the 'modelled surface concentrations are overestimated by approximately 10% during the Northern Hemisphere summer and autumn. A similar positive bias, albeit reduced, is also evident in the comparison at Mace Head'. Further in the same paragraph, O'Connor refer to this paper: 'More recent work by Hayman et al. (2014) also supports the hypothesis that the strength of the Fung et al. (1991) wetland emissions in the Northern Hemisphere (as used in this study) are overstated.'

We acknowledge in the present paper that this was an incorrect interpretation of the dataset. It results in much higher wetland emissions for boreal and higher latitudes, which is apparent in the comparisons with the surface atmospheric methane measurements and the atmospheric column methane observations. Although the dataset of Fung et al. was produced in the late 1980's/1990's, it is still widely used within the atmospheric chemistry community and provided the base wetland methane emission estimate for the TRANSCOM CH_4 model intercomparison (Patra et al., 2011 mentioned above).

In response to this comment, we have since undertaken a new model run using the Fung wetland inventory developed for the TRANSCOM CH4 model intercomparison (scaled to give annual wetland methane emissions of 181 Tg CH_4 yr^{-1}). We will include this new model run in the revised paper as appropriate.

Manuscript Changes:

The results from the new HadGEM2 run using the TRANSCOM FUNG wetland inventory are included in many places in the paper.

- Moved some text from the ACPD discussion to Section 3.3.1 (starting at line 366 on page 5)
- We have added the corresponding outputs from this run to Figures 2-6, 8-10 and Table 1 (in the main paper).
- We discuss this new run in Sections 3.1 (e.g., at lines 404, 543 on page 6), 3.2.2 (line 676 on page 7) and 3.3.1.
- We have also changed three HadGEM2 runs to four throughout the paper.

Detailed comments
Page 12988, line 12, Providing a numerical value for annual stratospheric loss rate would give some extra sense to the discussion on simulated stratospheric methane content.

Response:

We have calculated the global annual loss rate of stratospheric CH_4 (53±4 Tg CH_4 yr^{-1}) and compared it with other published estimates. We will alter the description of the UKCA tropospheric chemistry scheme (Section 2.1.2) and add the following to the current Section 3.2.1:

In the model runs carried out here, we derive the global annual loss rate of stratospheric CH_4 to be 53±4 Tg CH_4 yr^{-1}. This is higher than previous estimates (40 Tg CH_4 yr^{-1}, from Prather et al., 2001). Similar behaviour has however been seen in the stratospheric configuration of UKCA (Morgenstern et al., 2009). Given the different treatment of stratospheric CH_4 removal in the two UKCA configurations and that stratospheric chemical removal rates are much slower than transport timescales (Zahn et al., 2006), it is likely that the faster fall-off of modelled stratospheric CH_4 with height than observed is an indication that stratospheric transport timescales are too long.

Manuscript Changes:

Changes made to Sections 2.1.2 (starting line 225 on page 3) and 3.2.1 (starting line 618 on page 7).

Page 12988, line 5, Is it better to say “mapping-based” instead of “mapped-based”?

Response: Accept

Manuscript Changes:

Changed in Section 3.2.3 (line 812 on page 9).

Page 12988. When comparing with Amazon emissions it is useful to add comparison to results by Beck, V., et al., (Atmos. Chem. Phys., 13, 7961-7982, 2013)

Response:

Beck et al. (2013) derive emission estimates for the Amazon lowland region from measurements made during the BARCA aircraft campaign during the months of November 2008 and May 2009. The mean monthly CH_4 budget for the Amazon basin obtained from four different simulations is 3.3 Tg (range 1.5-4.8 Tg) for November 2008 and 3.3 Tg (range 1.3-5.5 Tg) for May 2009. We have extracted the wetland methane emissions for the months of May and November (average between 1999 and 2007) for the JULES and JULES-GIEMS wetland emission inventories for a rectangular domain closely approximately the irregular Amazon lowland domain used by Beck et al. and find:

- JULES May: 6.5 Tg CH_4, November: 5.7 Tg CH_4
- JULES-GIEMS May: 3.9 Tg CH_4 November: 2.2 Tg CH_4

The JULES-GIEMS emission estimate is within the range given by Beck et al. but the JULES is higher. As we state in the paper, the JULES wetland emissions are too high in this region.

We will include this paper in the discussion of Section 4.2 on comparison with other wetland estimates and add an entry to Table 2.

Manuscript Changes:

A sentence is added to Section 3.2.3 (starting at line 834 on page 9). A row added to Table 2 and text to the Note to the Table. This is not shown as a difference.

Page 12986, line 24. A need to reduce non-wetland emissions over India was cited by Patra et al, (J. Meteorol. Soc. Jpn., 87(4), 635-663, 2009), adding the citation may help convincing the reader that the JULES estimates are going in right direction.

Response:

We thank the reviewer for this. We will add a sentence to the end of Section 4.1 that Patra et al. (2009) also found that the emissions in the Indian Ganges region were overstated.

Manuscript Changes:

A sentence is added to the end of Section 3.2.2 (starting at line 766 on page 8).

Other Changes

Main Paper

1. Abstract and other places: Meaning of acronyms.
2. Page 2, line 85: Updated with newer study.
3. Page 3, end of Introduction. There is now a single section (Section 3) for the Results and Discussion.
4. Various: Amended references in the main paper to figures and tables found in the Supplement to account for insertion of new figures and tables.
5. Acknowledgements (Page 10): Added acknowledgement to the MONSOON supercomputer facility, used for the HadGEM2 runs.
6. Reference section: Included additional references cited in the revised paper.

Supplement

1. Figure 3 (Page 5): TRANSCOM FUNG inventory added to plots and caption amended. Also corrected errors in assignment of line colours.
2. Table 2 (Page 7): Added TRANSCOM-FUNG to header column
3. Table 3 (Page 7): Modified caption and added TRANSCOM-FUNG to header column
4. Figure 5 (Page 9): New table with time series and annual cycle of emissions used in the TRANSCOM-FUNG HadGEM2 run.
5. Figure 16 (Page 25): New figure comparing time series of the surface atmospheric methane concentrations as observed and from the TRANSCOM-FUNG HadGEM2 run.
6. Table 6 (Page 28): Added corresponding metrics and statistical parameters for the TRANSCOM-FUNG HadGEM2 run. Reduced the number of decimal places on certain entries to enhance clarity.
7. Section 2.2: It is conventional to capitalise the name of the SCIAMACHY satellite instruments.
8. New section (Section 3) added with definition of metrics used in the main paper and Supplement.

Manuscript prepared for Atmos. Chem. Phys.
with version 2014/07/29 7.12 Copernicus papers of the LaTeX class copernicus.cls.
Date: 22 October 2014

Comparison of the HadGEM2 climate-chemistry model against in-situ and SCIAMACHY atmospheric methane data

G. D. Hayman[1], F. M. O'Connor[2], M. Dalvi[2], D. B. Clark[1], N. Gedney[3], C. Huntingford[1], C. Prigent[4], M. Buchwitz[5], O. Schneising[5], J. P. Burrows[5], C. Wilson[6], N. Richards[6], and M. Chipperfield[6]

[1]Centre for Ecology and Hydrology, Crowmarsh Gifford, Wallingford, Oxfordshire, OX10 8BB, UK
[2]Met Office Hadley Centre, FitzRoy Road, Exeter, EX1 3PB, UK
[3]Joint Centre for Hydrometeorological Research, Met Office Hadley Centre, Crowmarsh Gifford, Wallingford, Oxfordshire, OX10 8BB, UK
[4]CNRS-LERMA, Observatoire de Paris, 61 avenue de l'Observatoire, 75014 Paris, France
[5]Institute of Environmental Physics, University of Bremen FB1, P. O. Box 330440, Otto Hahn Allee 1, 28334 Bremen, Germany
[6]School of Earth and Environment, University of Leeds, Leeds, LS2 9JT, UK

Correspondence to: G. D. Hayman (garr@ceh.ac.uk)

Abstract. Wetlands are a major emission source of methane (CH_4) globally. In this study, we have evaluated wetland emission estimates derived using the UK community land surface model (JULES, the Joint UK Land Earth Simulator) against atmospheric observations of methane, including, for the first time, total methane columns derived from the SCIAMACHY instrument on board the ENVISAT satellite.

Two JULES wetland emission estimates were investigated: (a) from an offline run driven with Climatic Research Unit - National Centers for Environmental Prediction (CRUNCEP) meteorological data and (b) from the same offline run in which the modelled wetland fractions were replaced with those derived from the Global Inundation Extent from Multi-Satellites (GIEMS) remote sensing product. The mean annual emission assumed for each inventory (181 $\mathrm{Tg\,CH_4}$ per annum over the period 1999–2007) is in line with other recently-published estimates. There are regional differences as the unconstrained JULES inventory gave significantly higher emissions in the Amazon (by $\sim 36\,\mathrm{Tg\,CH_4\,yr^{-1}}$) and lower emissions in other regions compared (by $\sim 10\,\mathrm{Tg\,CH_4\,yr^{-1}}$) to the JULES estimates constrained with the GIEMS product.

Using the UK Hadley Centre's Earth System model with atmospheric chemistry (HadGEM2), we have evaluated these JULES wetland emissions against atmospheric observations of methane. We obtained improved agreement with the surface concentration measurements, especially at northern high latitudes, compared to previous HadGEM2 runs using the wetland emission dataset of Fung et al. (1991). Although the modelled monthly atmospheric methane columns reproduced the large–scale patterns in the SCIAMACHY observations, they were biased low by 50 part per billion by volume (ppb). Replacing the HadGEM2 modelled concentrations above 300 hPa with HALOE–ACE assimilated TOMCAT output resulted in a significantly better agreement with the SCIAMACHY observations. The use of the GIEMS product to constrain the JULES-derived wetland fraction improved the ~~description~~ representation of the wetland emissions in JULES and gave a good description of the seasonality observed at surface sites influenced by wetlands, especially at high latitudes. We found that the annual cycles observed in the SCIAMACHY measurements and at many of the surface sites influenced by non-wetland sources could not be reproduced in these HadGEM2 runs. This suggests that the emissions over certain regions (e.g., India and China) are possibly too high and/or the monthly emission patterns for specific sectors are incorrect.

The comparisons presented in this paper have shown that the performance of the JULES wetland scheme is comparable to that of other process-based land surface models. We have identified areas for improvement in this and the atmospheric chemistry components of the HadGEM Earth System model. The Earth Observation datasets used here will be of continued value in future evaluations of JULES and the HadGEM family of models.

1 Introduction

The global mean atmospheric concentration of methane (CH_4) has increased from ~ 700 parts per billion by volume (ppb) at the start of the industrial era to ~ 1808 ppb in 2012 (Blunden and Arndt, 2013) and constitutes $\sim 20\,\%$ of the anthropogenic radiative forcing by greenhouse gases (Forster et al., 2007). Increases in atmospheric CH_4 concentrations potentially have a large impact on the global climate, through its direct radiative forcing effect (the radiative efficiency of CH_4 is about ten times greater than that of carbon dioxide per tonne emitted: Ramaswamy et al., 2001) and, indirectly, through the formation of tropospheric ozone and aerosols (Shindell et al., 2009). In consequence, control of CH_4 emissions is potentially an important lever for international climate change policy and possible (short-term) mitigation actions (e.g., Shindell et al., 2012; Bowerman et al., 2013). An accurate knowledge of its contemporary sources and sinks is therefore essential.

CH_4 is emitted to the atmosphere from a number of sources (Denman et al., 2007): (a) biogenic sources, covering wetlands, agriculture (livestock and rice production), landfills, forests, oceans and termites, and (b) non-biogenic sources, comprising fossil-fuel mining and burning, biomass burning, waste treatment and geological sources. The major removal process for CH_4 in the atmosphere is reaction with hydroxyl (OH) radicals. Minor sinks are reactions with chlorine ~~atoms, with~~ (Cl) atoms in the boundary layer, reactions with OH, Cl, and excited oxygen atoms ($O(^1D)$) in the stratosphere, and uptake by soils. The overall atmospheric lifetime of CH_4 is estimated to be ~~8.7 ± 1.3~~9.1 ± 1.9 years ~~(Stevenson et al., 2006; Denman et al., 2007)~~ (Prather et al., 2012).

In-situ measurements of CH_4 concentrations have been made from global networks of surface atmospheric sites since the 1980s (Steele et al., 1987, 1992; Blake and Rowland, 1988; Dlugokencky et al., 1994b, 1998, 2001, 2003, 2009, 2011; Rigby et al., 2008). The globally-averaged CH_4 growth rate, derived from the surface measurements, has fallen from a high of $16\,\mathrm{ppb\,yr^{-1}}$ in the late 1970s/early 1980s (Blake and Rowland, 1988; Steele et al., 1992; Dlugokencky et al., 1998) to almost zero between 1999 and 2006 (Dlugokencky et al., 2011). This period of declining or low growth was however interspersed with years of positive growth-rate anomalies (e.g., in 1991–1992, 1998–1999 and 2002–2003). Since 2007, renewed growth has been evident (Rigby et al., 2008; Dlugokencky et al., 2009), with the largest increases observed to originate over polar northern latitudes and the Southern Hemisphere in 2007 and in the tropics in 2008. There is significant concern that this might be the restart of an on–going upward trend in atmospheric CH_4 concentrations.

The observed inter-annual variability in atmospheric CH_4 concentrations and the associated changes in growth rates have variously been ascribed to changes in the different CH_4 sources and sinks: (a) CH_4 sources directly influenced by human activities, such as fossil fuel production (Dlugokencky et al., 1994b, 2011; Bousquet et al., 2006; Bergamaschi et al., 2013; Kirschke et al., 2013), (b) wetland emissions (Bousquet et al., 2006, 2011; Ringeval et al., 2010; Kirschke et al., 2013; Pison et al., 2013) and (c) biomass burning, especially during the intense El Niño years in 1997 and 1998 (Dlugokencky et al., 2001; Kirschke et al., 2013). The most likely causes of the CH_4 anomalies observed during 2007 and 2008 were the anomalously high temperatures in the Arctic (Dlugokencky et al., 2009) or larger CH_4 emissions from natural wetlands in tropical South America and boreal Eurasia (Bousquet et al., 2011).

Atmospheric column CH_4 measurements with sensitivity to the surface and lower troposphere are now available from satellite instruments: SCIAMACHY on ENVISAT from 2003 (Buchwitz et al., 2005; Frankenberg et al., 2005; Schneising et al., 2009, 2011) and, since 2009, the Greenhouse Gas Observing Satellite (GOSAT, Kuze et al., 2009). The satellite measurements complement the observations from the sparse network of surface sites. Frankenberg et al. (2006) concluded that the SCIAMACHY measurements could be used in inverse modelling and were an important step in reducing the uncertainties in the global methane budget. Bergamaschi et al. (2007) extended the inverse modelling analysis to include both surface and satellite observations. Their results indicated significantly greater CH_4 emissions in the tropics compared to either the a priori estimates or the inversion based on the surface measurements alone. The discrepancy was partially reduced after taking account of spectroscopic changes to interfering water vapour absorption lines (Frankenberg et al., 2008; Meirink et al., 2008). More recently, Fraser et al. (2013) have used column CH_4 measurements from the Thermal And Near-infrared Sensor for carbon Observation (TANSO) on the GOSAT to estimate global and regional monthly CH_4 fluxes.

The surface and satellite atmospheric measurements have been used to constrain the total global annual source strength of CH_4 (in Tg $CH_4\,yr^{-1}$): 550 ± 50 (Frankenberg et al., 2005); 582 (Denman et al., 2007); 515 ± 3 [1999–2006], 536 [2007] and 533 [2008] (Bousquet et al., 2011); 513 ± 9 [1990s] and 514 ± 14 [2000s] (TRANSCOM Methane Model Intercomparison, Patra et al., 2011), 510–516 [2009–2010] (Fraser et al., 2013) and 551(500–592) [1980s], 554(529–596) [1990s] and 548(526–569) [2000s] (Kirschke et al., 2013). However, there still remain considerable uncertainties in the partitioning of sources and their spatial and temporal distribution (Kirschke et al., 2013).

Wetlands are generally accepted as being the largest, but least well quantified, single natural source of CH_4, with global emission estimates ranging from 100–231 Tg $CH_4\,yr^{-1}$ (Denman et al., 2007; USEPA, 2010). The modelling of wetlands and their associated emissions of CH_4 has become the subject of much current interest. The review by Melton et al. (2013) provides a summary of the current state of knowledge on wetlands and the outcome of

the WETland and wetland CH_4 Inter-comparison of Models project (WETCHIMP). Melton et al. (2013) found a large variation in the wetland areas and associated CH_4 emissions from the participating models and varying responses to climate change (as represented by increases in the driving CO_2 concentrations, temperature and precipitation).

Wetland emissions are particularly sensitive to climate change (O'Connor et al., 2010; Melton et al., 2013). Gedney et al. (2004) concluded that the wetlands model used in the Joint UK Land Earth Simulator (JULES, the UK community land surface model), would lead to a ~~-~~doubling of CH_4 emissions from wetlands by 2100 for the IPCC IS92a scenario considered. As a ~~-~~major emission source of CH_4 which responds strongly to climate change, it is vital that the description of wetlands and the associated emissions of CH_4 used in land surface and climate models reflects current understanding and the implications of emerging datasets. In this paper, we use atmospheric observations of CH_4 (surface concentrations and total columns derived from the SCIAMACHY instrument) to evaluate simulations of the Hadley Centre's Global Environmental Model (HadGEM2, Collins et al., 2011) and hence to assess the wetland methane emission parameterisation used in the UK community land surface model, JULES. The paper is structured as follows~~:~~ ~~-~~. Sect. 2 provides a ~~-~~brief description of the ~~model~~models, the experimental set-up and the key datasets used in the model runs and subsequent analysis~~, and~~ . Sect. 3 compares the modelled CH_4 concentrations with atmospheric methane measurements ~~. The paper concludes with Discussions (~~and includes discussion of the results. Finally, conclusions can be found in Sect. ~~3.1) and Conclusions (Sect. 4)~~4.

2 Approach and methodology

2.1 HadGEM2

2.1.1 Model configuration and nudging

The UK Hadley Centre's Global Environmental Model (HadGEM) is a ~~-~~family of models which have been designed to simulate and understand the ~~centennial-scale~~ centennial-scale evolution of climate, including biogeochemical feedbacks, ~~and~~ in response to anthropogenic ~~greenhouse gas~~ and natural greenhouse gas and aerosol-precursor emissions. In this study, we used version 2 of HadGEM (HadGEM2: Collins et al., 2011) in an atmosphere-only configuration. The model was driven with sea surface temperature and sea ice fields taken from the second Atmosphere Model Intercomparison Project (www-pcmdi.llnl.gov/projects/amip). The dynamics and temperatures of the climate model were "nudged" (Telford et al., 2008) towards ~~ECMWF~~ the European Centre for Medium-Range Weather Forecasts (ECMWF) ERA-40 reanalyses (Uppala et al., 2005) of the atmospheric state of temperature, surface pressure and the horizontal wind components. Hence, the synoptic variability would be similar to that observed, improving the comparison with observations of atmospheric trace constituents.

2.1.2 Atmospheric chemistry

For the runs reported here, we use the Standard Tropospheric chemistry scheme (O'Connor et al., 2014) from the UK Chemistry and Aerosol (UKCA; http://www.ukca.ac.uk) model, which has been implemented into HadGEM2. This chemistry scheme comprises 46 chemical species (of which 26 are advected tracers), 129 reactions (102 gas-phase and 27 photolysis reactions) and interactive deposition schemes. The chemistry scheme simulates the chemical cycles of odd oxygen (O_x), odd hydrogen (HO_x) and nitrogen oxide (NO_x) and the oxidation of carbon monoxide (CO), methane (CH_4), ethane (C_2H_6) and propane (C_3H_8). There are 8 emitted species: CO, NO_x, CH_4, C_2H_6, C_3H_8, HCHO (formaldehyde), CH_3CHO (acetaldehyde) and CH_3CHOCH_3 (acetone). ~~As a result of the upper model boundary being at 39, there is oxidation of by in the model~~In relation to CH_4, although the dominant loss of CH_4 in the troposphere is through oxidation by the hydroxyl radical (OH), oxidation in the stratosphere is solely represented by reactions with both OH and $O(^1D)$; there is no oxidation by Cl. However, because ~~of the low model lid, it~~ the upper model boundary is at 39 km, oxidation by $O(^1D)$ does not provide a ~~-~~sufficiently large sink for ~~- the bulk of the stratospheric removal occurs above 39, hence, the need for~~ CH_4. Hence, an explicit loss term is applied at the top of the model domain to compensate for the lack of stratospheric CH_4 oxidation. Further details on the Standard Troposphere chemistry scheme and its evaluation can be found in O'Connor et al. (2014).

2.1.3 Land surface module

JULES is a ~~-~~physically-based model that describes the water, energy and carbon balances and includes temperature, moisture and carbon stores (Best et al., 2011; Clark et al., 2011). JULES can be run as a ~~-~~stand-alone model using appropriate driving meteorological data or as the land surface component in UK climate or Earth System models (Note that HadGEM2 strictly uses the Met Office Surface Exchange System, an earlier version of JULES, as the land surface component).

JULES uses a ~~-~~tiled approach to describe sub-grid scale heterogeneity. Nine surface types are used, of which five are vegetation-related. The fractions of surface types within each land-surface grid-box can either be modelled or prescribed. Air temperature, humidity, wind speed and incident radiation above the surface and soil temperatures and moisture contents below the surface are treated as homogeneous across a ~~-~~grid cell; other parameters are calculated for each surface type.

The current version of JULES uses a methane wetland emission parameterization, developed and tested by Gedney et al. (2004) for use at large spatial scales. The wetland parameterization is coupled to the large-scale hydrology scheme of Gedney and Cox (2003), which predicts the distribution of sub-grid scale water table depth and wetland fraction (f_w) from the overall soil moisture content and the sub-grid scale topography. The methane flux from wetlands $F_w(CH_4$ in $kg\,C\,m^{-2}\,s^{-1})$ is given in terms of the main controls of temperature, water table height and substrate availability:

$$F_w(CH_4) = f_w\ k(CH_4)\ C_s\ Q_{10}(T_{soil})^{(T_{soil}-T_0)/10} \quad (1)$$

where T_{soil} is the soil temperature (in K) averaged over the top 10 cm and $k(CH_4)$ is a global constant which is calibrated to give the required global methane flux. Soil carbon content (C_s in $kg\,C\,m^{-2}$) was used as there is a lack of global data on substrate availability. The default parameter values are $k(CH_4) = 7.4\times10^{-12}\,s^{-1}$, $T_0 = 273.15$ K and $Q_{10}(T_0) = 3.7$ (Clark et al., 2011).

2.2 Earth Observation datasets

We have used a number of key Earth Observation datasets, either to constrain the land surface and ~~climate-chemistry~~ chemistry-climate models or to evaluate the models. These are briefly described in the following sections.

2.2.1 Wetland and inundation dynamics

A globally applicable remote-sensing technique, employing a suite of complementary satellite observations, has been developed to derive wetland inundation extents: the Global Inundation Extent from Multi-Satellites (GIEMS) (Prigent et al., 2001b, 2007; Papa et al., 2010; Prigent et al., 2012). The method estimates inundation and its seasonal and spatial dynamics at the global scale using 3 sensors. Detection of inundation primarily relies on the passive microwave land-surface signal between 19 and 85 GHz from the Special Sensor Microwave/Imager (SSM/I). Relative to non-flooded lands, inundated regions are characterized by low microwave emissivities and high emissivity polarization difference, even under dense canopies. In semi-arid regions where bare surfaces and inundation can produce similar SSM/I signatures, the Normalized Difference Vegetation Index (NDVI), derived from visible and near-infrared reflectances from the Advanced Very High Resolution Radiometer (AVHRR), is used to resolve ambiguities. Active microwave backscattering at 5.25 GHz from the ASCAT scatterometer (the original method used the scatterometer on board the European Remote Sensing (ERS) satellite) is very sensitive to vegetation density (Prigent et al., 2001a). These measurements are used to assess vegetation contributions and to quantify the fraction of inundation within the pixel. The GIEMS dataset is now available on a monthly basis from 1993 to 2007 globally, and mapped on an equal area grid of 773 km^2 (equivalent to $0.25^\circ \times 0.25^\circ$ at the equator) (Prigent et al., 2012). This and the earlier datasets have been thoroughly evaluated by comparison with other static estimates of wetland extent. This product is the only dynamic estimate available. It has also been compared with related hydrological variables such as rain rate, river gauges and river heights (Prigent et al., 2001b, 2007; Papa et al., 2006a, b, 2007, 2008a, b).

2.2.2 SCIAMACHY atmospheric column methane

Atmospheric column-averaged CH_4 dry-air mixing ratios (XCH_4 in ppb) are available from the SCIAMACHY instrument on the ENVISAT satellite (Schneising et al., 2009, 2011). The SCIAMACHY data product used in this study was retrieved from nadir measurements using the Weighting Function Modified Differential Optical Absorption Spectroscopy (WFM-DOAS) processing algorithm (version 2.3, WFMDv2.3). WFMDv2.3 is an improved version of WFMDv2.0.2 (Schneising et al., 2011, 2012), using a correction factor depending on simultaneously retrieved water vapour abundance (from the same fitting window as CO_2, which is used as a proxy for the light path) to account for spectroscopic interferences. The WFM-DOAS algorithm is one of the algorithms currently being compared in the ~~ESA~~ European Space Agency (ESA) project: Greenhouse Gases Climate Change Initiative (GHG-CCI; Buchwitz et al., 2013). The SCIAMACHY dataset has been validated and its relative accuracy, a quality measure quantifying regional biases, is 7.8 ppb (Dils et al., 2014). The SCIAMACHY XCH_4 dataset was provided on a $0.5^\circ \times 0.5^\circ$ grid at monthly intervals for the time period 2003–2009. The SCIAMACHY dataset was regridded to the spatial resolution of the HadGEM2 model to enable direct comparison with the model.

2.2.3 HALOE–ACE assimilated TOMCAT

The HALogen Occultation Experiment (HALOE, Russell et al., 1993) provides solar occultation observations of a range of trace gases including CH_4 (Park et al., 1996) from September 1991 until November 2005. Observations were obtained at about 15 sunrise and sunset locations per day. The Atmospheric Chemistry Experiment (ACE, Bernath et al., 2005) was launched onboard SCISAT-1 in August 2003 and since then has been providing solar occultation observations of trace gases including CH_4 (De Mazière et al., 2008). Despite the geographical sparseness of these datasets, the long-atmospheric lifetime of CH_4 means that this solar occultation data is sufficient to constrain a stratospheric Chemical Transport Model (CTM) through data assimilation (see Chipperfield et al., 2002). In this study, we use the TOMCAT off-line 3-D CTM (Chipperfield, 2006; Breider et al., 2010; Monks et al., 2012), with data assimilation of the HALOE and ACE measurements, to provide monthly CH_4 concentration fields

for the upper troposphere and stratosphere for the years 2000 through to 2007 (see Sect. 3.2.1).

2.3 Model runs and emission inventories

2.3.1 Wetland methane emissions

For their CH_4 wetland emissions, O'Connor et al. (2014), aggregate the wetlands, bogs, swamps and tundra components in the dataset of Fung et al. (1991), available from http://data.giss.nasa.gov/ch4_fung/. This ~~dataset~~aggregated wetland emission dataset (totally 181 $Tg\,CH_4\,yr^{-1}$), together with the other CH_4 emission sources used, was found to give very reasonable atmospheric CH_4 lifetimes and burdens, global mean concentrations, and reasonably good comparisons with in-situ surface atmospheric observations. One of the runs undertaken in this study made use of this inventory (denoted hereinafter FUNG). We now believe our use of the dataset to be incorrect. The components in the dataset represent 2 different emission scenarios with different assumptions on seasonality (Fung et al., 1991). We also use the version of the Fung inventory produced for the TRANSCOM–CH_4 study (Patra et al., 2009, 2011), denoted hereinafter TRANSCOM-FUNG. This was further scaled to give a global annual emission flux of 181 $Tg\,CH_4\,yr^{-1}$, as this was the nominal total wetland emission used in previous work.

The other runs reported here use methane wetland emissions derived from an offline global run of the JULES land surface model (see Sect. 2.1.3), driven with CRU-NCEP meteorological data (Viovy and Ciais, 2009), for $0.5° \times 0.5°$ terrestrial grid squares (denoted JULES). A ~~-~~second emission estimate is derived from this offline JULES run by replacing the modelled wetland fraction in Eq. (1) with the wetland fraction derived from the regridded GIEMS product (denoted JULES-GIEMS). As the GIEMS inundation product does not discriminate between natural wetlands and managed water areas such as rice paddy fields, the GIEMS product is corrected for such rice paddy fields, using information on the area of cultivation of rice from both irrigated and rain-fed cultivation (Portmann et al., 2010). The two JULES emission estimates are separately scaled so that the average global annual emission flux over the period of the model runs (1999–2007) is 181 $Tg\,CH_4\,yr^{-1}$, for the reason given in the previous paragraph.

The most noticeable differences between the JULES emission datasets and ~~that~~ those of Fung et al. (1991) are the significantly higher emissions in the boreal region ~~in~~ (> 50° N) in both the FUNG dataset as used by O'Connor et al. (2014) ~~(~~and the TRANSCOM-FUNG inventory compared to the JULES-based inventories (FUNG: ~ 90; TRANSCOM-FUNG: ~ 52; JULES: ~ 5 and JULES-GIEMS: ~ 15 $Tg\,CH_4\,yr^{-1}$)~~and ~~, and conversely the higher emissions in the tropics (30° S-30° N) in the JULES-based inventories (~~~ 160 and ~~~ 123FUNG: ~ 67; TRANSCOM-FUNG: ~ 100; JULES: ~ 167 and JULES-GIEMS: ~ 127 $Tg\,CH_4\,yr^{-1}$~~for JULESand JULES-GIEMS, respectively~~). This can be seen in Fig. 1 (see subsequent discussion in Sect. 3.1.1) and also Fig. 3 of the Supplement.

Additional information on the wetlands and their associated emissions of methane is provided in Sect. 1.1 of the Supplement.

2.3.2 Other emissions

We generate year- and month-specific emission datasets for the period from 1997 to 2009 for the emitted species in the UKCA standard tropospheric chemistry scheme (see Sect. 2.1.2). The approach adopted varies depending on the source sector:

- *Anthropogenic*: year- and month-specific emission datasets are derived from the decadal-averaged emission inventories compiled by Lamarque et al. (2010), by scaling the emission totals for the different years and source sectors using sector and species-specific scaling factors based on the annual trends given in various EDGAR time series.

- *Biomass burning*: year-specific emission inventories are available from the Global Fire Emissions Database (GFED, v3.1) for the years 1997 to 2009 (van der Werf et al., 2010), on a monthly timestep. The CH_4 emissions are rescaled to give the same period mean (25 $Tg\,CH_4$ per annum), as used in the UKCA runs of O'Connor et al. (2014).

- *Other*: sources such as termites and hydrates for CH_4 and oceanic emissions of CH_4 and other volatile organic compounds are taken from various sources, as described in O'Connor et al. (2014). These datasets contain a ~~-~~single annual cycle, which is assumed to apply for all years.

A ~~-~~number of studies (e.g., Monteil et al., 2011; Patra et al., 2011) find that the anthropogenic trend in the 2000s as given in the EDGAR v4.2 emission time series is not consistent with surface atmospheric measurements of methane and its ^{13}C isotope for the period from 2000 to 2006. For this reason, we prefer to use the earlier EDGAR v3.2 emission time series. The recently-published papers by Bergamaschi et al. (2013) and Kirschke et al. (2013) provide justification for this choice.

Additional information on the emission datasets used for the other emitted species in the model runs is provided in Sect. 1.2 of the Supplement.

3 Results and Discussion

Three Four HadGEM2 runs were undertaken for the period 1999–2007, which differed only in the wetland emission inventory used (FUNG, TRANSCOM-FUNG, JULES and JULES-GIEMS). Figure 2 shows the spatial distribution of the global annual methane emissions for the year 2000 for the three four runs. The model runs all used the same previously-derived initial conditions, which represented a spun-up atmosphere for the early 2000's.

3.1 Comparison with surface measurements

We use the surface measurements of atmospheric CH_4 dry air mole fractions made at sites in the NOAA ESRL GMD National Oceanic & Atmospheric Administration's Earth System Research Laboratory (NOAA ESRL) Carbon Cycle Cooperative Global Air Sampling Network (Dlugokencky et al., 2012). Section 2.1 in the Supplement includes a map of the monitoring sites and has time series of the observed and modelled atmospheric CH_4 concentrations between the years 2000 and 2010 at 16 of the 64 sites, covering both northern Northern and Southern Hemisphere locations, for the different model runs. Figure 3 shows a comparison of the latitudinal distribution of the observed monthly surface atmospheric methane mixing ratios from all the sites for the months of January, April, July and October (as a mean of the available measurements between 2000 and 2010) with the corresponding values derived from the three four HadGEM2 runs. All three four model runs reproduce the increase in methane mixing ratio between the Southern and Northern Hemispheres (SH, NH). The model runs also capture the variability (or lack thereof) in the Northern Hemisphere (in the Southern Hemisphere). The runs also reproduce the annual cycles observed at many of the Southern Hemisphere sites.

There is a difference are differences in the modelled annual cycles at the Northern Hemisphere sites for the three four runs, which is more clearly seen in Fig. 4. The model run using the FUNG wetland emissions gives very high surface CH_4 concentrations and an incorrect seasonality at all the high and mid–latitude NH sites (illustrated here by the Barrow, Pallas-Sammaltunturi and Mace Head sites). This has been seen by other authors (e.g. Patra et al., 2011) and is also seen to a lesser extent in the run using the TRANSCOM-FUNG wetland inventory. The runs using the JULES wetland emission inventories are generally better in terms of amplitude and seasonality for these sites. We subsequently evaluate the model outputs using various metrics (see below). There is further evidence of the different spatial and temporal patterns between the wetland emission inventories at other mid-latitude NH sites (Hegyhatsal, Hungary; Ulaan Uul, Mongolia; Southern Great Plains, USA and Plateau Assy, Kazakstan). The modelled concentrations at the Arembepe site in Brazil provide evidence of the over-prediction of the CH_4 emissions from the JULES wetland inventories. All three model runs show similar behaviour at a number of the other At many of the sites (e.g., Ulaan Uul, Mongolia; Southern Great Plains, USA; Tae-ahn Peninsula, Korea; Mount Waliguan, China; Mahe Island, Seychelles). At many of these sites, the concentrations in the winter months are significantly overestimated, suggesting that the annual pattern of the non-wetland methane emissions may not be correct. The remote SH sites (illustrated here by the South Pole site Tierra del Fuego and South Pole sites) are located a long distance from the large CH_4 sources (which are mainly in the NH) and are representative of the remote and well-mixed Southern Hemisphere, although there is evidence of the higher SH wetland emissions in the JULES and JULES-GIEMS runs.

The HadGEM2 configuration used for these runs does not provide 'tagged' or 'coloured' outputs (i.e., the contribution of the different methane source sectors cannot be derived). Instead, we estimate the contribution from the various source sectors (anthropogenic, rice paddy fields, shipping, wetlands, biomass burning, termites and oceanic/hydrates) using the sector emissions local to that region. In Tab. 4 of the Supplement, we present the relative contribution of the emissions sectors for a $20° \times 20°$ box centred on the Barrow and Plateau Assy sites. At Barrow, the emissions in the TRANSCOM-FUNG run are mainly from wetlands (>62%), whereas the wetland emissions are smaller in the JULES and JULES-GIEMS runs and the emissions from anthropogenic sources make the largest contribution. A similar pattern is also observed at the Pallas-Sammaltunturi site. At the Plateau Assy site, anthropogenic emissions are the largest contributing sector with wetlands at 25-29% (TRANSCOM-FUNG), 0.3-6.0% (JULES) and 11-13% (JULES-GIEMS).

A wide variety of methods have been developed within the atmospheric composition and air pollution community to assess model performance (e.g., Yu et al., 2006; Dennis et al., 2010). For each of the HadGEM2 runs, we derived these different metrics (linear regression, bias, normalized mean bias, index of agreement (IOA), hit rate - see Sect. 3 in the Supplement) for each site where there were at least 20 co-located monthly observed and modelled concentrations. The valid data from all sites for a given run were then aggregated and the same set of metrics derived for this "global" dataset. Table 1 provides the output of this analysis. There are some remarkably good fits with slopes close to unity and high correlation coefficients ($R^2 = 0.82$ for the JULES-GIEMS inventory). That said, there are specific sites where the performance appears superficially good but is less robust on closer inspection (see Table 5 6 in Sect. 2.1 of the Supplement). This can also be seen in Fig. 5, which shows a Taylor plot for the 3 Taylor plot (Taylor, 2001) for the 4 runs (FUNG, TRANSCOM-FUNG, JULES and JULES-GIEMS). The JULES-based inventories represent an improvement over the FUNG wetland inventory; where the and, to a lesser extent, the TRANSCOM-FUNG wetland inventories, where a negative correlation between the observed and modelled

concentrations at high latitude NH sites is evident for the latter. The index of agreement (and, to a ~~–~~lesser extent, the hit rate) did show some discrimination between the model runs. The IOA varies between 0.76 (FUNG) and 0.94 (JULES-GIEMS)~~. The run which gives the highest index of agreement uses the wetland emission inventory~~ , the run in which the ~~modelled~~ JULES-modelled wetland fraction is replaced with the EO-derived value. The run using the JULES-modelled wetland fraction gave an ~~index of agreement of~~ IOA of 0.91, showing that the JULES-based emission inventories are, in general, a ~~–~~considerable improvement over run using the FUNG inventory (but not the run using TRANSCOM-FUNG inventory, for which an IOA of 0.91 is derived).

Of more relevance is whether the model can reproduce the observed growth rates and hence explain the origin of the positive anomalies. Following Dlugokencky et al. (1994a) and references therein, the average trend and seasonal cycle in the modelled or observed concentrations were approximated by a ~~–~~second-order polynomial and four harmonics. A ~~–~~low-pass filter was then applied to the residuals of the fit to remove variations occurring on timescales less than ~ 1 year. The smoothed residuals were added to the quadratic portion to give a ~~–~~deseasonalised trend. The growth rate was derived as the derivative of the monthly concentrations of this deseasonlised trend. Figure 6 shows the growth rates derived from the observed and calculated surface concentrations at 6 sites (Alert, Niwot Ridge, Mauna Loa, Ascension Island, Bukit Kototabang and South Pole) for ~~the three~~ all the runs. The modelled growth rates are similar to each other and generally larger than those observed, reflecting the generally larger modelled annual cycles (see Figures in Sect. 2.1 of the Supplement). It is less clear that the JULES-based inventories are generally better. The correspondence at many sites is variable and there is some indication that the modelled changes are more rapid than those observed.

3.2 Comparison with SCIAMACHY measurements

3.2.1 Initial comparison

We convert the modelled 4-D methane mass mixing ratio fields (longitude, latitude, altitude, time) into 3-D fields (longitude, latitude, time) of the mean dry–air atmospheric column methane mixing ratio, using the SCIAMACHY averaging kernels (Schneising et al., 2009). We then derive contour maps of the mean atmospheric mixing ratios of methane from the HadGEM2 model runs and the regridded version of the SCIAMACHY product (v2.3, Sect. 2.2.2) for the period 2003 to 2007. The model outputs are only sampled at the valid space and time points present in the SCIAMACHY product and a ~~–~~land–sea mask is applied to remove all data over the oceans as the SCIAMACHY dataset only includes measurements over the oceans for the period between 2003 and 2005. As shown in Fig. ~~17~~ 19 in the Supplement, there is a ~~–~~clear underprediction in the modelled atmospheric column methane mixing ratios by ~ 50 ppb ~~–~~(i.e., $\sim 3\%$ of a typically observed mean column mixing ratio).

We attribute the underprediction to a ~~–~~faster fall-off in modelled methane concentrations with altitude than that observed. To test this, we initially replaced the HadGEM2 model outputs above 400 hPa with methane mixing ratios derived from the thermal infrared (TIR) channel of the Tropospheric Emission Spectrometer (TES, AURA, 2004–2011: Beer, 2006), because of its availability and ease of use. As discussed by Worden et al. (2012), the CH_4 in the upper troposphere is biased high relative to the lower troposphere by 4 % on average. Given this and the poor temporal overlap with the SCIAMACHY dataset, we subsequently constrained the HadGEM2 output above 300 hPa with data from HALOE/ACE-assimilated TOMCAT output (see Sect. 2.2.3), which covered the entire period of the HadGEM2 runs (2000–2007) and the SCIAMACHY measurements. Figure 7 shows a ~~–~~typical comparison of the HadGEM2 modelled vertical concentration profile of CH_4 with the corresponding profiles from TES and the HALOE/ACE-assimilated TOMCAT model for the grid square centred on ~~point (1~~the location (10° ~~E, 10~~N, 1° ~~N~~E) in July 2005. The figure also shows the revised profiles derived by replacing the HadGEM2 modelled concentrations with interpolated TES measurements (above 400 hPa) and the HALOE-assimilated TOMCAT output (above 300 hPa). The derived mean atmospheric methane column mixing ratios (in ppb) were: 1725.9 (HadGEM2, original), 1780.2 (HadGEM2+TES) and 1766.4 (HadGEM2+HALOE-TOMCAT), compared to the SCIAMACHY measurement of 1760.9 ppb.

~~O'Connor et al. (2014)~~ (O'Connor et al., 2014) introduce an explicit loss term in the Standard Tropospheric Chemistry scheme to ~~represent the oxidation~~ compensate for the lack of CH_4 ~~by~~ oxidation in the stratosphere~~(see Sect.)~~. However, the faster fall-off with height cannot be attributed to this additional explicit loss term (see Sec. 2.1.2). ~~We initially believed that this might be the cause of~~ In the model runs carried out here, although the global annual loss rate of stratospheric CH_4 is higher than previous estimates (53 ± 4 Tg CH_4 $year^{-1}$) compared to 40 Tg CH_4 $year^{-1}$ from Prather et al. (2001)), similar behaviour has been seen in the stratospheric configuration of UKCA (Morgenstern et al., 2009) . Given the different treatment of stratospheric CH_4 removal in the two UKCA configurations and that stratospheric chemical removal rates are much slower than transport timescales (Zahn et al., 2006) , it is likely that the faster ~~fall-off. However, unpublished results obtained with a new version of the UKCA (F. M. O'Connor, personal communication, 2013), including both tropospheric and stratospheric chemistry, indicate that this faster~~ fall-off ~~is still present. Further work is in progress to address this.~~ of modelled stratospheric CH_4 with height than observed

is an indication that stratospheric transport timescales are too long. Constraining the modelled CH_4 concentrations at model levels above 300 hPa improved the agreement with the SCIAMACHY SWIR CH_4 product (Fig. ~~17~~ 19 in the Supplement). All subsequent comparisons with the SCIAMACHY product are based on the merged HadGEM2 and HALOE/ACE-assimilated TOMCAT outputs. As our emphasis is on testing different wetland CH_4 emission configurations, ~~we adopt~~ this extra constraint ~~of our atmospheric modelling structure~~being applied to HadGEM2 output is appropriate.

3.2.2 Comparisons in space and time

Figure 8 compares the mean atmospheric column measurements of methane derived from the regridded SCIAMACHY product for the period 2003–2007 and the HadGEM2 runs using the FUNG, TRANSCOM-FUNG, JULES and JULES-GIEMS methane wetland emission inventories, constrained as described in the previous section. We note that (i) the model reproduces the latitudinal gradient in the atmospheric methane column, with higher methane columns in the Northern Hemisphere; (ii) the model captures the high emission areas over South and South East Asia, although the modelled concentrations are much higher than those observed; (iii) the different spatial patterns of the wetland methane emissions used are evident in the maps. We see enhanced atmospheric columns over the boreal Eurasia region in the run using the FUNG wetland inventory and over the Amazon in the run using the JULES wetland inventory.

We compare the latitudinal distributions in Fig. 9. The run using the TRANSCOM-FUNG wetland inventory gives a remarkably good description. The larger emissions present at temperate and higher Northern Hemisphere latitudes in the ~~wetland inventory of Fung et al. (1991)~~ FUNG wetland inventory result in higher zonal averages at these latitudes compared to both TRANSCOM-FUNG and the JULES-based inventories. ~~On the other hand, the~~ The JULES-based inventories give better agreement in the tropics and Southern Hemisphere compared to the FUNG inventory but underestimate the atmospheric column at boreal and higher northern latitudes. The high modelled mixing ratios over the Ganges Valley in India are evident in the peaks in the modelled profiles between 20–30° N in all four runs.

Figure 10 shows time series and annual cycles of the area-weighted mean atmospheric column methane mixing ratios between January 2003 and December 2007 from the SCIAMACHY data and the ~~three~~ four HadGEM2 runs for all land surface points and for the 11 terrestrial TRANSCOM regions (see map at http://transcom.project.asu.edu/transcom03_protocol_basisMap.php). ~~A noticeable difference in the model runs is the larger annual cycle seen using the Fung et al. dataset, especially in the boreal region (~~In Fig. 20 in the Supplement, we include similar time series and annual cycle plots using the unconstrained HadGEM2 model outputs. We know that the FUNG wetland emission inventory used here gives too much emission at boreal and higher latitudes. This is apparent from the very strong annual cycles with summer maxima (30–50 ppb enhancements) for Europe and the two boreal zones in North America and Eurasia~~), Europe and, to a lesser extent, Southern Africa~~. The run using ~~the wetland emissions of Fung et al. (1991) results in very large~~ TRANSCOM-FUNG wetland inventory also has annual cycles with ~~strong summer maxima (30–50enhancement)~~ summer maxima for Europe and the two boreal zones in North America and Eurasia. The JULES-based inventories, on the other hand, show summer mimima, similar to the behaviour seen in the surface measurement sites (see Fig. 4). It is also evident that the monthly emission profiles of some source sectors appear incorrect. In the Tropical Asia region, the annual cycle shows a ~~-~~minimum in July for all ~~three~~ four runs whereas the SCIAMACHY data show a ~~-~~maximum in the late summer/early autumn. Also included in each panel of Fig. 10 are the Indices of Agreement derived for the ~~three~~ four HadGEM2 runs. ~~The~~ As presented, the values generally show that the model run using the FUNG wetland emission inventory performed the best when all land surface points are considered together (IOA = 0.86) and for some of the TRANSCOM regions in the Northern Hemsiphere. However, the JULES-based inventories were better in the Southern Hemisphere (e.g., IOA for JULES-GIEMS = 0.59 for South American Temperate, Southern Africa and Australia). ~~From this comparison with the SCIAMACHY measurements, there is no one preferred~~ The high modelled mixing ratios over the Ganges Valley in India, evident in Figs. 8 and 9 in all four runs, occur in the winter months. This suggests that the stronger summer emissions in the FUNG wetland emission inventory ~~as each are better in some TRANSCOM regions than others.~~ compensates for the lack of or opposite seasonality in the emissions from other source sectors (see Figs. 4-7 in the Supplement).

4 ~~Discussion~~

3.1 Discussion

3.2 ~~Comparison against measurements~~

3.1.1 Comparison against measurements

The comparison of the model outputs against the in-situ surface atmospheric and atmospheric column measurements of methane have indicated varying levels of agreement. The run using the JULES-GIEMS wetland emission inventory gives the best description of the surface observations and the derived growth rates. The observed growth rates clearly show the positive anomalies in 1997/1998, 2002/2003 and the increase in methane after 2007 (see Fig. 6). The model captures these events with varying degrees of success. There is also evidence from the high latitude Southern Hemisphere (SH)

sites that the modelled atmospheric burden is increasing too quickly.

We expect the in-situ surface atmospheric measurements to be more sensitive to the methane emissions, whereas the atmospheric column measurements integrate the effects of emissions, chemistry and atmospheric transport. The large amplitudes seen in the annual cycles of the in-situ surface atmospheric observations (Fig. 4), especially at the high NH latitude sites, are less apparent in the modelled atmospheric columns, possibly because of the limited number of SCIAMACHY observations at these latitudes and the model outputs were only sampled if there was a valid SCIAMACHY measurement. Figure 10 and Fig. 20 in the Supplement show comparisons of the observed SCIAMACHY and modelled time series and annual cycles for the constrained and unconstrained HadGEM2 model outputs, respectively. The amplitudes of the annual cycles appear larger in the unconstrained model outputs, especially the FUNG and TRANSCOM-FUNG runs, as these effectively have larger contributions from the model levels close to the surface and these levels are more affected by the surface emissions. Generally, we see similar trends and patterns between the constrained and unconstrained model outputs, suggesting that the different emission distributions largely account for the differences in the modelled atmospheric concentrations and columns between the model runs.

Compared to the SCIAMACHY observations, the constrained model run using the Fung-derived inventory appears better in terms of the annual cycle (Fig. 10), although its annual cycle in the boreal zone is larger. The JULES-based inventories on the other hand exhibit a smaller seasonal cycle (for the JULES inventory, this is because the wetland emissions are dominated by those from the Amazon and these are modelled to have little seasonality). The high concentrations modelled over the Ganges in India in all ~~three~~ four runs indicates that the magnitude of the non-wetland emissions in this region and their monthly variability may be too large (see Fig. 9) or that the boundary layer mixing in this region, close to the Himalayan mountains, is not well represented. There is evidence in the comparison with the inverse emission estimates that part of the explanation is that the emissions are overstated in this region (and these are largely CH_4 emissions from non–wetland sources). Further support for this interpretation is provided by (Patra et al., 2009), who found that the methane emission from India were lower by 13 $Tg\,CH_4\,yr^{-1}$ in their optimised emission scenario.

3.2 ~~Comparison with other wetland estimates~~

3.1.1 Comparison with other wetland estimates

Wetlands are generally accepted as being the largest, but least well quantified, single natural source of CH_4 (Denman et al., 2007; USEPA, 2010). In this work, the mean annual global emission between 1999 and 2007 was effectively fixed at 181 $Tg\,CH_4\,yr^{-1}$; the value used by O'Connor et al. (2014) in earlier HadGEM2 model runs. The total is however consistent with other recent estimates. Bousquet et al. (2011) derived a value of 165 $CH_4\,yr^{-1}$ from their inverse modelling study. Melton et al. (2013) reported an ensemble mean of the annual global emissions of 190 $Tg\,CH_4\,yr^{-1}$ with a spread of $\pm 40\,\%$ from the wetland models participating in the WETCHIMP wetland model intercomparison. Fraser et al. (2013) obtained wetland emissions between 184 and 195 $Tg\,CH_4\,yr^{-1}$ from inversions of surface and/or GOSAT measurements between 2009 and 2010. In a synthesis paper, Kirschke et al. (2013) estimated methane emissions from natural wetlands for the period from 2000–2009 to be in the range from 142 to 208 $Tg\,CH_4\,yr^{-1}$ with a mean value of 175 $Tg\,CH_4\,yr^{-1}$ using inverse modelling methods and in the range from 177 to 284 $Tg\,CH_4\,yr^{-1}$ with a mean value of 217 $Tg\,CH_4\,yr^{-1}$ from process-based approaches (see Table 2).

As the long-term mean annual emissions were fixed, the emphasis here has been on the spatial patterns and intra and inter-annual variability. As shown in Fig. 2 in the Supplement, the JULES wetland emissions are concentrated in the tropics and especially the Amazon. The JULES-GIEMS still has more emissions in the tropics but these are located more in India and SE Asia (and a smaller increase in the Boreal emissions). In Table 2, we compare wetland emission estimates from JULES and JULES-GIEMS with other recent global and regional literature estimates. Petrescu et al. (2010) found a wide variation in methane emission fluxes from wetlands and floodplains above 30° N for the years 2001 to 2006 for different estimates of wetland extents (37.7 to 157.3 $Tg\,CH_4\,yr^{-1}$). The corresponding JULES-GIEMS estimate for the same period is 35.1 $Tg\,CH_4\,yr^{-1}$, although we believe that this is an underestimate from the comparison against the atmospheric measurements. For the West Siberian Lowlands, Glagolev et al. (2011), using more measurement sites, revised the ~~mapped-based~~ mapping-based estimate given by Kim et al. (2011) to 2.93 ± 0.97 $Tg\,CH_4\,yr^{-1}$. The corresponding JULES estimates are lower, which we believe arises from the absence of peatland soils in JULES. There is better agreement for the JULES-GIEMS inventory with the estimate of Pickett-Heaps et al. (2011) for the Hudson Bay Lowlands. Bloom et al. (2010, 2012) report a 7 % rise in global wetland CH_4 emissions over 2003–2007, due to warming of mid-latitude and Arctic wetland regions. Following the introduction of a time-decay of the substrate carbon to account for the observed seasonal lag between CH_4 concentrations and the peak in the equivalent water height, used as a proxy for a wetland, Bloom et al. (2012) derive revised global CH_4 emissions for 2003–2009. Tropical emissions amount to 111.1 $Tg\,CH_4\,yr^{-1}$, of which 24 % is emitted from Amazon wetlands. As expected, the emissions in the tropics for 1999–2007 from

the JULES and JULES-GIEMS inventories are higher, at 159 $\mathrm{Tg\,CH_4\,yr^{-1}}$ (for the Tropics with the Amazon accounting for 89 $\mathrm{Tg\,CH_4\,yr^{-1}}$) and 123 $\mathrm{Tg\,CH_4\,yr^{-1}}$ (~~for the Tropics~~ with the Amazon contributing 53 $\mathrm{Tg\,CH_4\,yr^{-1}}$), respectively. We see that the JULES-GIEMS inventory is in reasonable agreement with these regional estimates. The JULES–GIEMS inventory is also in good agreement with the emission estimates obtained by Beck et al. (2013) for the Amazon Lowlands for November 2008 and May 2009. The JULES inventory again overestimates the emissions. In Fig. 12, we compare the regional emission totals given by the two JULES-based inventories with the corresponding information given in Kirschke et al. (2013) from their top–down and bottom–up approaches for the period from 2000–2009. The comparison again indicates that the wetland emissions are too high in the Amazon for the JULES emission inventory and too low at boreal and higher latitudes. The JULES-GIEMS emission estimates are an improvement in that respect.

~~One of the runs undertaken here used the same FUNG wetland emission dataset that was used in previous HadGEM2 model runs (O'Connor et al., 2014) . The dataset was prepared by aggregating the wetlands, bogs, swamps and tundra components of Fung et al. (1991) (see Sect. 2.3.1). As shown in Fig. 1 and also Table 2, this dataset has much higher emissions at mid- and higher NH latitudes and its use resulted in the large amplitudes and incorrect seasonality seen in both the comparisons against the surface and SCIAMACHY measurements at these latitudes. We now believe our use of the dataset to be incorrect. The components in the dataset represent 2 different emission scenarios with different assumptions on seasonality (Fung et al., 1991) . However, our use of this inventory in this work does provide an upper limit on the wetland emissions at mid- and higher-NH latitudes.~~

3.2 ~~Comparison with inverse emission estimates~~

3.1.1 Comparison with inverse emission estimates

In Fig. 11, we compare the anomalies in the deseasonalised global and wetland methane emissions used in the ~~3~~ HadGEM2 runs and from two inverse flux estimates derived by Bousquet et al. (2011) from surface atmospheric methane measurements, specifically, using prior wetland emission estimates based on Fung et al. (1991) and Kaplan (as described in Bergamaschi et al., 2007). The FUNG dataset as used here shows no change in the anomaly of the wetland emissions as a single annual dataset is used for all years; this is also the case for other methane sources, apart from biomass burning. Any anomalies in the emissions therefore largely result from biomass burning. The variability shown in the JULES model run is largely from the biomass burning – the wetlands show a ~~-~~steady increase. On the other hand, there is more interannual variability in the model run using the JULES-GIEMS wetland emission inventory. The inventories used here confirm other studies that link the 1997/1998 and the 2002/2003 positive growth anomalies in surface atmospheric methane concentrations to biomass burning (see Introduction, Dlugokencky et al., 2001; Simmonds et al., 2005). There is some ~~sugestion~~ suggestion from the JULES-GIEMS runs that wetland emissions contributed to the 2002/2003 anomaly (see Fig. 11).

The JULES inventory shows an upward trend over time while there is more interannual variability in the JULES emission dataset driven with the EO inundation product (see Fig. 1). We compare the annual methane emission totals derived from the JULES-based estimates used here with two optimised inverse estimates of Bousquet et al. (2011)~~, which use wetland methane emission priors based on Fung et al. (1991) and Kaplan (Bergamaschi et al., 2007)~~. The mean (minimum–maximum) annual emissions between 1999 and 2007 are: JULES, 181(178–184) $\mathrm{Tg\,CH_4\,yr^{-1}}$; JULES-GIEMS, 181(165–192) $\mathrm{Tg\,CH_4\,yr^{-1}}$; Bousquet–Fung, 161(143–180) $\mathrm{Tg\,CH_4\,yr^{-1}}$ and Bousquet–Kaplan, 174(156–198) $\mathrm{Tg\,CH_4\,yr^{-1}}$. There is some agreement between the JULES-GIEMS and the inverse Bousquet–Kaplan emission inventories but also differences in the annual emission trends.

Figure 13 shows maps of the global annual emissions for the year 2000 for the inverse emission inventory estimates derived by Bousquet et al. (2011) using the wetland emission prior based on Fung for all methane sources and for wetlands. The figure also includes difference maps between the JULES-GIEMS emission estimates and the inverse emission inventory estimates derived by Bousquet et al. (2011) using emission priors based on the Fung (panels b and e) and Kaplan (panels c and f) wetland datasets. There is some agreement, which is not surprising, as similar datasets were used but that there are also differences, most noticeably in the wetlands. The JULES-GIEMS inventory has some similarities with the inverse inventory using the Kaplan wetland dataset (see material and figures in Sect. 1.3 of the Supplement. The monthly GIEMS dataset of Prigent et al. (2012) has been used in this work as it provides a ~~-~~long-term global dataset derived using a ~~-~~consistent methodology. As part of the wetland model intercomparison, Melton et al. (2013) noted that there were significant differences between this dataset and the wetland maps derived by Kaplan (as described in Bergamaschi et al., 2007). The inundation product showed more wetlands in Europe and the Canadian Arctic but less in the Hudson Bay Lowlands. Melton et al. (2013) identified a number of reasons for these differences: (i) classification of water bodies and wetlands; (ii) distinguishing agricultural (i.e., man-made) and natural wetlands; (iii) the ability of the inundation product to resolve saturated areas with high water tables close to the surface. Many of these differences can be seen in the difference maps.

4 Conclusions

In this paper, we have evaluated wetland emission estimates derived using the UK community land surface model (JULES, the Joint UK Land Earth Simulator) against atmospheric observations of methane, including, for the first time, total methane columns derived from the SCIAMACHY instrument on board the ENVISAT satellite. The modelled atmospheric methane columns were biased low (by 50 ppb) compared to those derived from the SCIAMACHY instrument, a consequence of the faster fall-off in the modelled methane concentrations with altitude than that observed. Constraining the modelled concentrations above 300 hPa with vertically-resolved methane data from the HALOE-ACE assimilated TOMCAT output resulted in a significantly better agreement with the SCIAMACHY observations. The model performed significantly better against measurements of surface atmospheric methane concentrations.

The wetland emission totals used in this work were consistent with other recently-published estimates, although there remains considerable differences between wetlands models as highlighted in the recent WETCHIMP model intercomparison study (Melton et al., 2013). While progress has been made, the JULES methane emission parameterisation overestimates the methane emissions in the tropics and underestimates them at mid- and higher-NH latitudes. The use of the GIEMS product to constrain JULES-derived wetland fraction improved the ~~description~~ representation of the wetland emissions in JULES and gave a good description of the seasonality observed at surface sites influenced by wetlands, especially at high latitudes. We found that the annual cycles observed in the SCIAMACHY measurements and at many of the surface sites influenced by non-wetland sources could not be reproduced in these HadGEM2 runs. This suggests that the emissions over certain regions (e.g., India and China) are possibly too high and/or the monthly emission patterns for specific sectors are incorrect.

The comparisons presented in this paper have identified areas for improvements in aspects of two components ~~of the HadGEM2 Earth System model~~ in the HadGEM family of models – the land surface and atmospheric chemistry modules. Current and future work will look to improve (a) the description of wetlands and the associated emissions of methane in JULES through the inclusion of an organic soil type related more closely to peatlands, and (b) ~~the representation of~~ on understanding and addressing the cause(s) of the faster fall-off, with potentially a particular emphasis on the model's stratospheric transport timescale. The inclusion of whole-domain methane chemistry in UKCA by implementing a ~~-~~combined troposphere-stratosphere chemistry scheme (Telford et al., 2014) may help in this regard. The EO datasets used here (and to be extended in the future) are essential for the future evaluations of JULES, UKCA and the HadGEM family of models.

The Supplement related to this article is available online at doi:10.5194/acp-0-1-2014-supplement.

Acknowledgements. This work was supported from a number of sources: (a) the European Space Agency through its Support to Science Element initiative (ALANIS Methane), Climate Change Initiative on Greenhouse Gases (GHG-CCI) and CARBONGASES; (b) the Centre for Ecology and Hydrology's Science Budget Programme; (c) the UK National Centre for Earth Observation; and (d) the Joint DECC/Defra Met Office Hadley Centre Climate Programme (GA01101). We gratefully acknowledge the support of these funding bodies.

We are grateful to N. Viovy and P. Ciais for providing the CRUNCEP meteorological dataset used to drive the JULES model. We are also grateful to P. Bousquet for providing the inverse emission estimates. GDH acknowledges the assistance provided by L. Abraham from the UKCA team at the University of Cambridge with the HadGEM model and ancillary datasets.

We acknowledge the use of the MONSooN supercomputer facility for the HadGEM2 runs reported here. The MONSooN system is a collaborative facility supplied under the Joint Weather and Climate Research Programme, which is a strategic partnership between the Met Office and the Natural Environment Research Council.

References

Beck, V., Gerbig, C., Koch, T., Bela, M. M., Longo, K. M., Freitas, S. R., Kaplan, J. O., Prigent, C., Bergamaschi, P. and Heimann, M.: WRF-Chem simulations in the Amazon region during wet and dry season transitions: evaluation of methane models and wetland inundation maps, Atmos. Chem. Phys., 13, 7961–7982, doi:10.5194/acp-13-7961-2013, 2013.

Beer, R.: TES on the aura mission: scientific objectives, measurements, and analysis overview, IEEE T. Geosci. Remote, 44, 1102–1105, doi:10.1109/TGRS.2005.863716, 2006.

Bergamaschi, P., Frankenberg, C., Meirink, J. F., Krol, M., Dentener, F., Wagner, T., Platt, U., Kaplan, J. O., Körner, S., Heimann, M., Dlugokencky, E. J., and Goede, A.: Satellite chartography of atmospheric methane from SCIAMACHY on board ENVISAT: 2. Evaluation based on inverse model simulations, J. Geophys. Res.-Atmos., 112, D02304, doi:10.1029/2006JD007268, 2007.

Bergamaschi, P., Houweling, S., Segers, A., Krol, M., Frankenberg, C., Scheepmaker, R. A., Dlugokencky, E., Wofsy, S. C., Kort, E. A., Sweeney, C., Schuck, T., Brenninkmeijer, C., Chen, H., Beck, V., and Gerbig, C.: Atmospheric CH4 in the first decade of the 21st century: inverse modeling analysis using SCIAMACHY satellite retrievals and NOAA surface measurements, J. Geophys. Res.-Atmos., 118, 7350–7369, doi:10.1002/jgrd.50480, 2013.

Bernath, P. F., McElroy, C. T., Abrams, M. C., Boone, C. D., Butler, M., Camy-Peyret, C., Carleer, M., Clerbaux, C., Coheur, P.-F., Colin, R., DeCola, P., DeMazière, M., Drummond, J. R., Dufour, D., Evans, W. F. J., Fast, H., Fussen, D., Gilbert, K., Jennings, D. E., Llewellyn, E. J., Lowe, R. P., Mahieu, E., Mc-

Connell, J. C., McHugh, M., McLeod, S. D., Michaud, R., Midwinter, C., Nassar, R., Nichitiu, F., Nowlan, C., Rinsland, C. P., Rochon, Y. J., Rowlands, N., Semeniuk, K., Simon, P., Skelton, R., Sloan, J. J., Soucy, M.-A., Strong, K., Tremblay, P., Turnbull, D., Walker, K. A., Walkty, I., Wardle, D. A., Wehrle, V., Zander, R., and Zou, J.: Atmospheric Chemistry Experiment (ACE): mission overview, Geophys. Res. Lett., 32, L15S01, doi:10.1029/2005GL022386, 2005.

Best, M. J., Pryor, M., Clark, D. B., Rooney, G. G., Essery, R. L. H., Ménard, C. B., Edwards, J. M., Hendry, M. A., Porson, A., Gedney, N., Mercado, L. M., Sitch, S., Blyth, E., Boucher, O., Cox, P. M., Grimmond, C. S. B., and Harding, R. J.: The Joint UK Land Environment Simulator (JULES), model description – Part 1: Energy and water fluxes, Geosci. Model Dev., 4, 677–699, doi:10.5194/gmd-4-677-2011, 2011.

Blake, D. R. and Rowland, F. S.: Continuing worldwide increase in tropospheric methane, 1978 to 1987, Science, 239, 1129–1131, doi:10.1126/science.239.4844.1129, 1988.

Bloom, A. A., Palmer, P. I., Fraser, A., Reay, D. S., and Frankenberg, C.: Large-scale controls of methanogenesis inferred from methane and gravity spaceborne data, Science, 327, 322–325, doi:10.1126/science.1175176, 2010.

Bloom, A. A., Palmer, P. I., Fraser, A., and Reay, D. S.: Seasonal variability of tropical wetland CH_4 emissions: the role of the methanogen-available carbon pool, Biogeosciences, 9, 2821–2830, doi:10.5194/bg-9-2821-2012, 2012.

Blunden, J. and Arndt, D. S.: State of the Climate in 2012, B. Am. Meteorol. Soc., 94, S1–S258, doi:10.1175/2013BAMSStateoftheClimate.1, 2013.

Bousquet, P., Ciais, P., Miller, J. B., Dlugokencky, E. J., Hauglustaine, D. A., Prigent, C., Van der Werf, G. R., Peylin, P., Brunke, E.-G., Carouge, C., Langenfelds, R. L., Lathiere, J., Papa, F., Ramonet, M., Schmidt, M., Steele, L. P., Tyler, S. C., and White, J.: Contribution of anthropogenic and natural sources to atmospheric methane variability, Nature, 443, 439–443, doi:10.1038/nature05132, 2006.

Bousquet, P., Ringeval, B., Pison, I., Dlugokencky, E. J., Brunke, E.-G., Carouge, C., Chevallier, F., Fortems-Cheiney, A., Frankenberg, C., Hauglustaine, D. A., Krummel, P. B., Langenfelds, R. L., Ramonet, M., Schmidt, M., Steele, L. P., Szopa, S., Yver, C., Viovy, N., and Ciais, P.: Source attribution of the changes in atmospheric methane for 2006–2008, Atmos. Chem. Phys., 11, 3689–3700, doi:10.5194/acp-11-3689-2011, 2011.

Bowerman, N. H. A., Frame, D. J., Huntingford, C., Lowe, J. A., Smith, S. M., and Allen, M. R.: The role of short-lived climate pollutants in meeting temperature goals, Nature Climate Change, 3, 1021–1024, doi:10.1038/nclimate2034, 2013.

Breider, T. J., Chipperfield, M. P., Richards, N. A. D., Carslaw, K. S., Mann, G. W., and Spracklen, D. V.: Impact of BrO on dimethylsulfide in the remote marine boundary layer, Geophys. Res. Lett., 37, L02807, doi:10.1029/2009GL040868, 2010.

Buchwitz, M., de Beek, R., Burrows, J. P., Bovensmann, H., Warneke, T., Notholt, J., Meirink, J. F., Goede, A. P. H., Bergamaschi, P., Körner, S., Heimann, M., and Schulz, A.: Atmospheric methane and carbon dioxide from SCIAMACHY satellite data: initial comparison with chemistry and transport models, Atmos. Chem. Phys., 5, 941–962, doi:10.5194/acp-5-941-2005, 2005.

Buchwitz, M., Reuter, M., Schneising, O., Boesch, H., Guerlet, S., Dils, B., Aben, I., Armante, R., Bergamaschi, P., Blumenstock, T., Bovensmann, H., Brunner, D., Buchmann, B., Burrows, J., Butz, A., Chédin, A., Chevallier, F., Crevoisier, C., Deutscher, N., Frankenberg, C., Hase, F., Hasekamp, O., Heymann, J., Kaminski, T., Laeng, A., Lichtenberg, G., Mazière, M. D., Noël, S., Notholt, J., Orphal, J., Popp, C., Parker, R., Scholze, M., Sussmann, R., Stiller, G., Warneke, T., Zehner, C., Bril, A., Crisp, D., Griffith, D., Kuze, A., O'Dell, C., Oshchepkov, S., Sherlock, V., Suto, H., Wennberg, P., Wunch, D., Yokota, T., and Yoshida, Y.: The Greenhouse Gas Climate Change Initiative (GHG-CCI): comparison and quality assessment of near-surface-sensitive satellite-derived CO_2 and CH_4 global data sets, Remote Sens. Environ., in press, doi:10.1016/j.rse.2013.04.024, 2013.

Chipperfield, M. P.: New version of the TOMCAT/SLIMCAT offline chemical transport model: Intercomparison of stratospheric tracer experiments, Q. J. Roy. Meteor. Soc., 132, 1179–1203, doi:10.1256/qj.05.51, 2006.

Chipperfield, M. P., Khattatov, B. V., and Lary, D. J.: Sequential assimilation of stratospheric chemical observations in a three-dimensional model, J. Geophys. Res.-Atmos., 107, ACH 8–1–ACH 8–14, doi:10.1029/2002JD002110, 2002.

Clark, D. B., Mercado, L. M., Sitch, S., Jones, C. D., Gedney, N., Best, M. J., Pryor, M., Rooney, G. G., Essery, R. L. H., Blyth, E., Boucher, O., Harding, R. J., Huntingford, C., and Cox, P. M.: The Joint UK Land Environment Simulator (JULES), model description – Part 2: Carbon fluxes and vegetation dynamics, Geosci. Model Dev., 4, 701–722, doi:10.5194/gmd-4-701-2011, 2011.

Collins, W. J., Bellouin, N., Doutriaux-Boucher, M., Gedney, N., Halloran, P., Hinton, T., Hughes, J., Jones, C. D., Joshi, M., Liddicoat, S., Martin, G., O'Connor, F., Rae, J., Senior, C., Sitch, S., Totterdell, I., Wiltshire, A., and Woodward, S.: Development and evaluation of an Earth-System model – HadGEM2, Geosci. Model Dev., 4, 1051–1075, doi:10.5194/gmd-4-1051-2011, 2011.

De Mazière, M., Vigouroux, C., Bernath, P. F., Baron, P., Blumenstock, T., Boone, C., Brogniez, C., Catoire, V., Coffey, M., Duchatelet, P., Griffith, D., Hannigan, J., Kasai, Y., Kramer, I., Jones, N., Mahieu, E., Manney, G. L., Piccolo, C., Randall, C., Robert, C., Senten, C., Strong, K., Taylor, J., Tétard, C., Walker, K. A., and Wood, S.: Validation of ACE-FTS v2.2 methane profiles from the upper troposphere to the lower mesosphere, Atmos. Chem. Phys., 8, 2421–2435, doi:10.5194/acp-8-2421-2008, 2008.

Denman, K., Brasseur, G., Chidthaisong, A., Ciais, P., Cox, P., Dickinson, R., Hauglustaine, D., Heinze, C., Holland, E., Jacob, D., Lohmann, U., Ramachandran, S., da Silva Dias, P., Wofsy, S., and Zhang, X.: Couplings between changes in the climate system and biogeochemistry, in: Climate Change 2007: The Physical Science Basis, Contribution of Working Group I to the Fourth Assessment Report of the Intergovernmental Panel on Climate Change, edited by: Solomon, S., Qin, D., Manning, M., Chen, Z., Marquis, M., Averyt, K. B., Tignor, M., and Miller, H. L., Cambridge University Press, Cambridge, UK and New York, NY, USA, 2007.

Dennis, R., Fox, T., Fuentes, M., Gilliland, A., Hanna, S., Hogrefe, C., Irwin, J., Rao, S., Scheffe, R., Schere, K., Steyn, D., and Venkatram, A.: A framework for evaluating regional–scale

numerical photochemical modeling systems, Environ. Fluid Mech., 10, 471–489, doi:10.1007/s10652-009-9163-2, 2010.

Dils, B. and Buchwitz, M., Reuter, M., Schneising, O., Boesch, H., Parker, R., Guerlet, S., Aben, I., Blumenstock, T., Burrows, J. P., Butz, A., Deutscher, N. M., Frankenberg, C., Hase, F., Hasekamp, O. P., Heymann, J., De Mazière, M., Notholt, J., Sussmann, R., Warneke, T., Griffith, D., Sherlock, V., Wunch, D.: The Greenhouse Gas Climate Change Initiative (GHG-CCI): comparative validation of GHG-CCI SCIAMACHY/ENVISAT and TANSO-FTS/GOSAT CO_2 and CH_4 retrieval algorithm products with measurements from the TCCON, Atmos. Meas. Tech., 7, 1723–1744, doi:10.5194/amt-7-1723-2014, 2014.

Dlugokencky, E. J., Masaire, K. A., Lang, P. M., Tans, P. P., Steele, L. P., and Nisbet, E. G.: A dramatic decrease in the growth rate of atmospheric methane in the Northern Hemisphere during 1992, Geophys. Res. Lett., 21, 45–48, doi:10.1029/93GL03070, 1994a.

Dlugokencky, E. J., Steele, L. P., Lang, P. M., and Masarie, K. A.: The growth rate and distribution of atmospheric methane, J. Geophys. Res.-Atmos., 99, 17021–17043, doi:10.1029/94JD01245, 1994b.

Dlugokencky, E. J., Masarie, K. A., Lang, P. M., and Tans, P. P.: Continuing decline in the growth rate of the atmospheric methane burden, Nature, 393, 447–450, doi:10.1038/30934, 1998.

Dlugokencky, E. J., Walter, B. P., Masarie, K. A., Lang, P. M., and Kasischke, E. S.: Measurements of an anomalous global methane increase during 1998, Geophys. Res. Lett., 28, 499–502, doi:10.1029/2000GL012119, 2001.

Dlugokencky, E. J., Houweling, S., Bruhwiler, L., Masarie, K. A., Lang, P. M., Miller, J. B., and Tans, P. P.: Atmospheric methane levels off: temporary pause or a new steady-state?, Geophys. Res. Lett., 30, 1992, doi:10.1029/2003GL018126, 2003.

Dlugokencky, E. J., Bruhwiler, L., White, J. W. C., Emmons, L. K., Novelli, P. C., Montzka, S. A., Masarie, K. A., Lang, P. M., Crotwell, A. M., Miller, J. B., and Gatti, L. V.: Observational constraints on recent increases in the atmospheric CH_4 burden, Geophys. Res. Lett., 36, L18803, doi:10.1029/2009GL039780, 2009.

Dlugokencky, E. J., Nisbet, E. G., Fisher, R., and Lowry, D.: Global atmospheric methane: budget, changes and dangers, Philos. T. R. Soc. A, 369, 2058–2072, doi:10.1098/rsta.2010.0341, 2011.

Dlugokencky, E. J., Lang, P. M., Crotwell, A. M., and Masarie, K. A.: Atmospheric Methane Dry Air Mole Fractions from the NOAA ESRL Carbon Cycle Co-operative Global Air Sampling Network, 1983–2011, Version: 24 September 2012, ftp://aftp.cmdl.noaa.gov/data/trace_gases/ch4/flask/surface/ (last access date of updated and extended dataset: 9 May 2014), 2012.

Forster, P., Ramaswamy, V., Artaxo, P., Berntsen, T., Betts, R., Fahey, D., Haywood, J., Lean, J., Lowe, D., Myhre, G., Nganga, J., Prinn, R., Raga, G., Schulz, M., and Van Dorland, R.: Changes in atmospheric constituents and in radiative forcing, in: Climate Change 2007: The Physical Science Basis, Contribution of Working Group I to the Fourth Assessment Report of the Intergovernmental Panel on Climate Change, edited by: Solomon, S., Qin, D., Manning, M., Chen, Z., Marquis, M., Averyt, K. B., Tignor, M., and Miller, H. L., Cambridge University Press, Cambridge, UK and New York, NY, USA, 2007.

Frankenberg, C., Meirink, J. F., van Weele, M., Platt, U., and Wagner, T.: Assessing methane emissions from global space-borne observations, Science, 308, 1010–1014, doi:10.1126/science.1106644, 2005.

Frankenberg, C., Meirink, J. F., Bergamaschi, P., Goede, A. P. H., Heimann, M., Körner, S., Platt, U., van Weele, M., and Wagner, T.: Satellite chartography of atmospheric methane from SCIAMACHY on board ENVISAT: analysis of the years 2003 and 2004, J. Geophys. Res.-Atmos., 111, D07303, doi:10.1029/2005JD006235, 2006.

Frankenberg, C., Bergamaschi, P., Butz, A., Houweling, S., Meirink, J. F., Notholt, J., Petersen, A. K., Schrijver, H., Warneke, T., and Aben, I.: Tropical methane emissions: a revised view from SCIAMACHY onboard ENVISAT, Geophys. Res. Lett., 35, L15811, doi:10.1029/2008GL034300, 2008.

Fraser, A., Palmer, P. I., Feng, L., Boesch, H., Cogan, A., Parker, R., Dlugokencky, E. J., Fraser, P. J., Krummel, P. B., Langenfelds, R. L., O'Doherty, S., Prinn, R. G., Steele, L. P., van der Schoot, M., and Weiss, R. F.: Estimating regional methane surface fluxes: the relative importance of surface and GOSAT mole fraction measurements, Atmos. Chem. Phys., 13, 5697–5713, doi:10.5194/acp-13-5697-2013, 2013.

Fung, I., John, J., Lerner, J., Matthews, E., Prather, M., Steele, L. P., and Fraser, P. J.: Three-dimensional model synthesis of the global methane cycle, J. Geophys. Res.-Atmos., 96, 13033–13065, doi:10.1029/91JD01247, 1991.

Gedney, N. and Cox, P. M.: The sensitivity of global climate model simulations to the representation of soil moisture heterogeneity, J. Hydrometeorol., 4, 1265–1275, doi:10.1175/1525-7541(2003)004<1265:TSOGCM>2.0.CO;2, 2003.

Gedney, N., Cox, P. M., and Huntingford, C.: Climate feedback from wetland methane emissions, Geophys. Res. Lett., 31, L20503, doi:10.1029/2004GL020919, 2004.

Glagolev, M., Kleptsova, I., Filippov, I., Maksyutov, S., and Machida, T.: Regional methane emission from West Siberia mire landscapes, Environ. Res. Lett., 6, 045214, doi:10.1088/1748-9326/6/4/045214, 2011.

Kim, H.-S., Maksyutov, S., Glagolev, M. V., Machida, T., Patra, P. K., Sudo, K., and Inoue, G.: Evaluation of methane emissions from West Siberian wetlands based on inverse modeling, Environ. Res. Lett., 6, 035201, doi:10.1088/1748-9326/6/3/035201, 2011.

Kirschke, S., Bousquet, P., Ciais, P., Saunois, M., Canadell, J. G., Dlugokencky, E. J., Bergamaschi, P., Bergmann, D., Blake, D. R., Bruhwiler, L., Cameron-Smith, P., Castaldi, S., Chevallier, F., Feng, L., Fraser, A., Heimann, M., Hodson, E. L., Houweling, S., Josse, B., Fraser, P. J., Krummel, P. B., Lamarque, J.-F., Langenfelds, R. L., Le Quere, C., Naik, V., O'Doherty, S., Palmer, P. I., Pison, I., Plummer, D., Poulter, B., Prinn, R. G., Rigby, M., Ringeval, B., Santini, M., Schmidt, M., Shindell, D. T., Simpson, I. J., Spahni, R., Steele, L. P., Strode, S. A., Sudo, K., Szopa, S., van der Werf, G. R., Voulgarakis, A., van Weele, M., Weiss, R. F., Williams, J. E., and Zeng, G.: Three decades of global methane sources and sinks, Nat. Geosci., 6, 813–823, 2013.

Kuze, A., Suto, H., Nakajima, M., and Hamazaki, T.: Thermal and near infrared sensor for carbon observation Fourier-transform spectrometer on the Greenhouse Gases Observing Satellite for greenhouse gases monitoring, Appl. Optics, 48, 6716–6733, doi:10.1364/AO.48.006716, 2009.

Lamarque, J.-F., Bond, T. C., Eyring, V., Granier, C., Heil, A., Klimont, Z., Lee, D., Liousse, C., Mieville, A., Owen, B., Schultz, M. G., Shindell, D., Smith, S. J., Stehfest, E., Van Aardenne, J., Cooper, O. R., Kainuma, M., Mahowald, N., McConnell, J. R., Naik, V., Riahi, K., and van Vuuren, D. P.: Historical (1850–2000) gridded anthropogenic and biomass burning emissions of reactive gases and aerosols: methodology and application, Atmos. Chem. Phys., 10, 7017–7039, doi:10.5194/acp-10-7017-2010, 2010.

Meirink, J. F., Bergamaschi, P., Frankenberg, C., d'Amelio, M. T. S., Dlugokencky, E. J., Gatti, L. V., Houweling, S., Miller, J. B., Röckmann, T., Villani, M. G., and Krol, M. C.: Four-dimensional variational data assimilation for inverse modeling of atmospheric methane emissions: analysis of SCIAMACHY observations, J. Geophys. Res.-Atmos., 113, D17301, doi:10.1029/2007JD009740, 2008.

Melton, J. R., Wania, R., Hodson, E. L., Poulter, B., Ringeval, B., Spahni, R., Bohn, T., Avis, C. A., Beerling, D. J., Chen, G., Eliseev, A. V., Denisov, S. N., Hopcroft, P. O., Lettenmaier, D. P., Riley, W. J., Singarayer, J. S., Subin, Z. M., Tian, H., Zürcher, S., Brovkin, V., van Bodegom, P. M., Kleinen, T., Yu, Z. C., and Kaplan, J. O.: Present state of global wetland extent and wetland methane modelling: conclusions from a model intercomparison project (WETCHIMP), Biogeosciences, 10, 753–788, doi:10.5194/bg-10-753-2013, 2013.

Monks, S. A., Arnold, S. R., and Chipperfield, M. P.: Evidence for El Niño–Southern Oscillation (ENSO) influence on Arctic CO interannual variability through biomass burning emissions, Geophys. Res. Lett., 39, L14804, doi:10.1029/2012GL052512, 2012.

Monteil, G., Houweling, S., Dlugockenky, E. J., Maenhout, G., Vaughn, B. H., White, J. W. C., and Rockmann, T.: Interpreting methane variations in the past two decades using measurements of CH_4 mixing ratio and isotopic composition, Atmos. Chem. Phys., 11, 9141–9153, doi:10.5194/acp-11-9141-2011, 2011.

Morgenstern, O., Braesicke, P., O'Connor, F. M., Bushell, A. C., Johnson, C. E., Osprey, S. M., Pyle, J. A.: Evaluation of the new UKCA climate-composition model – Part 1: The stratosphere, Geosci. Model Dev., 2, 43–57, doi:10.5194/gmd-2-43-2009, 2009.

O'Connor, F. M., Boucher, O., Gedney, N., Jones, C. D., Folberth, G. A., Coppell, R., Friedlingstein, P., Collins, W. J., Chappellaz, J., Ridley, J., and Johnson, C. E.: Possible role of wetlands, permafrost, and methane hydrates in the methane cycle under future climate change: a review, Rev. Geophys., 48, RG4005, doi:10.1029/2010RG000326, 2010.

O'Connor, F. M., Johnson, C. E., Morgenstern, O., Abraham, N. L., Braesicke, P., Dalvi, M., Folberth, G. A., Sanderson, M. G., Telford, P. J., Voulgarakis, A., Young, P. J., Zeng, G., Collins, W. J., and Pyle, J. A.: Evaluation of the new UKCA climate-composition model – Part 2: The Troposphere, Geosci. Model Dev., 7, 41–91, doi:10.5194/gmd-7-41-2014, 2014.

Papa, F., Prigent, C., Durand, F., and Rossow, W. B.: Wetland dynamics using a suite of satellite observations: a case study of application and evaluation for the Indian Subcontinent, Geophys. Res. Lett., 33, L08401, doi:10.1029/2006GL025767, 2006a.

Papa, F., Prigent, C., Rossow, W. B., Legresy, B., and Remy, F.: Inundated wetland dynamics over boreal regions from remote sensing: the use of TopexPoseidon dualfrequency radar altimeter observations, Int. J. Remote Sens., 27, 4847–4866, doi:10.1080/01431160600675887, 2006b.

Papa, F., Prigent, C., and Rossow, W. B.: Ob' River flood inundations from satellite observations: a relationship with winter snow parameters and river runoff, J. Geophys. Res.-Atmos., 112, D18103, doi:10.1029/2007JD008451, 2007.

Papa, F., Güntner, A., Frappart, F., Prigent, C., and Rossow, W. B.: Variations of surface water extent and water storage in large river basins: a comparison of different global data sources, Geophys. Res. Lett., 35, L11401, doi:10.1029/2008GL033857, 2008a.

Papa, F., Prigent, C., and Rossow, W.: Monitoring flood and discharge variations in the large Siberian rivers from a multi-satellite technique, Surv. Geophys., 29, 297–317, doi:10.1007/s10712-008-9036-0, 2008b.

Papa, F., Prigent, C., Aires, F., Jimenez, C., Rossow, W. B., and Matthews, E.: Interannual variability of surface water extent at the global scale, 1993–2004, J. Geophys. Res.-Atmos., 115, D12111, doi:10.1029/2009JD012674, 2010.

Park, J. H., Russell, J. M., Gordley, L. L., Drayson, S. R., Benner, D. C., McInerney, J. M., Gunson, M. R., Toon, G. C., Sen, B., Blavier, J.-F., Webster, C. R., Zipf, E. C., Erdman, P., Schmidt, U., and Schiller, C.: Validation of Halogen Occultation Experiment CH_4 measurements from the UARS, J. Geophys. Res.-Atmos., 101, 10183–10203, doi:10.1029/95JD02736, 1996.

Patra, P. K., Takigawa, M., Ishijima, K., Choi, B.–C., Cunnold, D., Dlugokencky, E., Fraser, P., Gomez-Pelaez, A., Goo,T.–Y., Kim, J.–S., Krummel, P., Langenfelds, R., Meinhardt, F., Mukai, H., O'Doherty, S., Prinn, R., Simmonds,P., Steele, P., Tohjima, Y., Tsuboi, K., Uhse, K., Weiss, R., Worthy, D., Nakazawa, T.: Growth Rate, Seasonal, Synoptic, Diurnal Variations and Budget of Methane in the Lower Atmosphere, J. Met. Soc. Japan. Ser. II, 87, 635–663, doi:10.2151/jmsj.87.635, 2009.

Patra, P. K., Houweling, S., Krol, M., Bousquet, P., Belikov, D., Bergmann, D., Bian, H., Cameron-Smith, P., Chipperfield, M. P., Corbin, K., Fortems-Cheiney, A., Fraser, A., Gloor, E., Hess, P., Ito, A., Kawa, S. R., Law, R. M., Loh, Z., Maksyutov, S., Meng, L., Palmer, P. I., Prinn, R. G., Rigby, M., Saito, R., and Wilson, C.: TransCom model simulations of CH_4 and related species: linking transport, surface flux and chemical loss with CH_4 variability in the troposphere and lower stratosphere, Atmos. Chem. Phys., 11, 12813–12837, doi:10.5194/acp-11-12813-2011, 2011.

Petrescu, A. M. R., van Beek, L. P. H., van Huissteden, J., Prigent, C., Sachs, T., Corradi, C. A. R., Parmentier, F. J. W., and Dolman, A. J.: Modeling regional to global CH_4 emissions of boreal and arctic wetlands, Global Biogeochem. Cy., 24, GB4009, doi:10.1029/2009GB003610, 2010.

Pickett-Heaps, C. A., Jacob, D. J., Wecht, K. J., Kort, E. A., Wofsy, S. C., Diskin, G. S., Worthy, D. E. J., Kaplan, J. O., Bey, I., and Drevet, J.: Magnitude and seasonality of wetland methane emissions from the Hudson Bay Lowlands (Canada), Atmos. Chem. Phys., 11, 3773–3779, doi:10.5194/acp-11-3773-2011, 2011.

Pison, I., Ringeval, B., Bousquet, P., Prigent, C., and Papa, F.: Stable atmospheric methane in the 2000s: key-role of emissions from natural wetlands, Atmos. Chem. Phys., 13, 11609–11623, doi:10.5194/acp-13-11609-2013, 2013.

Portmann, F. T., Siebert, S., and Döll, P.: MIRCA2000 – global monthly irrigated and rainfed crop areas around the year 2000: a new high-resolution data set for agricultural and hydrological modeling, Global Biogeochem. Cy., 24, GB1001, doi:10.1029/2008GB003435, 2010.

Prather, M., Ehhalt, D., Dentener, F., Derwent, R., Dlugokencky, E., Holland, E., Isaksen, I., Katima, J., Kirchhoff, V., Matson, P., Midgley, P., and Wang, M.: Atmospheric Chemistry and Greenhouse Gases. In: Climate Change 2001: The Scientific Basis. Contribution of Working Group I to the Third Assessment Report of the Intergovernmental Panel on Climate Change [Houghton, J.T., Y. Ding, D.J. Griggs, M. Noguer, P. J. van der Linden, X. Dai, K. Maskell, and C. A. Johnson (eds.)]. Cambridge University Press, Cambridge, United Kingdom and New York, NY, USA, 881pp., 2001.

Prather, Michael J. and Holmes, Christopher D. and Hsu, Juno: Reactive greenhouse gas scenarios: Systematic exploration of uncertainties and the role of atmospheric chemistry, Geophys. Res. Lett., 39, L09803, doi:10.1029/2012GL051440, 2012.

Prigent, C., Aires, F., Rossow, W., and Matthews, E.: Joint characterization of vegetation by satellite observations from visible to microwave wavelengths: a sensitivity analysis, J. Geophys. Res.-Atmos., 106, 20665–20685, doi:10.1029/2000JD900801, 2001a.

Prigent, C., Matthews, E., Aires, F., and Rossow, W. B.: Remote sensing of global wetland dynamics with multiple satellite data sets, Geophys. Res. Lett., 28, 4631–4634, doi:10.1029/2001GL013263, 2001b.

Prigent, C., Papa, F., Aires, F., Rossow, W. B., and Matthews, E.: Global inundation dynamics inferred from multiple satellite observations, 1993–2000, J. Geophys. Res.-Atmos., 112, D12107, doi:10.1029/2006JD007847, 2007.

Prigent, C., Papa, F., Aires, F., Jimenez, C., Rossow, W. B., and Matthews, E.: Changes in land surface water dynamics since the 1990s and relation to population pressure, Geophys. Res. Lett., 39, L08403, doi:10.1029/2012GL051276, 2012.

Ramaswamy, V., Boucher, O., Haigh, J., Hauglustaine, D., Haywood, J., Myhre, G., Nakajima, T., Shi, G., and Solomon, S.: 2001: radiative forcing of climate change, in: Climate Change 2001: the Scientific Basis. Contribution of Working Group I to the Third Assessment Report of the Intergovernmental Panel on Climate Change, edited by: Houghton, J. T., Ding, Y., Griggs, D. J., Noguer, M., van der Linden, P. J., Dai, X., Maskell, K., and Johnson, C. A., Cambridge University Press, Cambridge, UK and New York, NY, USA, 349–416, 2001.

Rigby, M., Prinn, R. G., Fraser, P. J., Simmonds, P. G., Langenfelds, R. L., Huang, J., Cunnold, D. M., Steele, L. P., Krummel, P. B., Weiss, R. F., O'Doherty, S., Salameh, P. K., Wang, H. J., Harth, C. M., Mühle, J., and Porter, L. W.: Renewed growth of atmospheric methane, Geophys. Res. Lett., 35, L22805, doi:10.1029/2008GL036037, 2008.

Ringeval, B., de Noblet-Ducoudré, N., Ciais, P., Bousquet, P., Prigent, C., Papa, F., and Rossow, W. B.: An attempt to quantify the impact of changes in wetland extent on methane emissions on the seasonal and interannual time scales, Global Biogeochem. Cy., 24, GB2003, doi:10.1029/2008GB003354, 2010.

Russell, J. M., Gordley, L. L., Park, J. H., Drayson, S. R., Hesketh, W. D., Cicerone, R. J., Tuck, A. F., Frederick, J. E., Harries, J. E., and Crutzen, P. J.: The Halogen Occultation Experiment, J. Geophys. Res.-Atmos., 98, 10777–10797, doi:10.1029/93JD00799, 1993.

Schneising, O., Buchwitz, M., Burrows, J. P., Bovensmann, H., Bergamaschi, P., and Peters, W.: Three years of greenhouse gas column-averaged dry air mole fractions retrieved from satellite – Part 2: Methane, Atmos. Chem. Phys., 9, 443–465, doi:10.5194/acp-9-443-2009, 2009.

Schneising, O., Buchwitz, M., Reuter, M., Heymann, J., Bovensmann, H., and Burrows, J. P.: Long-term analysis of carbon dioxide and methane column-averaged mole fractions retrieved from SCIAMACHY, Atmos. Chem. Phys., 11, 2863–2880, doi:10.5194/acp-11-2863-2011, 2011.

Schneising, O., Bergamaschi, P., Bovensmann, H., Buchwitz, M., Burrows, J. P., Deutscher, N. M., Griffith, D. W. T., Heymann, J., Macatangay, R., Messerschmidt, J., Notholt, J., Rettinger, M., Reuter, M., Sussmann, R., Velazco, V. A., Warneke, T., Wennberg, P. O., and Wunch, D.: Atmospheric greenhouse gases retrieved from SCIAMACHY: comparison to ground-based FTS measurements and model results, Atmos. Chem. Phys., 12, 1527–1540, doi:10.5194/acp-12-1527-2012, 2012.

Shindell, Drew T. and Faluvegi, Greg and Koch, Dorothy M. and Schmidt, Gavin A. and Unger, Nadine and Bauer, Susanne E.: Improved Attribution of Climate Forcing to Emissions, Science, 326, 716–718, doi:10.1126/science.1174760, 2009.

Shindell, D., Kuylenstierna, J. C. I., Vignati, E., van Dingenen, R., Amann, M., Klimont, Z., Anenberg, S. C., Muller, N., Janssens-Maenhout, G., Raes, F., Schwartz, J., Faluvegi, G., Pozzoli, L., Kupiainen, K., Höglund-Isaksson, L., Emberson, L., Streets, D., Ramanathan, V., Hicks, K., Oanh, N. T. K., Milly, G., Williams, M., Demkine, V., and Fowler, D.: Simultaneously mitigating near-term climate change and improving human health and food security, Science, 335, 183–189, doi:10.1126/science.1210026, 2012.

Simmonds, P., Manning, A., Derwent, R., Ciais, P., Ramonet, M., Kazan, V., and Ryall, D.: A burning question. Can recent growth rate anomalies in the greenhouse gases be attributed to large-scale biomass burning events?, Atmos. Environ., 39, 2513–2517, doi:10.1016/j.atmosenv.2005.02.018, 2005.

Steele, L., Fraser, P., Rasmussen, R., Khalil, M., Conway, T., Crawford, A., Gammon, R., Masarie, K., and Thoning, K.: The global distribution of methane in the troposphere, J. Atmos. Chem., 5, 125–171, doi:10.1007/BF00048857, 1987.

Steele, L. P., Dlugokencky, E. J., Lang, P. M., Tans, P. P., Martin, R. C., and Masarie, K. A.: Slowing down of the global accumulation of atmospheric methane during the 1980s, Nature, 358, 313–316, doi:10.1038/358313a0, 1992.

Stevenson, D. S., Dentener, F. J., Schultz, M. G., Ellingsen, K., van Noije, T. P. C., Wild, O., Zeng, G., Amann, M., Atherton, C. S., Bell, N., Bergmann, D. J., Bey, I., Butler, T., Cofala, J., Collins, W. J., Derwent, R. G., Doherty, R. M., Drevet, J., Eskes, H. J., Fiore, A. M., Gauss, M., Hauglustaine, D. A., Horowitz, L. W., Isaksen, I. S. A., Krol, M. C., Lamarque, J.-F., Lawrence, M. G., Montanaro, V., Müller, J.-F., Pitari, G., Prather, M. J., Pyle, J. A., Rast, S., Rodriguez, J. M., Sanderson, M. G., Savage, N. H., Shindell, D. T., Strahan, S. E., Sudo, K., and Szopa, S.: Multimodel ensemble simulations of present-day and near-future tropospheric ozone, J. Geophys. Res.-Atmos., 111, D08301, doi:10.1029/2005JD006338, 2006.

Taylor, Karl E.: Summarizing multiple aspects of model performance in a single diagram, J. Geophys. Res.-Atmos., 106, 7183–7192,doi:10.1029/2000JD900719, 2001.

Telford, P. J., Braesicke, P., Morgenstern, O., and Pyle, J. A.: Technical Note: Description and assessment of a nudged version of the new dynamics Unified Model, Atmos. Chem. Phys., 8, 1701–1712, doi:10.5194/acp-8-1701-2008, 2008.

Telford, P. J., Archibald, A. T., Abraham, N. L., Braesicke, P., Dalvi, M., Hommel, R., Keeble, J. M., Johnson, C. E, O'Connor, F. M., Squire, O. J., and Pyle, J. A.: Evaluation of the UM-UKCA model configuration for Chemistry of the Stratosphere and Troposphere (CheST), Geosci. Model Dev., in preparation, 2014.

Uppala, S. M., Kållberg, P. W., Simmons, A. J., Andrae, U., Bechtold, V. D. C., Fiorino, M., Gibson, J. K., Haseler, J., Hernandez, A., Kelly, G. A., Li, X., Onogi, K., Saarinen, S., Sokka, N., Allan, R. P., Andersson, E., Arpe, K., Balmaseda, M. A., Beljaars, A. C. M., Berg, L. V. D., Bidlot, J., Bormann, N., Caires, S., Chevallier, F., Dethof, A., Dragosavac, M., Fisher, M., Fuentes, M., Hagemann, S., Hólm, E., Hoskins, B. J., Isaksen, L., Janssen, P. A. E. M., Jenne, R., Mcnally, A. P., Mahfouf, J.-F., Morcrette, J.-J., Rayner, N. A., Saunders, R. W., Simon, P., Sterl, A., Trenberth, K. E., Untch, A., Vasiljevic, D., Viterbo, P., and Woollen, J.: The ERA-40 re-analysis, Q. J. Roy. Meteor. Soc., 131, 2961–3012, doi:10.1256/qj.04.176, 2005.

USEPA: Methane and nitrous oxide emissions from natural sources, Report (EPA 430-R-10-001) of the United States Environmental Protection Agency (Office of Atmospheric Programs), available at: http://www.epa.gov/methane/pdfs/Methane-and-Nitrous-Oxide-Emissions-From-Natural-Sources.pdf (last access: 9 May 2014), 2010.

van der Werf, G. R., Randerson, J. T., Giglio, L., Collatz, G. J., Mu, M., Kasibhatla, P. S., Morton, D. C., DeFries, R. S., Jin, Y., and van Leeuwen, T. T.: Global fire emissions and the contribution of deforestation, savanna, forest, agricultural, and peat fires (1997–2009), Atmos. Chem. Phys., 10, 11707–11735, doi:10.5194/acp-10-11707-2010, 2010.

Viovy, N. and Ciais, P.: A combined dataset for ecosystem modelling, available at: http://dods.extra.cea.fr/store/p529viov/cruncep/V4_1901_2012/ (last access date of updated and extended dataset: 9 May 2014), 2009.

Worden, J., Kulawik, S., Frankenberg, C., Payne, V., Bowman, K., Cady-Peirara, K., Wecht, K., Lee, J.-E., and Noone, D.: Profiles of CH_4, HDO, H_2O, and N_2O with improved lower tropospheric vertical resolution from Aura TES radiances, Atmos. Meas. Tech., 5, 397–411, doi:10.5194/amt-5-397-2012, 2012.

Yu, S., Eder, B., Dennis, R., Chu, S.-H., and Schwartz, S. E.: New unbiased symmetric metrics for evaluation of air quality models, Atmos. Sci. Lett., 7, 26–34, doi:10.1002/asl.125, 2006.

Zahn, A., Franz, P., Bechtel, C., Grooß, J.-U., Röckmann, T.: Modelling the budget of middle atmospheric water vapour isotopes, Atmos. Chem. Phys., 6, 2073–2090, doi:10.5194/acp-6-2073-2006, 2006.

Table 1. Statistical outputs from the "global" analysis of the observed and modelled surface methane concentrations for the ~~the three~~ HadGEM2 runs (FUNG, TRANSCOM-FUNG, JULES and JULES-GIEMS) using valid co-located data from all monitoring sites.

Statistic/Metric	FUNG	TRANSCOM-FUNG	JULES	JULES-GIEMS
Number of valid data pairs	5591	5591	5591	5591
Linear regression – slope	1.33	1.09	0.79	~~1.01~~ 0.99
Linear regression – intercept	~~−563.30~~ -563.3	~~391.56~~ -130.8	~~2.33~~ 391.6	30.8
Coefficient of determination ($~~R^2~~R^2$)	0.58	0.81	0.71	~~0.81~~ 0.82
Mean of Observations (in ppb)	~~1816.40~~ 1816.4	~~1816.40~~ 1816.4	~~1816.40~~ 1816.4	1816.4
Mean of Modelled Conc. (in ppb)	~~1849.84~~ 1849.8	~~1820.86~~ 1839.1	~~1831.57~~ 1820.9	1828.9
Mean normalised bias	0.02	0.01	0.003	0.01
Number of modelled results within a factor of 2	~~1.00~~ 1.0	~~1.00~~ 1.0	~~1.00~~ 1.0	1.0
Index of Agreement	0.76	0.91	~~0.93~~ 0.91	0.94
Hit Rate	0.93	0.97	0.99	0.98
Root Mean Square Error (RMSE in ppb)	~~78.37~~ 78.4	~~32.98~~ 38.7	~~33.25~~ 33.0	30.8
Coefficient of Variation in RMSE	0.04	0.02	0.02	0.02

Table 2. Comparison of global and regional estimates of methane emissions from wetlands.

Domain	*Observational-based Estimate* [*Ref.*]	*JULES (1997-2009)*	*JULES-GIEMS (1997-2009)*	*FUNG (as used here)*	*TRANSCOM/ FUNG*
Global	(TD: 2000s) 175 (142-208) [*1*] (BU: 2000s) 217 (177-284) [*1*]	181 (178-184)	181 (167-194)	181	149
Global - WETCHIMP	190 (141-264) [*2*]				
Boreal (>30°N)	37.7-157.3 [*3*]	12.6 (12.2-13.2)	35.1 (32.8-37.4)	109	58.5
Hudson Bay Lowlands	2.3±1.3 [*4*]	0.4 (0.3-0.6)	2.2 (1.8-2.6)	10.2	3.5
West Siberian Lowlands	2.93±0.97 [*5*]	0.5 (0.4-0.6)	1.6 (1.3-2.2)	19.1	8.0
Tropics (23°S-23°N)	111.1 [*6*]	159 (157-162)	123 (112-134)	57.3	69.4
Amazon	26.6 [*6*]	89 (85-91)	53 (46-59)	17	25
Amazon (Nov. 2008)	3.3 (1.5-4.8) [*7*]	5.7	2.2	1.2	1.4
Amazon (May 2009)	3.3 (1.3-5.5) [*7*]	6.5	3.9	0.6	1.4

Notes: For the JULES and JULES-GIEMS wetland inventories, we show the mean (minimum–maximum) annual emission of the years 1999–2007. The JULES-GIEMS wetland inventory was corrected for the area of rice paddy fields, as described in Sect. 2.3.1.
References: (1) top-down (TD) and bottom-up (BU) wetland emission estimates for the 2000's taken from Kirschke et al. (2013) ; (2) taken from the WETCHIMP wetland model intercomparison of Melton et al. (2013) ; (3) range of emission estimates from Petrescu et al. (2010) using the PEATLAND-VU wetland CH_4 emission and PCR-GLOBWB hydrological models, driven with different wetland datasets; (4) Pickett-Heaps et al. (2011) , domain taken to be 96–75° W and 50–60° N; (5) version (Bc8) of the "standard model" in Glagolev et al. (2011) , domain taken to be 65–85° E and 54–70° N; (6) Bloom et al. (2012) , the wetland emissions from the Amazon are 24 % of the total wetland emissions from the Tropics; (7) Mean(range of) emission estimates for Amazon Lowlands for November 2008 and May 2009 from Beck et al. (2013) .

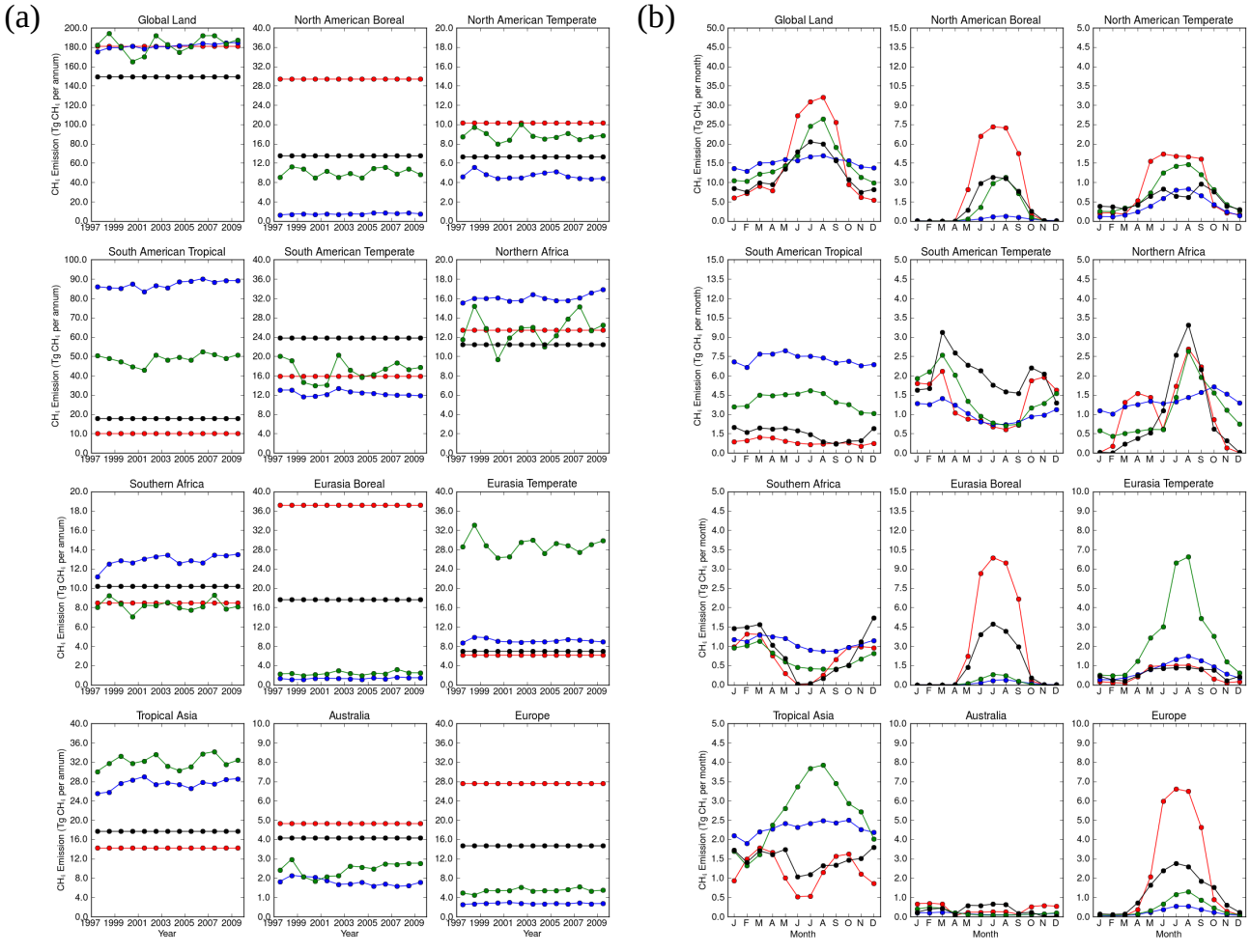

Figure 1. Time series of the area-weighted annual wetland emissions for all land surface points and for the 11 terrestrial TRANSCOM regions (left-hand panel) for the ~~Fung~~ Fung et al. (1991) wetland datasets (red: as used ~~here~~by O'Connor et al. (2014) ; black: ~~as used in the TRANSCOM-MIP~~TRANSCOM-FUNG) and for the JULES wetland estimates (blue: JULES; green: JULES-GIEMS). The right-hand panel shows the corresponding mean annual cycles.

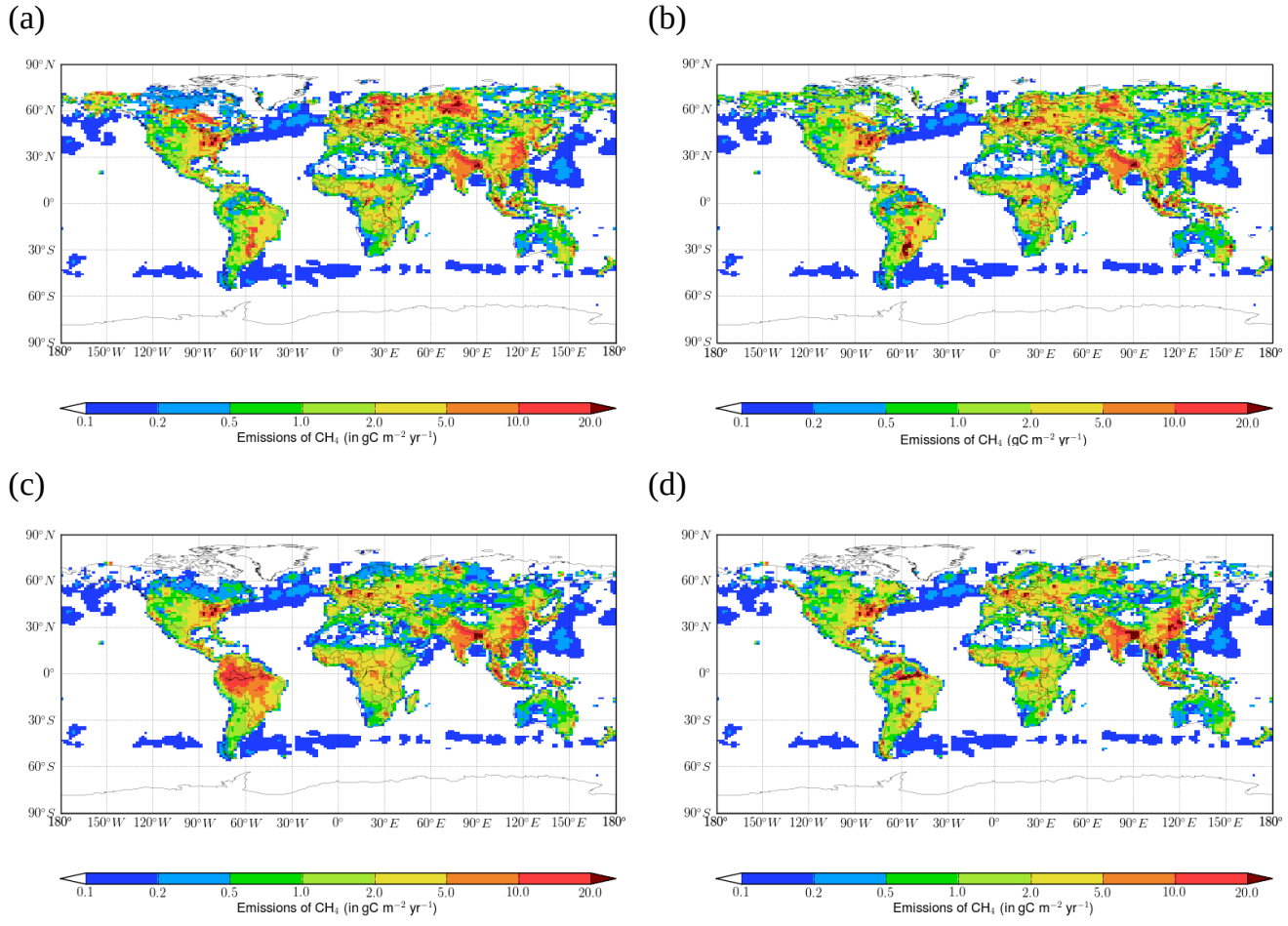

Figure 2. Maps of the global annual emissions of methane from all sources ~~in~~ for the year 2000 using wetland emissions based on ~~(a)~~ **(a, b)** the dataset of ~~Fung~~ Fung et al. (1991) (FUNG and TRANSCOM FUNG), ~~(b)~~ **(c)** an offline JULES run (JULES) and ~~(c)~~ **(d)** the same JULES run in which the modelled wetland fraction is replaced by that in the GIEMS product, corrected for rice paddyfields (JULES-GIEMS).

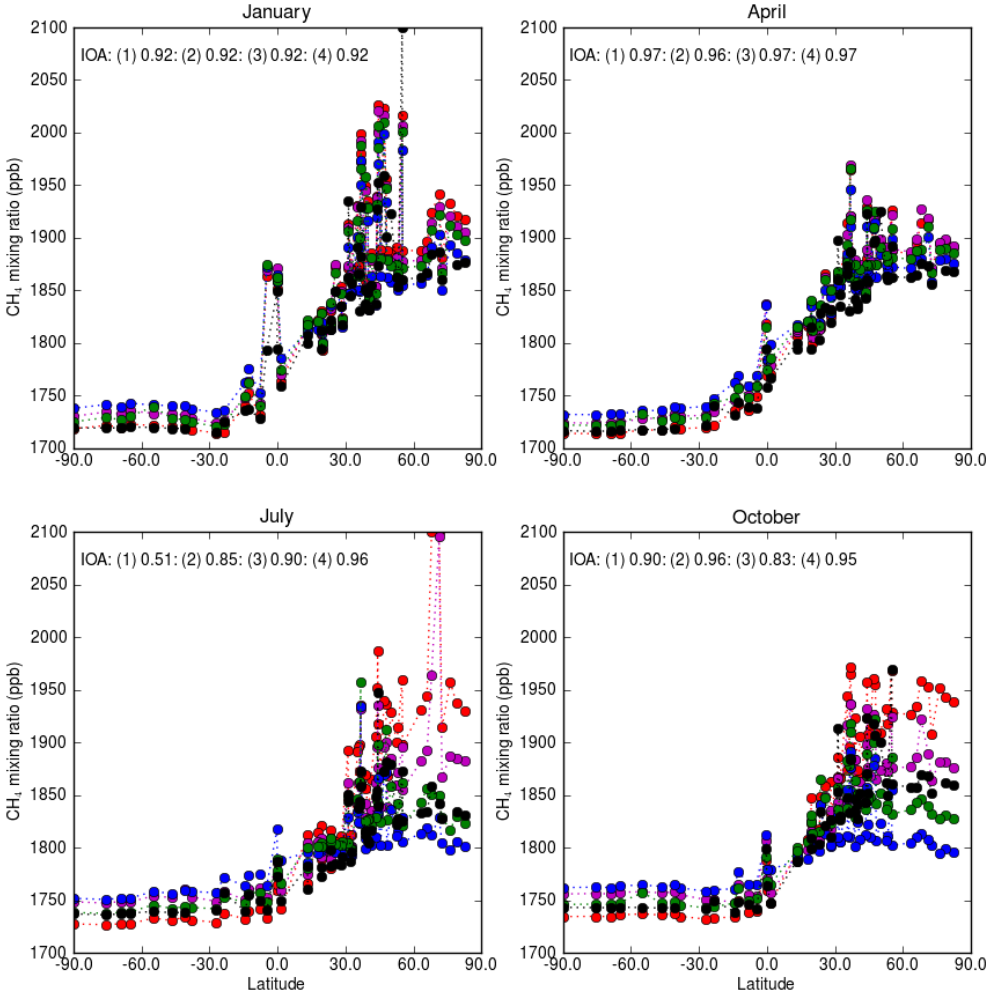

Figure 3. Comparison of the latitudinal distribution of the surface atmospheric methane mixing ratio (in ppb) as observed (black) and from the HadGEM2 runs using the following wetland emission inventories, (1) FUNG (red), (2) TRANSCOM-FUNG (magenta), (3) JULES (blue), and (~~3~~4) JULES-GIEMS (green) ~~at selected sites~~ between the years 2000 and 2010 for the months January, April, October and December. The index of agreement (IOA) is shown for each run (see Sect.3 of the Supplement for the definition of the IOA).

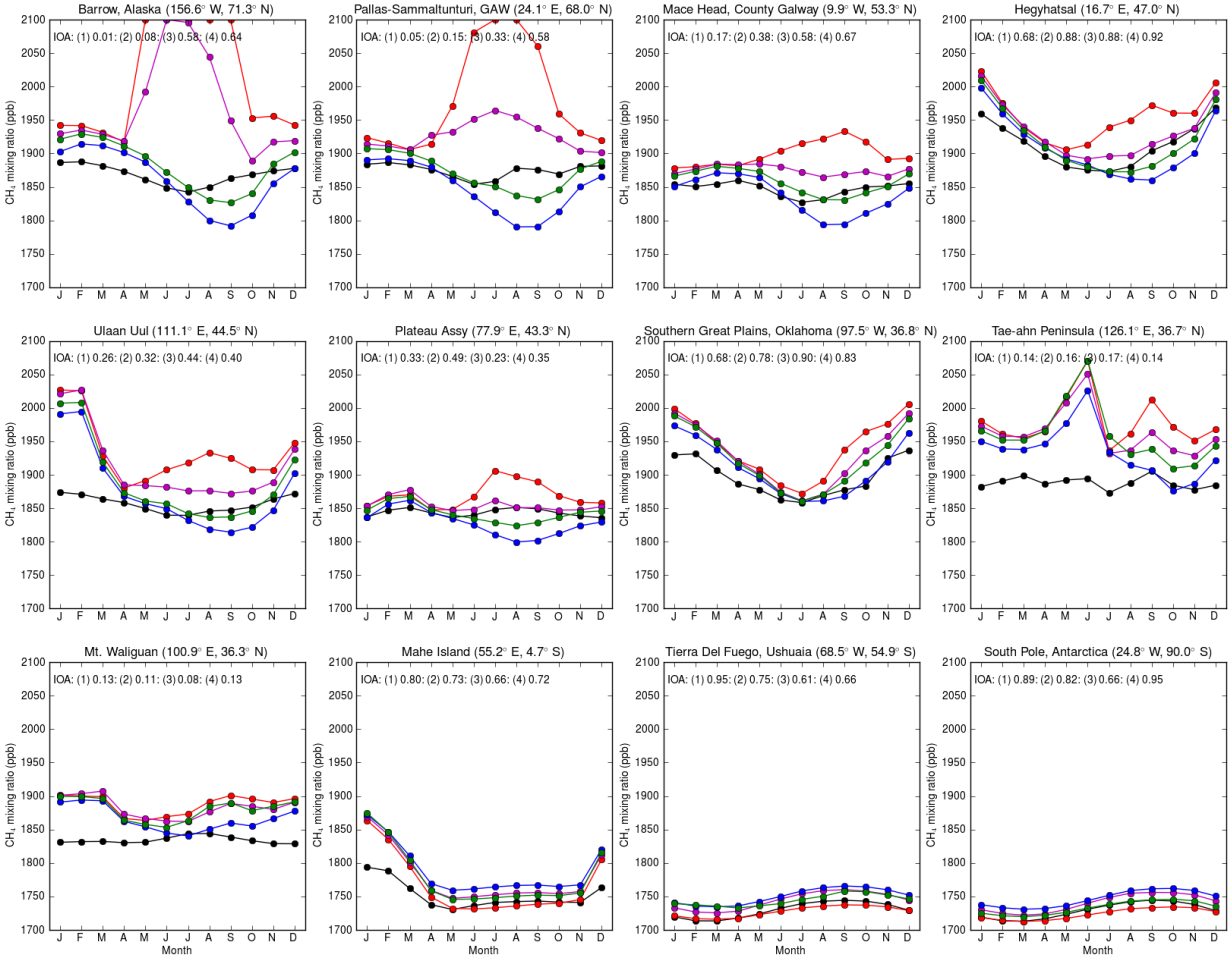

Figure 4. Comparison of the annual cycle in the surface atmospheric methane mixing ratio (in ppb) at selected sites between the years 2000 and 2010, as observed (black) and from the HadGEM2 runs using the following wetland emission inventories, (1) FUNG (red), (2) TRANSCOM-FUNG (magenta), (3) JULES (blue), and (4) JULES-GIEMS (green)~~at selected sites between 2000 and 2010.~~. The index of agreement (IOA) is shown for each run (see Sect.3 of the Supplement for the definition of the IOA).

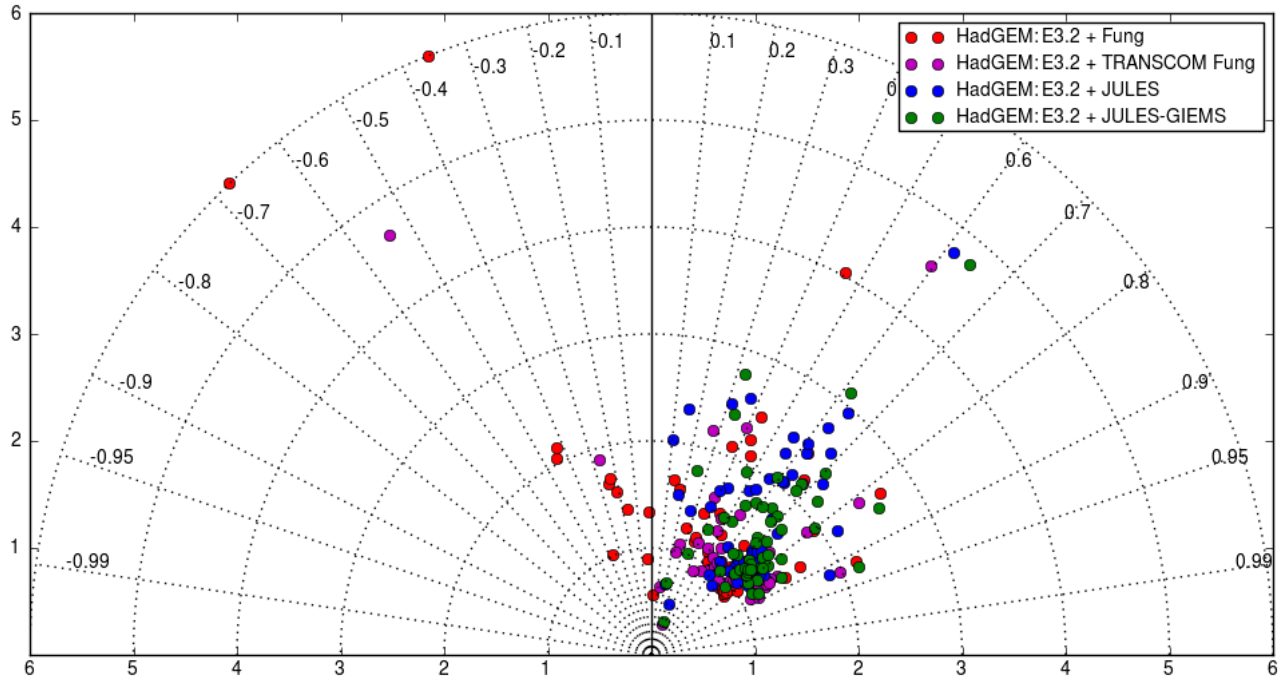

Figure 5. Taylor plot derived from the observed surface atmospheric methane mixing ratio (in ppb) and the HadGEM2 runs using the following wetland emission inventories, FUNG (red), TRANSCOM FUNG (magenta), JULES (blue) and JULES-GIEMS (green), for all co-located measurements from all sites.

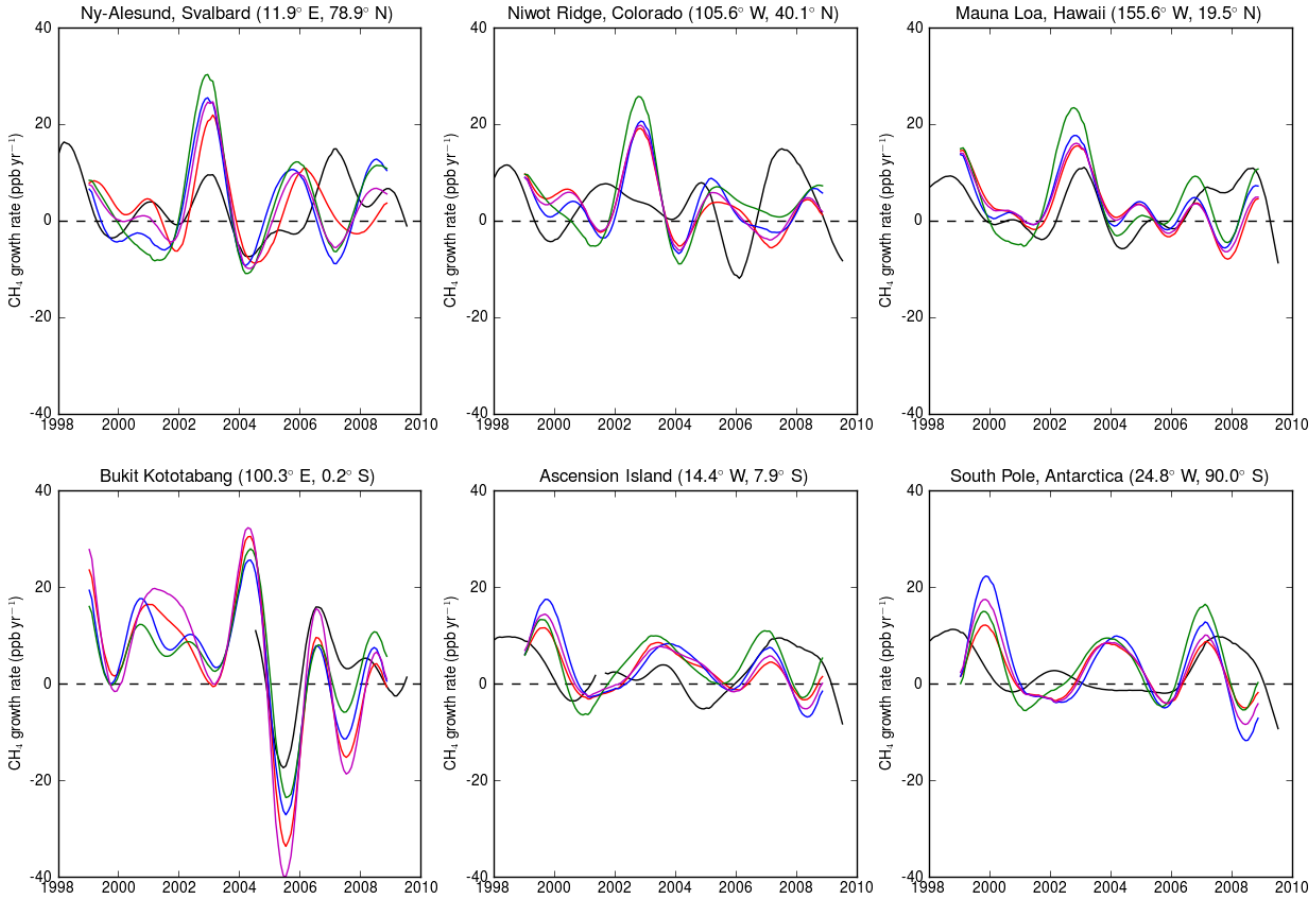

Figure 6. Comparison of the growth rates in the surface atmospheric methane mixing ratio (in ppb) as observed (black) and from and the HadGEM2 runs using the following wetland emission inventories, FUNG (red), TRANSCOM FUNG (magenta), JULES (blue) and JULES-GIEMS (green) at selected sites between the years 1998 and 2010.

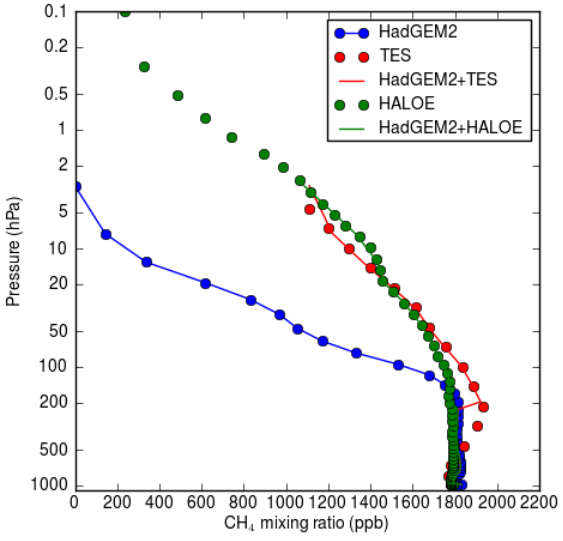

Figure 7. Comparison of the HadGEM2 modelled vertical concentration profile of CH_4 with the corresponding profiles from the Tropospheric Emission Spectrometer (red) and the HALOE-assimilated TOMCAT model for the grid point (~~1~~10° ~~E~~N, ~~1~~01° ~~N~~E) in July 2005. The red and green lines show the results from replacing the HadGEM2 modelled concentrations above 200 hPa with TES and the HALOE-assimilated TOMCAT output, respectively.

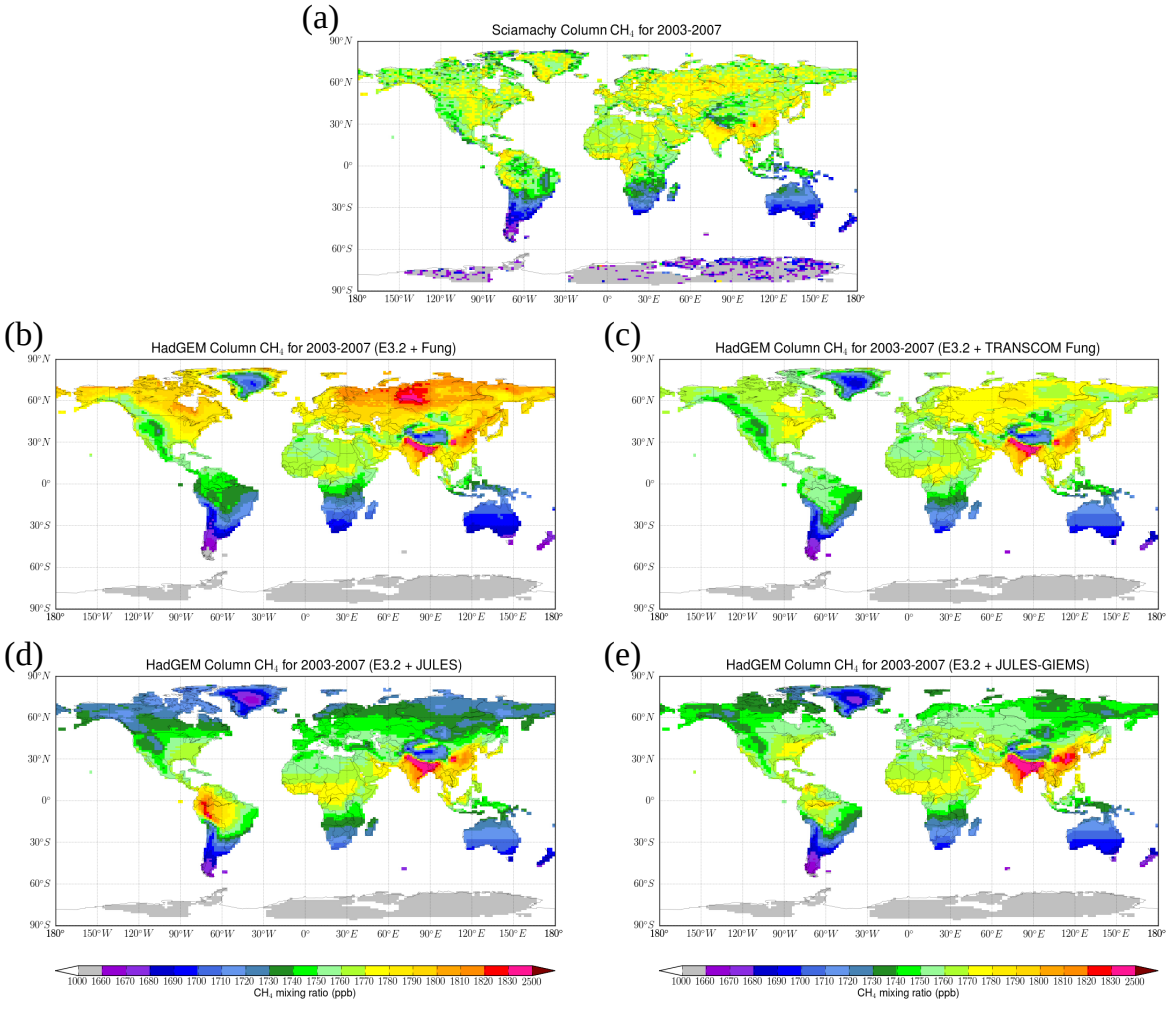

Figure 8. Contour maps of the average atmospheric column methane mixing ratio ~~for 2003–2007~~ between the years 2003 and 2007, as derived from monthly regridded SCIAMACHY data **(a)** and from the HadGEM2 runs using the FUNG **(b)**, TRANSCOM-FUNG **(c)**, the JULES ~~**(c)**~~ **(d)** and the JULES-GIEMS ~~**(d)**~~ **(e)** wetland emission inventories and the EDGAR v3.2 (E3.2) anthropogenic methane emission time series, sampled at co-located space and time points.

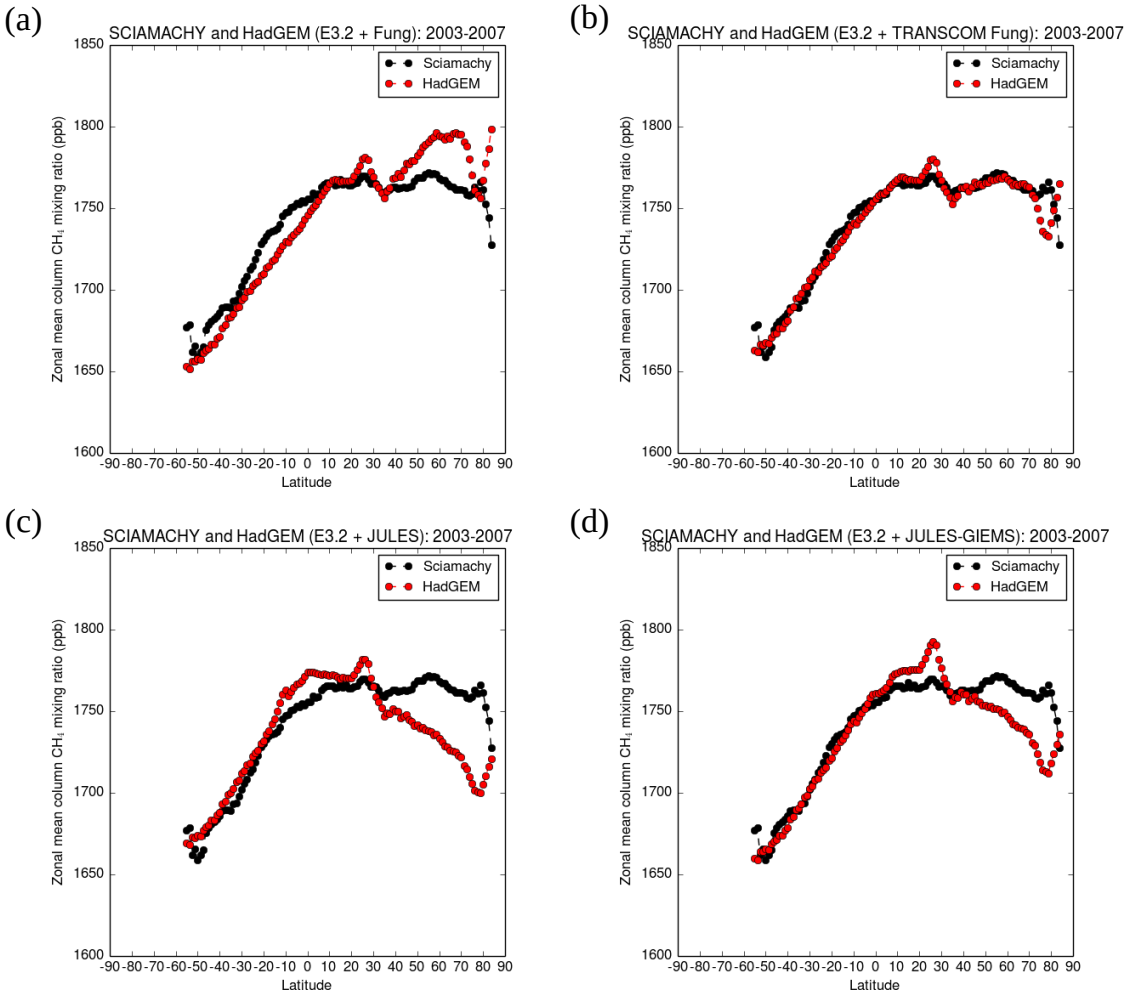

Figure 9. Comparisons of the latitudinal distribution of the average atmospheric column methane mixing ratio ~~for 2003–2007~~ between the years 2003 and 2007, as derived from monthly regridded SCIAMACHY data and from the HadGEM2 runs using the FUNG **(a)**, ~~the JULES~~ TRANSCOM-FUNG **(b)**, JULES **(c)** and the JULES-GIEMS ~~(c)~~ **(d)** wetland emission inventories and the EDGAR v3.2 (E3.2) anthropogenic methane emission time series, sampled at co-located space and time points. Note that the SCIAMACHY data between 60–90° S has been removed because of its sparsity and quality.

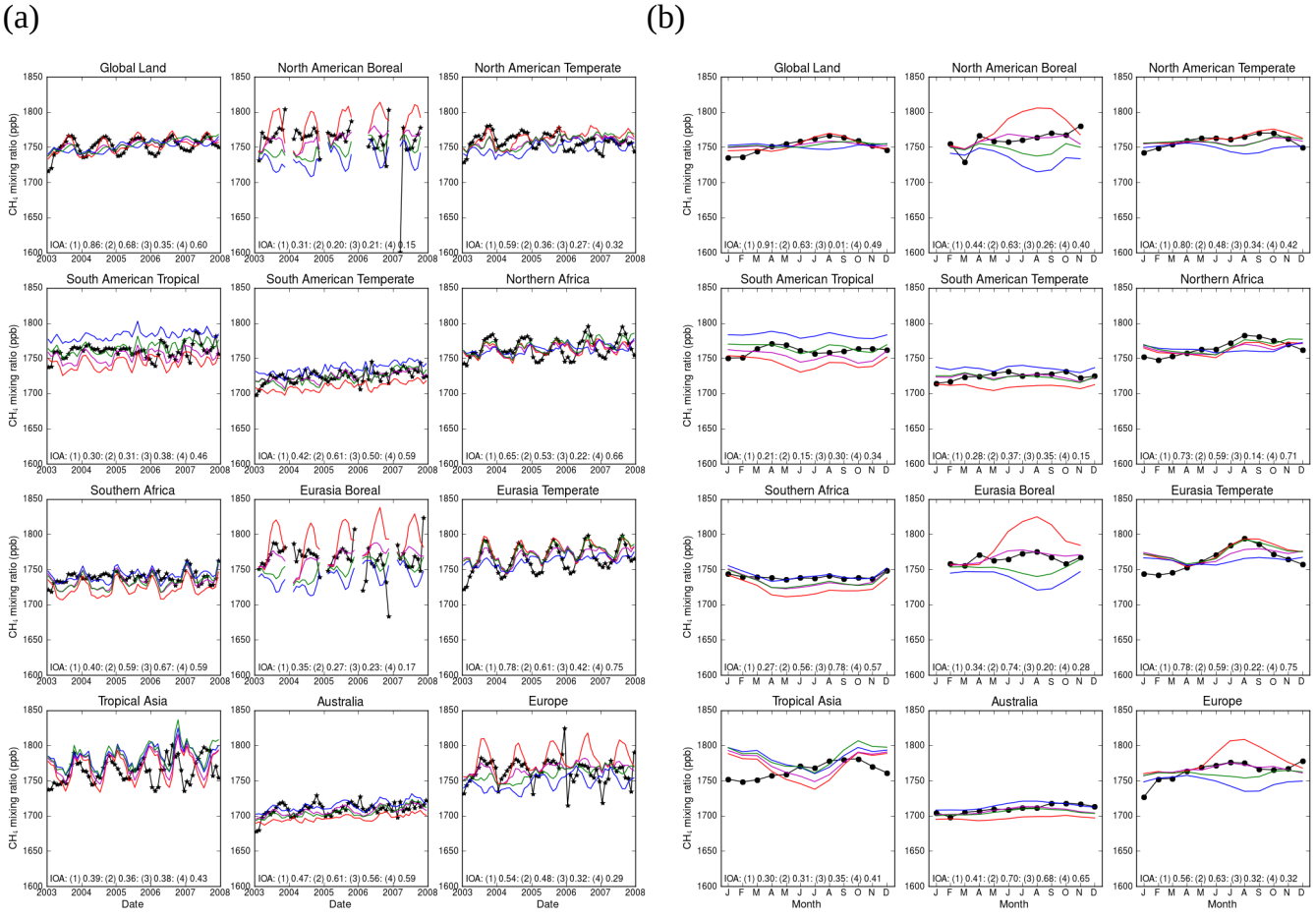

Figure 10. Time series of the area-weighted average atmospheric column methane mixing ratio from January 2003 to December 2007, as derived from monthly regridded SCIAMACHY data (v2.3) and from the ~~three~~ HadGEM2 runs using (1) the FUNG (red), (2) TRANSCOM FUNG (magenta), (3) the JULES (blue), and (~~3~~4) the JULES-GIEMS (green) wetland emission inventories and the EDGAR v3.2 (E3.2) anthropogenic methane emission time series, sampled at co-located space and time points for all land surface points and for the 11 terrestrial TRANSCOM regions **(a)**. **(b)** ~~-~~shows the corresponding annual cycles. The index of agreement (IOA) is shown for each run (see Sect.3 of the Supplement for the definition of the IOA).

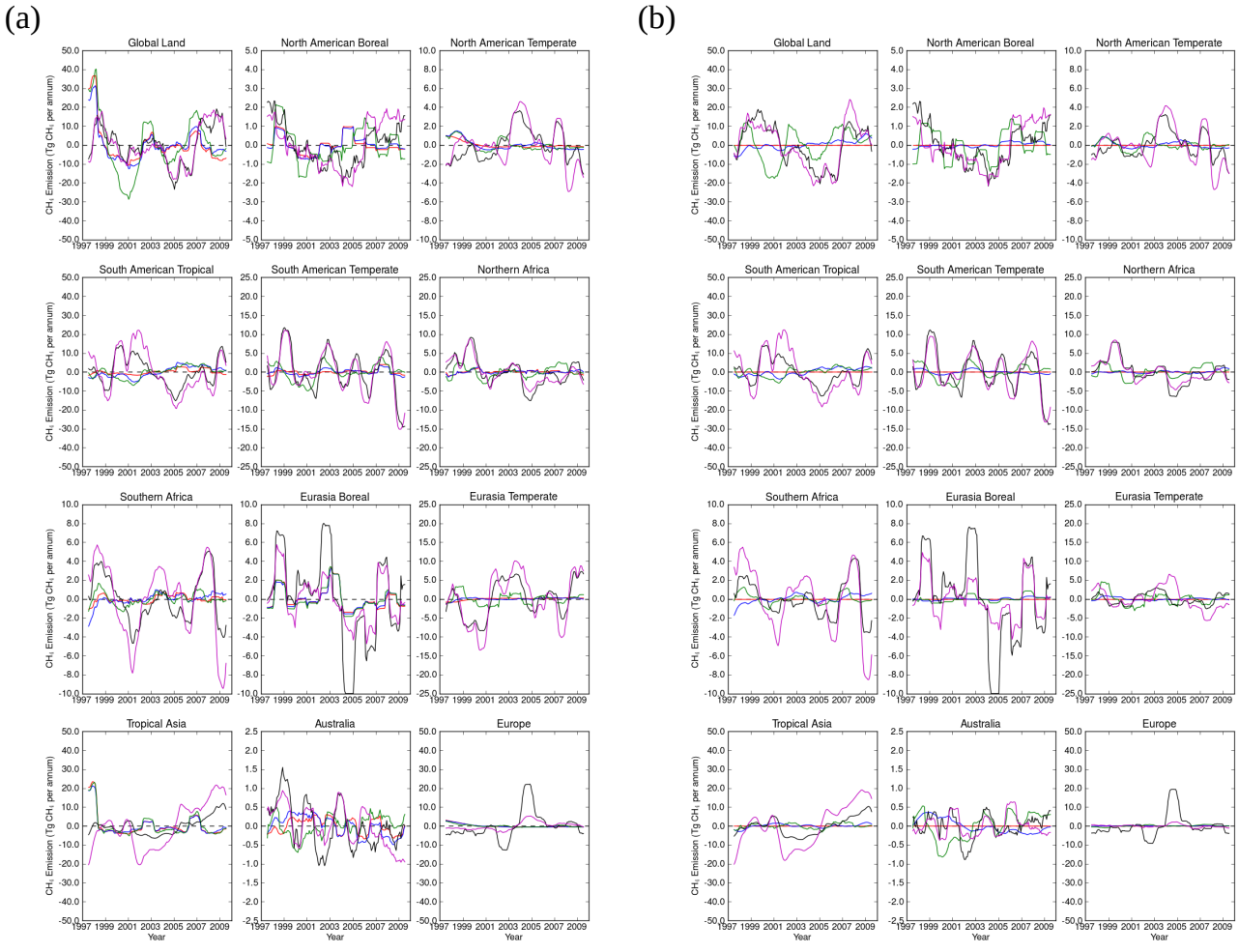

Figure 11. Comparison of the deseasonalised emission fluxes between 1997 and 2009 from the ~~three~~ HadGEM2 runs (using the wetland emission inventories: FUNG – red, JULES – blue and JULES-GIEMS – green) and the two inverse flux estimates of Bousquet et al. (2011) (black and purple). The left-hand panel shows the anomalies in the global methane emissions and the right-hand panel the anomalies in the wetland emissions.

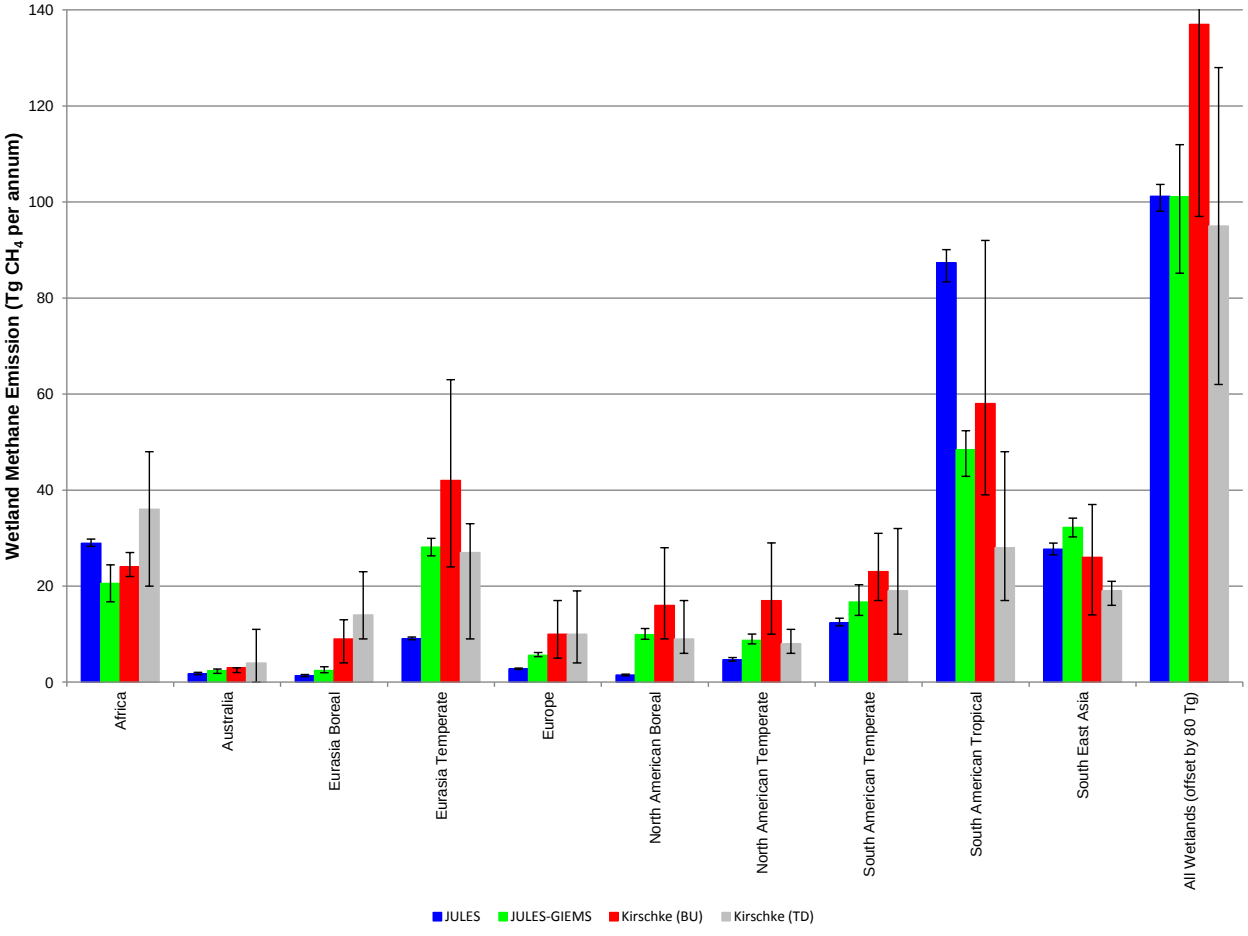

Figure 12. Mean annual methane emissions for the period 2000–2009 from the JULES (blue) and JULES-GIEMS (red) used in this work and the bottom–up (green) and top–down (purple) estimates of Kirschke et al. (2013). The "all wetlands" components have been offset by 80 $\mathrm{Tg\,CH_4\,yr^{-1}}$ for greater clarity. The error bars give the range of values.

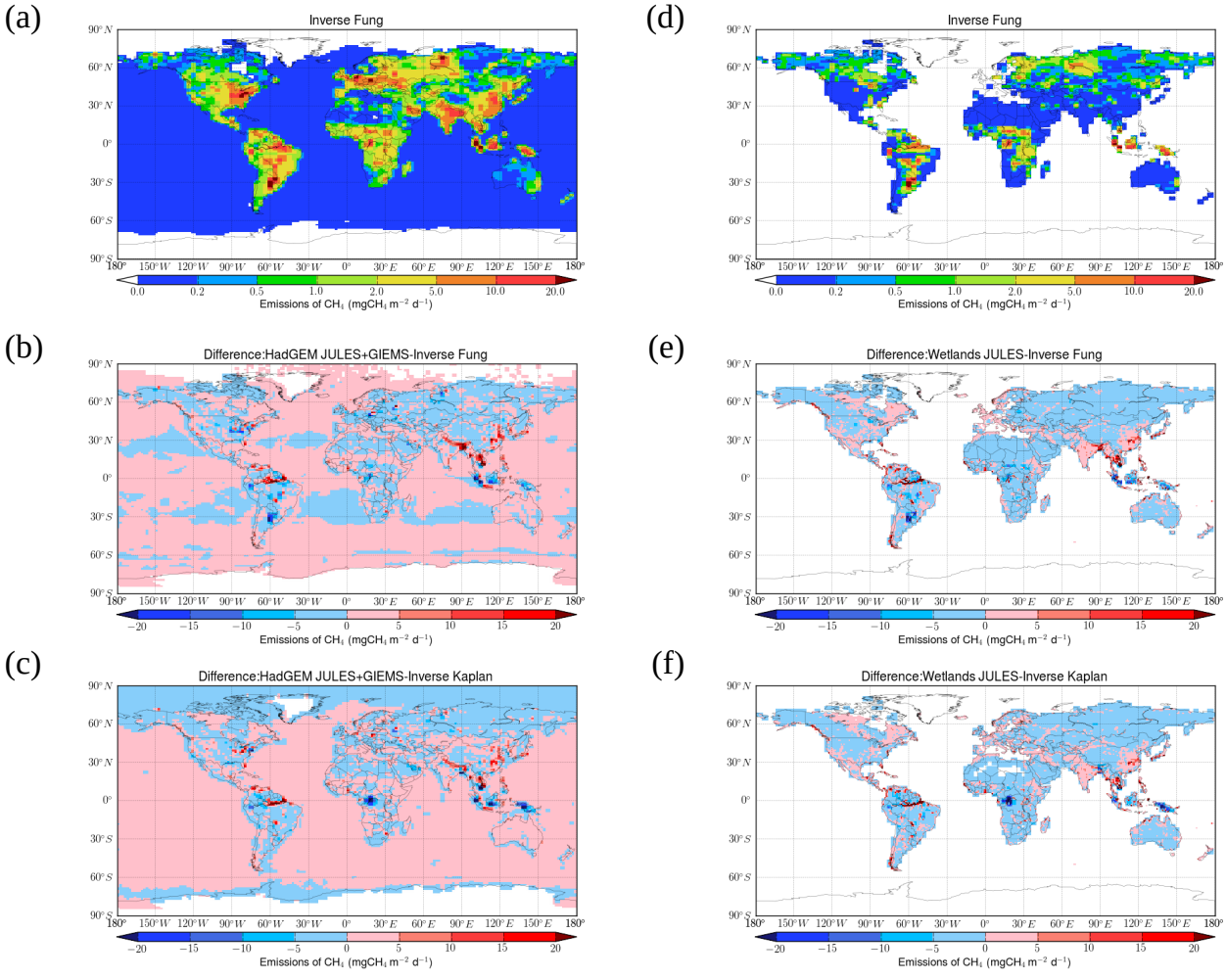

Figure 13. Annual methane emissions for 2000 from all sources (left-hand panels) and wetlands (right-hand panels). The upper panels **(a, d)** show the emission maps from the inverse modelling of Bousquet et al. (2011) using the dataset of ~~FUNG~~ Fung et al. (1991) for the prior wetland emissions. Panels (**b** and **e**) show difference maps between the emission estimates shown in Panels (**a** and **d**) and the corresponding inventories using the JULES-GIEMS wetland emission inventory. Panels (**c** and **f**) are the same as Panels (**b** and **e**) but replacing the wetland emission prior ~~derived from the dataset of Fung et al. (1991)~~ with that of Kaplan (as described in Bergamaschi et al., 2007).

Comparison of the HadGEM2 climate-chemistry model against in situ and SCIAMACHY atmospheric methane data

G. D. Hayman[1], F. O'Connor[2], M. Dalvi[2], D. B. Clark[1], C. Huntingford[1], N. Gedney[3], C. Prigent[4], M. Buchwitz[5], O. Schneising[5], J. P. Burrows[5], C. Wilson[6], N. Richards[6] and M. Chipperfield[6]

October 22, 2014

[1] Centre for Ecology and Hydrology, Crowmarsh Gifford, Wallingford, Oxfordshire, OX10 8BB, UK; [2] Climate, Chemistry, and Ecosystems Team, Met Office Hadley Centre, FitzRoy Road, Exeter, EX1 3PB, UK; [3] Joint Centre for Hydrometeorological Research, Met Office Hadley Centre, Maclean Building, Crowmarsh Gifford, Wallingford, Oxfordshire, OX10 8BB, UK; [4] CNRS-LERMA, Observatoire de Paris, 61 avenue de l'Observatoire, 75014 Paris, France; [5] Institute of Environmental Physics, University of Bremen FB1, P O Box 330440, Otto Hahn Allee 1, D-28334 Bremen, Germany; [6] School of Earth and Environment, University of Leeds, Leeds, LS2 9JT, UK.

Supplementary material

1 Emission Inventories

1.1 Wetlands and Wetland Emissions

The methane emissions from wetlands used in this study were based on an offline global monthly run of the JULES land-surface model for 0.5° x 0.5° terrestrial grid squares for the period from January 1980 to December 2010, using CRU-NCEP driving meteorological data (Viovy and Ciais, 2009). JULES (Joint UK land earth simulator) is a physically-based model that contains description of water, energy and carbon balances and temperature, moisture and carbon stores (Best et al., 2011; Clark et al., 2011). JULES (v3.1) uses a methane wetland emission parameterization, developed and tested by Gedney et al. (2004) for use at large spatial scales. The wetland parameterization is coupled to the large-scale hydrology scheme of Gedney and Cox (2003), which predicts the distribution of sub-grid scale water table depth and wetland fraction from the overall soil moisture content and the sub-grid scale topography.

Fig. 1 compares maps of the maximum inundation fraction in each grid square for monthly data from January 1993 to December 2007, as derived from (a) the offline JULES run described above and (b) regridding the global inundation extent multi-sensor (GIEMS) product of Prigent et al. (2012). While JULES captures the major wetland areas, it is clear that JULES underestimates the magnitude. The JULES wetlands areas are more extensive spatially, especially over the Amazon, and smoother. Collins et al. (2011) indicated that the greater spatial extent of wetlands over the Amazon was linked to the poor data on the underlying rock topography in this region incorporated into the ancillary topographic index dataset. Changes are being made to the JULES wetland parameterisation and these are currently being evaluated (Gedney, 2014).

In addition to the standard output (denoted *JULES*), a second wetland emission estimate was derived from this JULES offline run by replacing the modelled wetland fraction with the wetland fraction from the regridded GIEMS product (denoted *JULES–GIEMS*). Emission fluxes for the latter could only be derived for the period from January 1993 to December 2007. Fig. 2 shows maps of the annual emissions of methane from wetlands in 2000 derived from the above. The two JULES inventories were separately scaled to give a mean annual emission of 181 Tg CH_4 per annum for the years 1999-2007, the period of the HadGEM2 model runs.

In the *JULES* wetland emission dataset, most of the emissions occur from the tropics, especially from the Amazon. The use of the EO data is to slightly shift the emissions away from the tropics towards the boreal zone. This is more clearly seen in the zonal plots of Fig. 3, which compare the latitudinal distributions of the methane emissions derived from (a) the *JULES* and the *JULES–GIEMS* runs for the year 2000; (b) the inventory of Fung et al. (1991) for wetlands (=wetlands+bogs+swamps+tundra) and for wetlands and rice paddy fields. The JULES methane inventories have more emissions in the tropics compared to the wetlands dataset of Fung et al. (1991).

The EO wetland inundation product does not discriminate between natural wetlands and managed water areas such as rice paddy fields. A correction was made for the rice paddy fields in the EO wetland product using information on the area of cultivation of rice, from both irrigated and rain-fed cultivation (Portmann et al., 2010). The left-hand panel (a) has no correction to the EO wetland fraction. The right-hand panel (b) shows the effect of correcting the EO wetland inundation product for the area of rice paddy fields. The effect of correcting for the methane emissions from rice paddy fields is most noticeable in the latitude band between 10° and 30° N. The corrected wetland emission dataset was used in the HadGEM model run and an additional term of 40 Tg CH_4 per annum was added to the non-wetland methane sources to represent emissions from rice paddy fields.

(a)

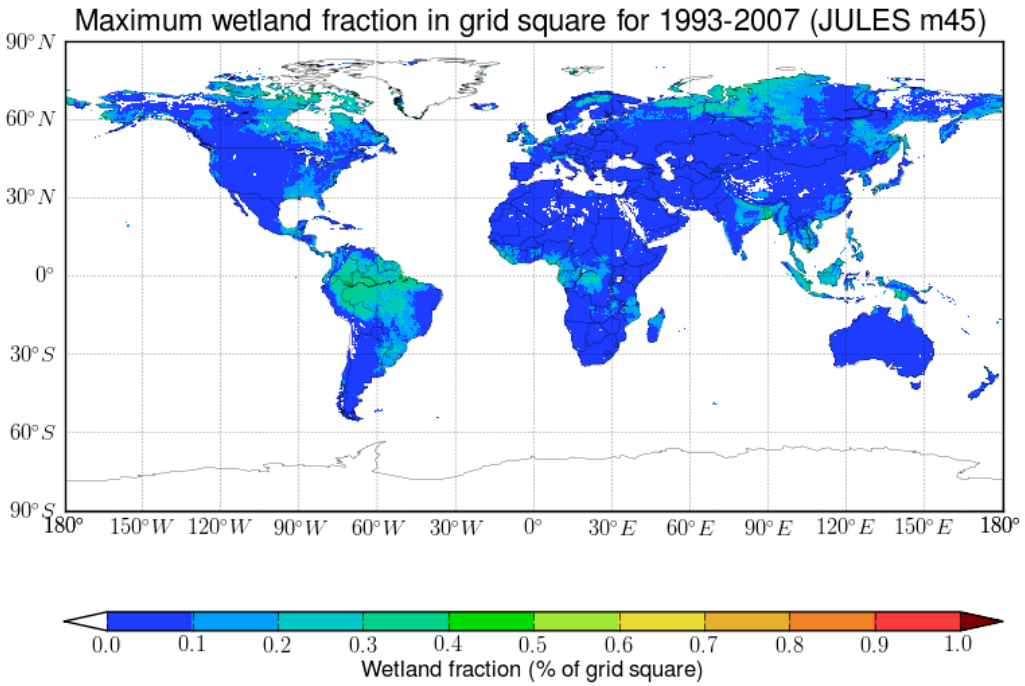

(b)

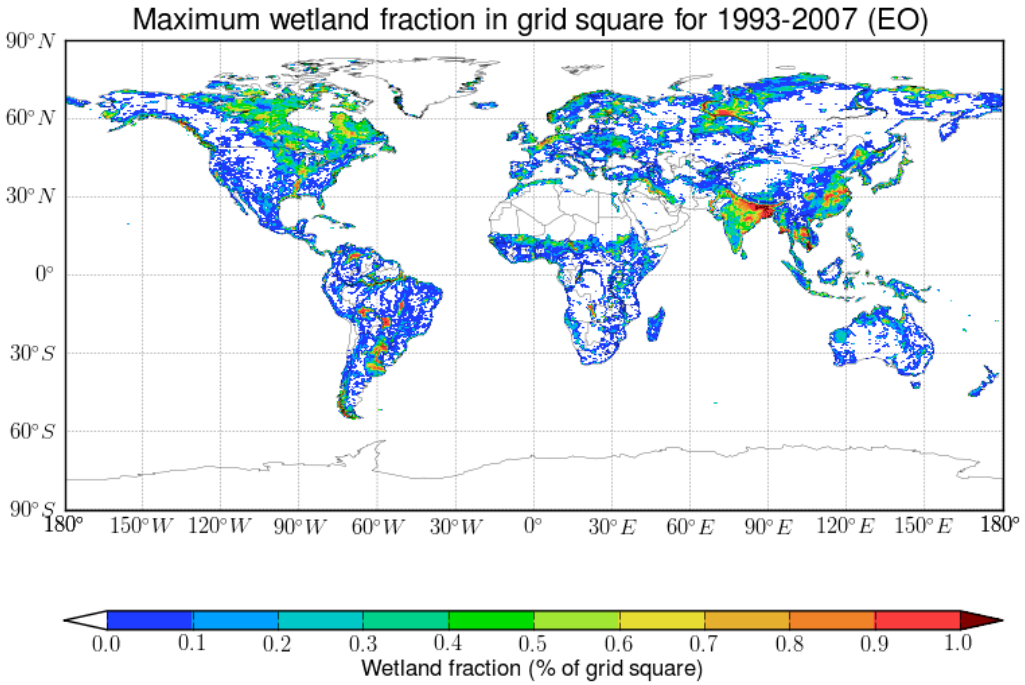

Figure 1: Maps of the maximum inundation fraction in each grid square for monthly data from January 1993 to December 2007, as derived from (a) an offline JULES run using the standard configuration and (b) the Earth Observation Global Inundation Extent Multi-Sensor (GIEMS) product of Prigent et al. (2012).

(a)

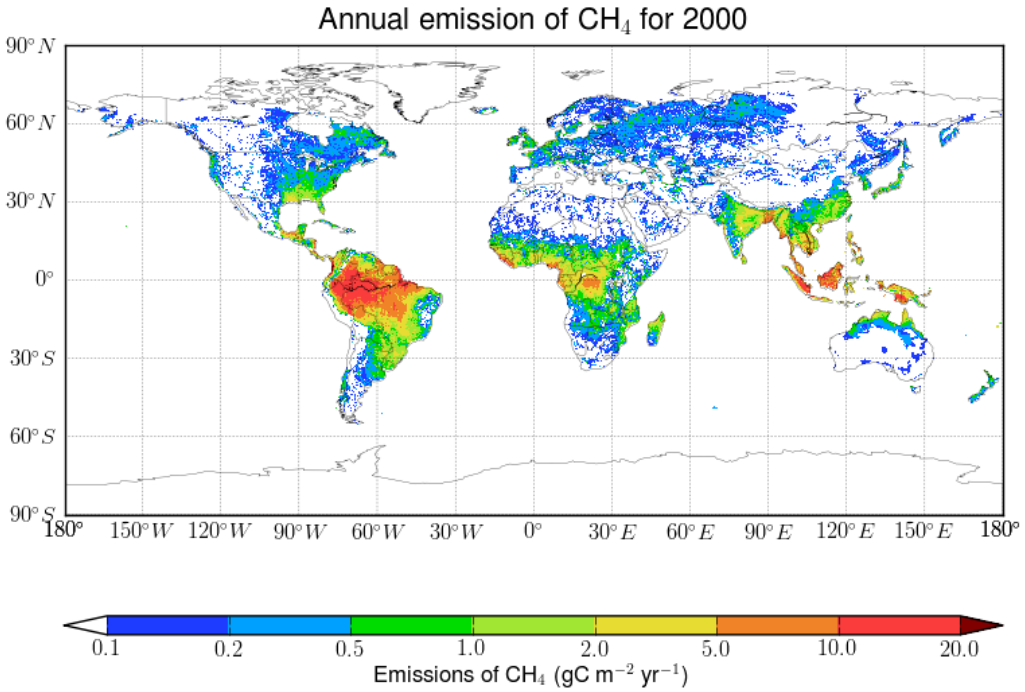

(b)

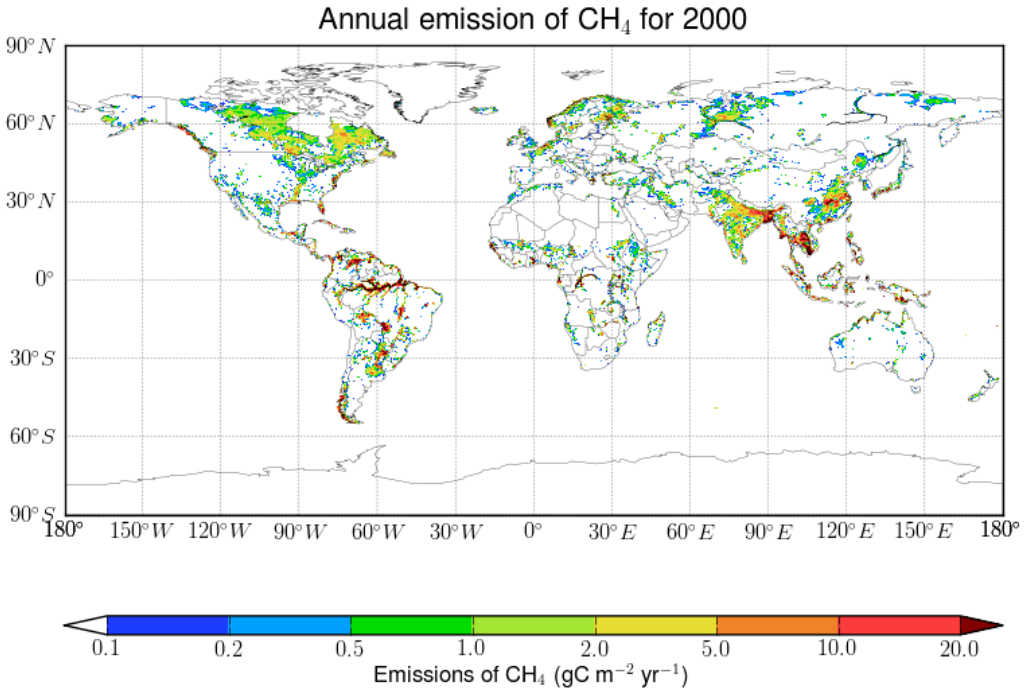

Figure 2: Maps of the annual emissions of methane from wetlands in 2000 from (a) an offline JULES run using the standard configuration and the modelled wetland fraction and (b) the same offline JULES run in which the modelled wetland fraction is replaced with the EO-derived wetland fraction.

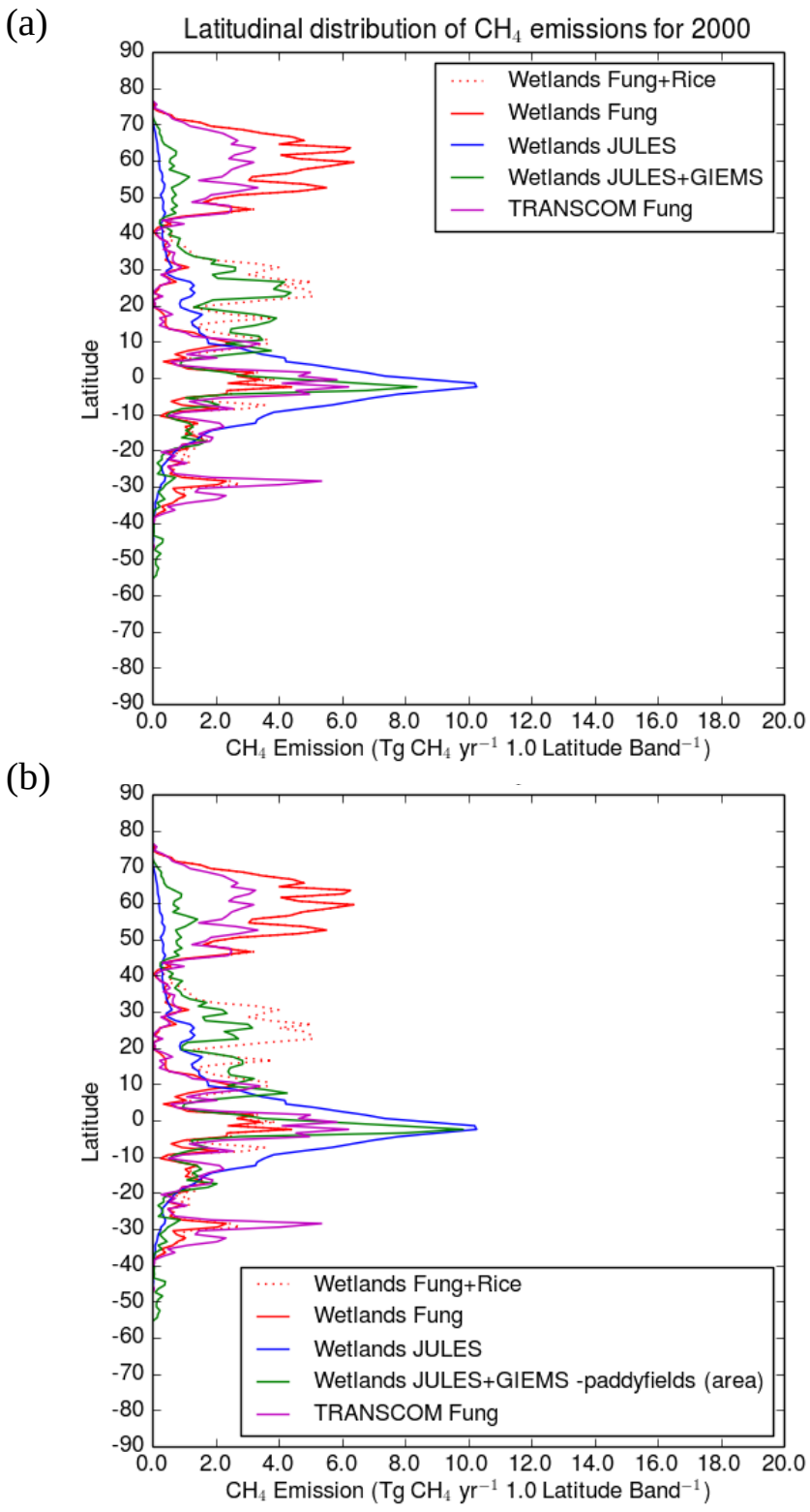

Figure 3: The latitudinal distributions of (i) the wetland methane emissions from JULES for the year 2000, denoted *JULES* (~~red~~ blue lines); (ii) the wetland methane emissions from JULES for the year 2000 with the ~~modeled~~ modelled wetland fraction replaced with an EO-derived wetland fraction, denoted *JULES EO* (~~blue~~ green lines); (iii) the methane emissions derived from the inventory of Fung et al. (1991) for wetlands (see text) [solid ~~black~~ red lines]; (iv) the methane emissions derived from the inventory of Fung et al. (1991) for wetlands and for rice paddy fields [dotted ~~black~~ red lines], and (v) the methane emissions derived from the inventory of Fung et al. (1991) , as used in the TRANSCOM-CH_4 model intercomparison of Patra et al. (2011) . Panel (a) has no correction to the EO wetland fraction. Panel (b) shows the effect of correcting the EO wetland inundation product for the area of rice paddy fields.

Tab. 1 summarises the latitudinal breakdown of the JULES-based global annual methane emissions from wetlands used in this study. The JULES methane inventories have more emissions in the tropics compared to the wetlands dataset of Fung et al. (1991).

Table 1: Latitudinal breakdown of different global annual methane emissions from wetlands for the year 2000.

Emission Dataset	Extratropical SH (90°S–30°S)	Tropical (30°S–30°N)	Extratropical NH (30°N–50°N)	Boreal/Arctic (50°N–90°N)	Global
FUNG Wetlands and Rice paddy fields	5.7	133.2	30.2	90.8	259.9
FUNG Wetlands	5.0	67.1	18.1	90.8	181.0
JULES Wetlands	1.5	167.4	7.7	4.5	181.1
JULES–GIEMS Wetlands: no correction	4.1	132.1	18.3	12.2	166.7
JULES–GIEMS Wetlands: correction	4.9	127.9	17.6	14.8	165.2

1.2 Global Emissions

Year- and month-specific emission datasets were generated for the period from 1997 to 2009 for (a) non-wetland methane sources and (b) the other emitted species in the UKCA standard ~~tropospheric~~ tropospheric chemistry scheme (CO, NO_x, HCHO, CH_4, C_2H_6, C_3H_8, CH_3CHO, CH_3CHOCH_3 O'Connor et al., 2013). The approach adopted varied depending on the source sector:

- **Anthropogenic**: The emissions from anthropogenic sources were based on the decadal-averaged emission inventories compiled by Lamarque et al. (2010) for the Coupled Carbon Cycle Climate Model Intercomparison Project (C4MIP) undertaken for the fifth IPCC assessment report (AR5). The decadal-averaged inventories were used to derive year-specific emission datasets by scaling the emission totals for the different years and source sectors using sector and species-specific scaling factors based on the annual trends given in various EDGAR time series: (a) version 4.2 for all species (except NMVOCs) and version 4.1 for NMVOCs; (b) v3.2. This approach was also applied to the emissions from aviation (only for oxides of nitrogen) and international shipping.

- **Biomass burning**: Year-specific emission inventories are available from the Global Fire Emissions Database (GFED, v3.1) for the years 1997 to 2009 (van der Werf et al., 2010), on a monthly timestep. The methane emissions were scaled to give the same decadal mean, 25 Tg CH_4 per annum averaged over 1997 to 2005, as used in the study of O'Connor et al. (2013) to evaluate the standard tropospheric chemistry scheme.

- **Other**: Sources such as termites and hydrates for methane and oceanic emissions of CH_4 and other volatile organic compounds were taken from various sources, as described in O'Connor et al. (2013). These datasets contain a single annual cycle, which was assumed to apply for all years.

1.2.1 Methane

Tab. 2 provides a breakdown by source sector of the global annual emissions of methane used in the different HadGEM2 model for the year 2000. Tab. 3 gives the annual global emissions for the different runs from 1997 to 2008.

Table 2: Comparison of the global annual emissions of methane for 2000 (in Tg CH_4 per annum) and their breakdown by major source sector for the HadGEM2 runs using the following wetland emission inventories, *FUNG*, *TRANSCOM-FUNG*, *JULES* and *JULES-GIEMS*.

Emission Sector	*FUNG* and *TRANSCOM-FUNG*	*JULES*	*JULES-GIEMS*
anthropogenic	299.2	299.2	299.2
shipping	0.4	0.4	0.4
wetlands	181.1	181.2	165.4
biomass burning	15.6	15.6	15.6
termites	20.0	20.0	20.0
hydrates & oceanic emissions	25.0	25.0	25.0
TOTAL	541.3	541.4	525.6

Note: The anthropogenic term includes 40 Tg CH_4 per annum of emissions from rice paddy fields.

Table 3: Time series of the global annual emissions of methane from 1997 to 2008 (in Tg per annum) used in the ~~ALANIS methane base case and scenario~~ HadGEM2 runs ~~and~~ using the ~~Hadley Centres decadal-averaged~~ following wetland emission inventories, *FUNG*, *TRANSCOM-FUNG*, *JULES* and *JULES-GIEMS*.

Year	*FUNG* and *TRANSCOM-FUNG*	*JULES*	*JULES-GIEMS*
1997	578.4	572.6	579.7
1998	556.0	554.1	569.4
1999	543.8	542.1	543.2
2000	541.3	541.4	525.6
2001	541.1	538.2	530.3
2002	551.4	550.8	562.4
2003	548.0	547.4	550.1
2004	546.9	547.6	540.7
2005	549.1	549.8	548.5
2006	554.2	556.8	565.0
2007	547.1	548.6	558.2
2008	542.4	545.7	545.1
2009	542.2	545.9	548.9

Fig. ~~??~~4-~~??~~ 7 show plots of (a) the time series of the annual methane emissions from ~~from~~ wetlands and (b) the mean annual cycle of these emissions for all land surfaces and for the 11 terrestrial TRANSCOM regions for ~~three of~~ the HadGEM2 runs (*FUNG*, *TRANSCOM-FUNG*, *JULES*, *JULES–GIEMS*).

Table 4 shows the contribution of different methane emission sources within a 20° x 20° box centred on two sites: Barrow (Alaska) and Plateau Assy.

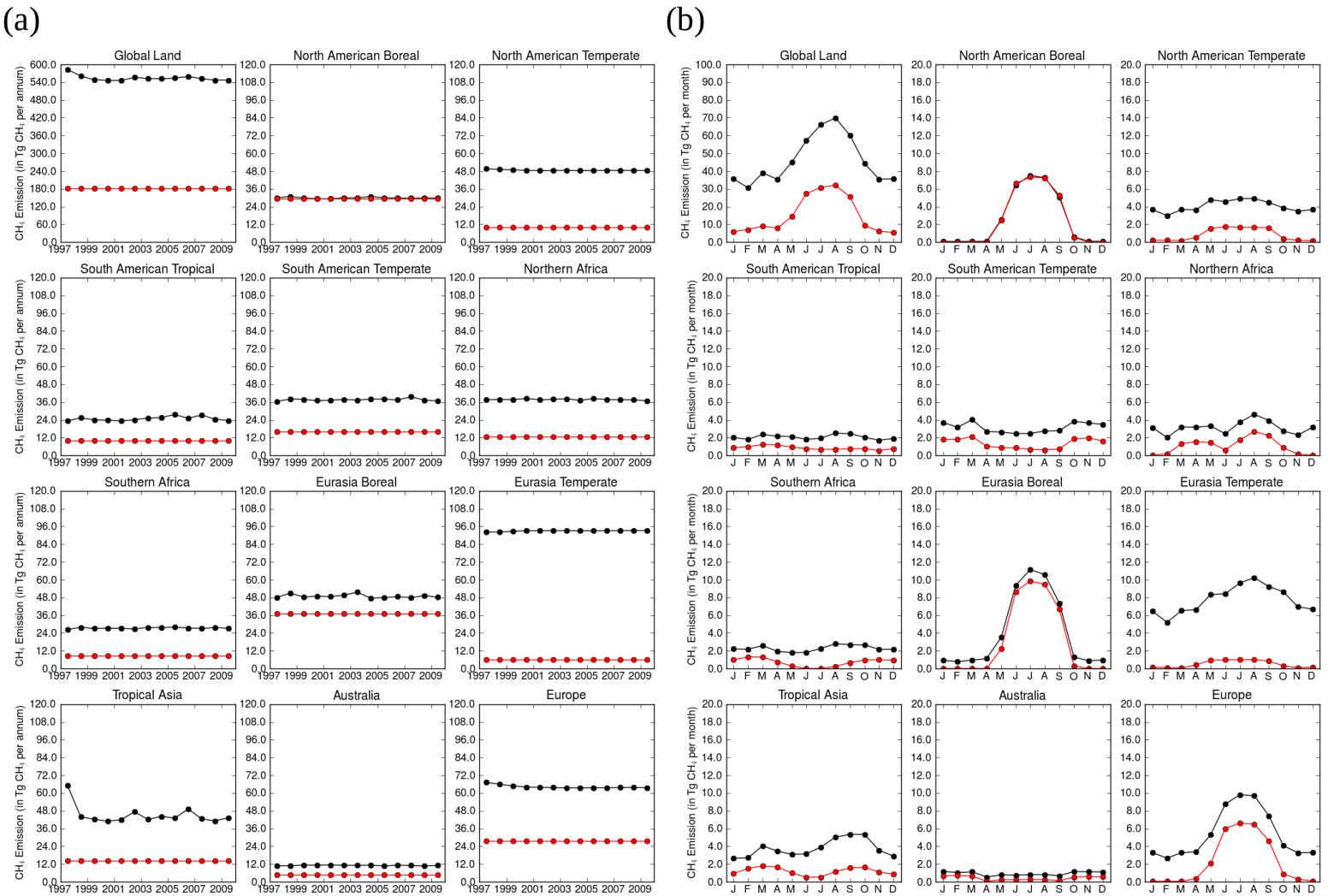

Figure 4: Time series of the annual emissions from 1993 to 2007 globally and for the 11 terrestrial TRANSCOM regions for the dataset of Fung et al. (1991). Panel (b) shows the corresponding annual cycles.

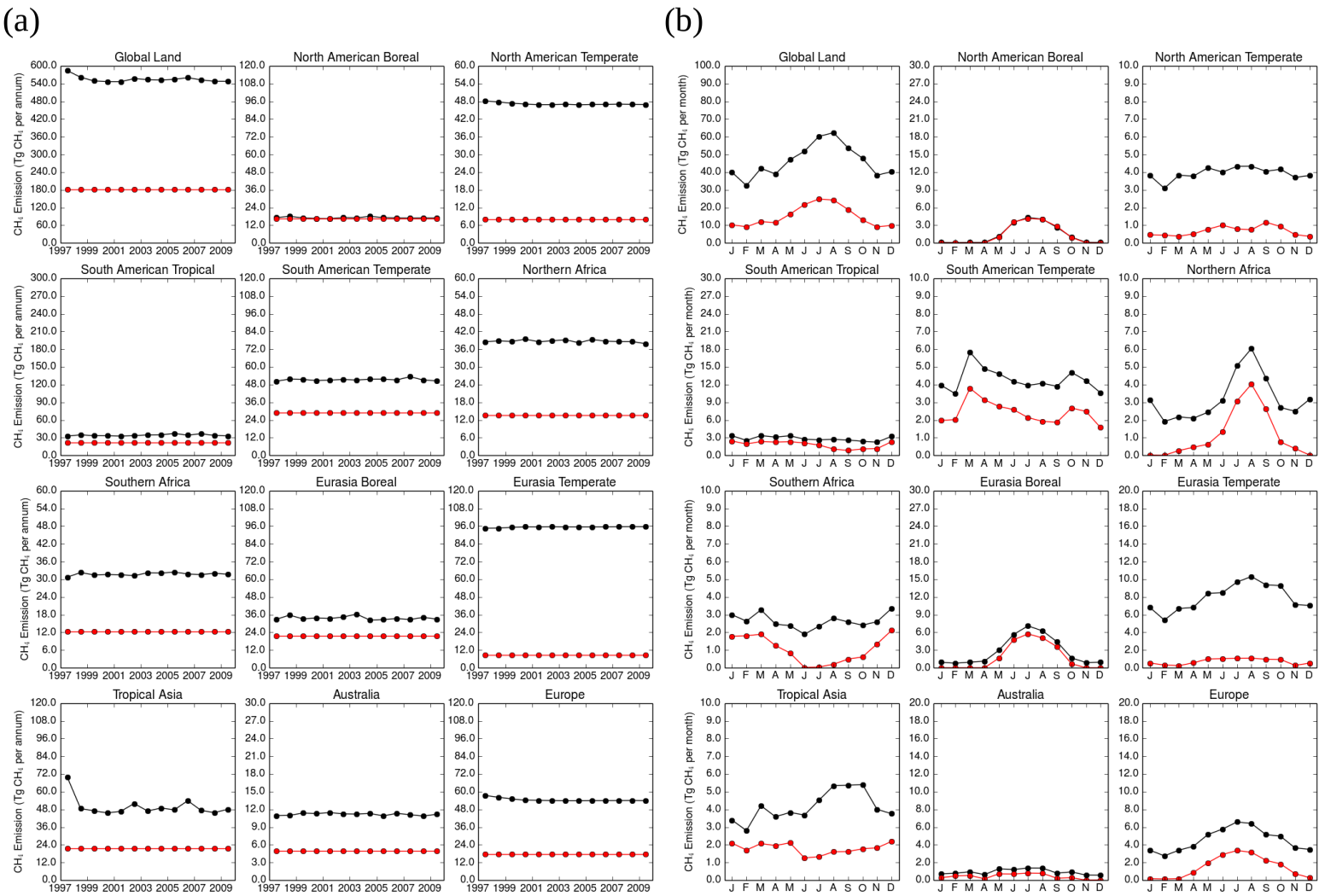

Figure 5: Time series of the annual emissions from 1993 to 2007 globally and for the 11 terrestrial TRANSCOM regions for the dataset of Fung et al. (1991) . Panel (b) shows the corresponding annual cycles.

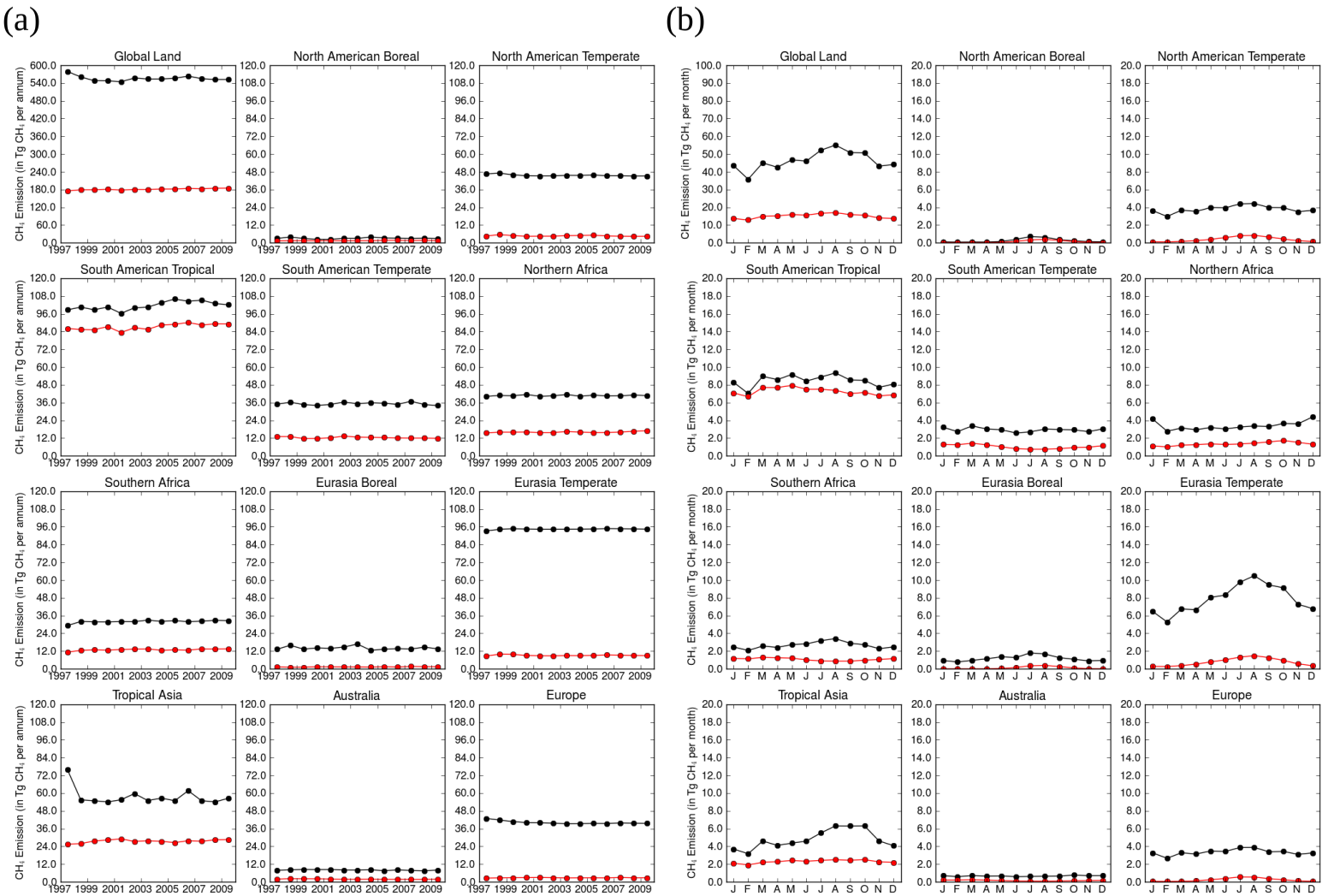

Figure 6: Time series of the annual emissions from 1993 to 2007 globally and for the 11 terrestrial TRANSCOM regions for the JULES wetland emission flux. Panel (b) shows the corresponding annual cycles.

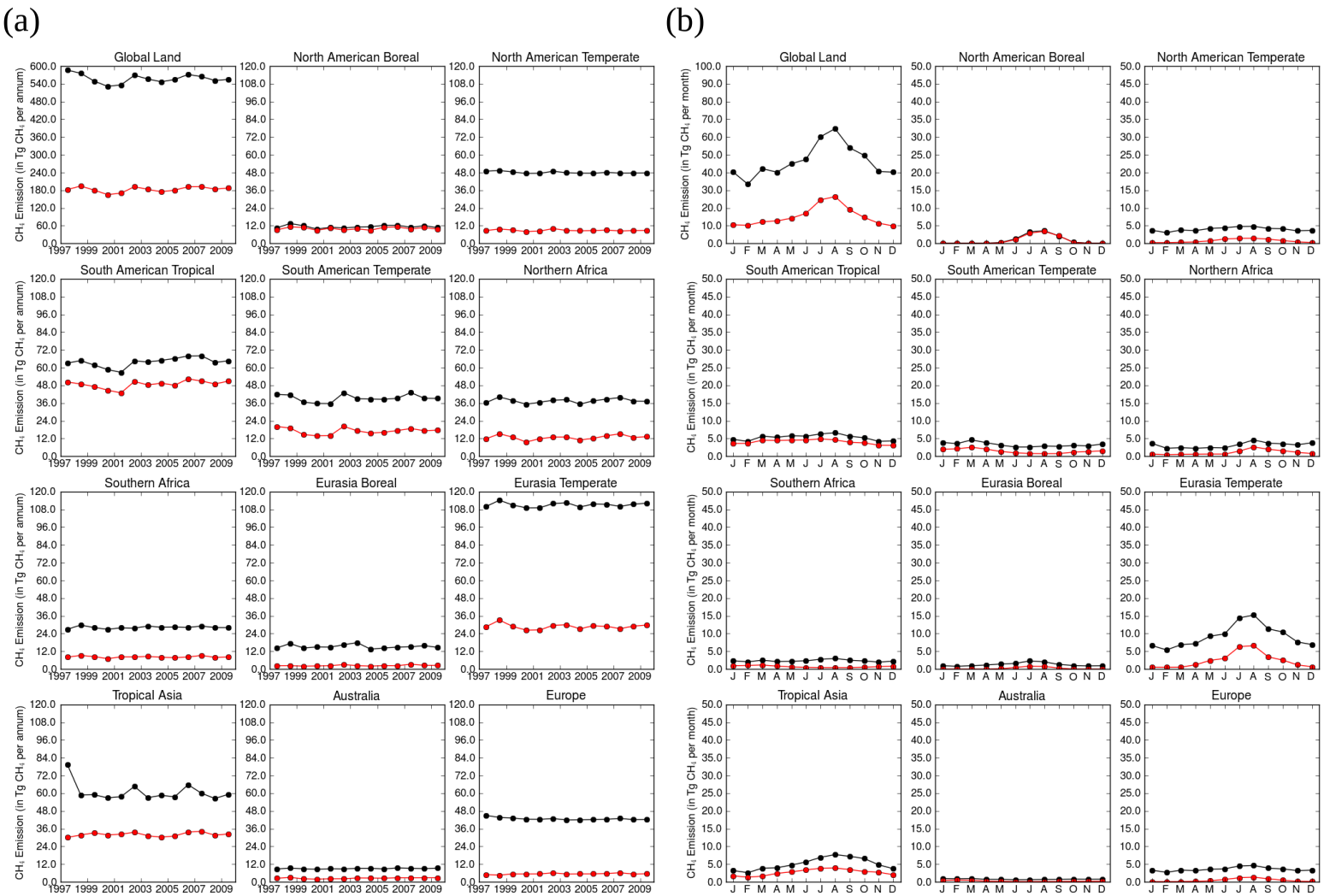

Figure 7: Time series of the annual emissions from 1993 to 2007 globally and for the 11 terrestrial TRANSCOM regions for the JULES wetland emission flux driven with the GIEMS EO product. Panel (b) shows the corresponding annual cycles.

Table 4: Contribution of different methane emission sources (Tg CH_4 yr^{-1}) within a 20° x 20° box centred on Barrow (Alaska) and Plateau Assy. The percentage contribution is shown in brackets.

(1) Barrow

a) Wetland Emission Inventory: Fung (as used here)

Year	Anthropogenic	Rice	Biomass Burning	Wetlands	Other	Total
1999	0.50 (12.1)	0.00 (0.0)	0.01 (0.3)	3.61 (87.3)	0.01 (0.3)	4.13
2000	0.49 (11.9)	0.00 (0.0)	0.02 (0.5)	3.61 (87.2)	0.01 (0.3)	4.13
2001	0.49 (11.8)	0.00 (0.0)	0.00 (0.0)	3.61 (87.8)	0.01 (0.4)	4.11
2002	0.48 (11.1)	0.00 (0.0)	0.19 (4.4)	3.61 (84.1)	0.01 (0.3)	4.29
2003	0.46 (11.3)	0.00 (0.0)	0.03 (0.6)	3.61 (87.7)	0.01 (0.3)	4.11
2004	0.45 (10.3)	0.00 (0.0)	0.27 (6.1)	3.61 (83.2)	0.01 (0.3)	4.33
2005	0.43 (9.9)	0.00 (0.0)	0.31 (7.2)	3.61 (82.6)	0.01 (0.3)	4.37
2006	0.42 (10.3)	0.00 (0.0)	0.02 (0.4)	3.61 (89.0)	0.01 (0.4)	4.05
2007	0.40 (9.9)	0.00 (0.0)	0.03 (0.8)	3.61 (88.9)	0.01 (0.4)	4.06

b) Wetland Emission Inventory: Fung (as used in the TRANSCOM-CH_4 model intercomparison and scaled to 181 Tg CH_4 yr^{-1})

Year	Anthropogenic	Rice	Biomass Burning	Wetlands	Other	Total
1999	0.50 (28.1)	0.00 (0.0)	0.01 (0.8)	1.25 (70.3)	0.01 (0.8)	1.77
2000	0.49 (27.7)	0.00 (0.0)	0.02 (1.2)	1.25 (70.2)	0.01 (0.8)	1.77
2001	0.49 (27.8)	0.00 (0.0)	0.00 (0.0)	1.25 (71.4)	0.01 (0.8)	1.74
2002	0.48 (24.8)	0.00 (0.0)	0.19 (9.8)	1.25 (64.6)	0.01 (0.7)	1.93
2003	0.46 (26.5)	0.00 (0.0)	0.03 (1.5)	1.25 (71.2)	0.01 (0.8)	1.75
2004	0.45 (22.7)	0.00 (0.0)	0.27 (13.5)	1.25 (63.1)	0.01 (0.7)	1.97
2005	0.43 (21.5)	0.00 (0.0)	0.31 (15.7)	1.25 (62.1)	0.01 (0.7)	2.01
2006	0.42 (24.6)	0.00 (0.0)	0.02 (1.0)	1.25 (73.6)	0.01 (0.8)	1.69
2007	0.40 (23.8)	0.00 (0.0)	0.03 (1.9)	1.25 (73.5)	0.01 (0.8)	1.69

c) Wetland Emission Inventory: JULES

Year	Anthropogenic	Rice	Biomass Burning	Wetlands	Other	Total
1999	0.50 (90.8)	0.00 (0.0)	0.01 (2.6)	0.02 (4.0)	0.01 (2.6)	0.55
2000	0.49 (87.9)	0.00 (0.0)	0.02 (3.8)	0.03 (5.7)	0.01 (2.6)	0.56
2001	0.49 (90.7)	0.00 (0.0)	0.00 (0.0)	0.04 (6.6)	0.01 (2.7)	0.53
2002	0.48 (69.1)	0.00 (0.0)	0.19 (27.3)	0.01 (1.5)	0.01 (2.1)	0.69
2003	0.46 (88.5)	0.00 (0.0)	0.03 (5.1)	0.02 (3.7)	0.01 (2.7)	0.52
2004	0.45 (61.3)	0.00 (0.0)	0.27 (36.4)	0.00 (0.3)	0.01 (2.0)	0.73
2005	0.43 (56.2)	0.00 (0.0)	0.31 (41.0)	0.01 (0.9)	0.01 (1.9)	0.77
2006	0.42 (90.6)	0.00 (0.0)	0.02 (3.7)	0.01 (2.6)	0.01 (3.1)	0.46
2007	0.40 (88.6)	0.00 (0.0)	0.03 (6.9)	0.01 (1.3)	0.01 (3.2)	0.46

d) Wetland Emission Inventory: JULES-GIEMS

Year	Anthropogenic	Rice	Biomass Burning	Wetlands	Other	Total
1999	0.50 (81.7)	0.00 (0.0)	0.01 (2.3)	0.08 (13.6)	0.01 (2.4)	0.61
2000	0.49 (79.7)	0.00 (0.0)	0.02 (3.5)	0.09 (14.5)	0.01 (2.3)	0.62
2001	0.49 (81.5)	0.00 (0.0)	0.00 (0.0)	0.10 (16.1)	0.01 (2.4)	0.60
2002	0.48 (61.0)	0.00 (0.0)	0.19 (24.1)	0.10 (13.1)	0.01 (1.8)	0.78
2003	0.46 (76.6)	0.00 (0.0)	0.03 (4.4)	0.10 (16.6)	0.01 (2.4)	0.60
2004	0.45 (52.9)	0.00 (0.0)	0.27 (31.4)	0.12 (14.0)	0.01 (1.7)	0.85
2005	0.43 (49.4)	0.00 (0.0)	0.31 (36.1)	0.11 (12.9)	0.01 (1.6)	0.87
2006	0.42 (75.1)	0.00 (0.0)	0.02 (3.1)	0.11 (19.2)	0.01 (2.6)	0.55
2007	0.40 (73.0)	0.00 (0.0)	0.03 (5.7)	0.10 (18.7)	0.01 (2.6)	0.55

Table 4 (continued): Contribution of different methane emission sources (Tg CH_4 yr^{-1}) within a 20° x 20° box centred on Barrow (Alaska) and Plateau Assy. The percentage contribution is shown in brackets.

(2) Plateau Assy

a) Wetland Emission Inventory: Fung (as used here)

Year	Anthropogenic	Rice	Biomass Burning	Wetlands	Other	Total
1999	3.72 (75.1)	0.14 (2.9)	0.03 (0.7)	0.78 (15.7)	0.28 (5.6)	4.96
2000	3.64 (74.5)	0.14 (3.0)	0.05 (0.9)	0.78 (15.9)	0.28 (5.7)	4.89
2001	3.57 (74.1)	0.14 (3.0)	0.05 (1.0)	0.78 (16.2)	0.28 (5.8)	4.81
2002	3.48 (72.1)	0.14 (3.0)	0.15 (3.0)	0.78 (16.1)	0.28 (5.8)	4.83
2003	3.39 (72.8)	0.14 (3.1)	0.06 (1.3)	0.78 (16.8)	0.28 (6.0)	4.65
2004	3.29 (72.4)	0.14 (3.2)	0.05 (1.2)	0.78 (17.1)	0.28 (6.1)	4.55
2005	3.19 (72.0)	0.14 (3.3)	0.04 (0.9)	0.78 (17.6)	0.28 (6.3)	4.43
2006	3.09 (71.3)	0.14 (3.3)	0.04 (1.0)	0.78 (18.0)	0.28 (6.4)	4.34
2007	3.01 (70.6)	0.14 (3.4)	0.06 (1.3)	0.78 (18.2)	0.28 (6.5)	4.27

b) Wetland Emission Inventory: Fung (as used in the TRANSCOM-CH_4 model intercomparison and scaled to 181 Tg CH_4 yr^{-1})

Year	Anthropogenic	Rice	Biomass Burning	Wetlands	Other	Total
1999	3.72 (66.3)	0.14 (2.6)	0.03 (0.6)	1.44 (25.6)	0.28 (5.0)	5.61
2000	3.64 (65.7)	0.14 (2.6)	0.05 (0.8)	1.44 (25.9)	0.28 (5.0)	5.55
2001	3.57 (65.2)	0.14 (2.6)	0.05 (0.9)	1.44 (26.3)	0.28 (5.1)	5.47
2002	3.48 (63.5)	0.14 (2.6)	0.15 (2.7)	1.44 (26.2)	0.28 (5.1)	5.49
2003	3.39 (63.8)	0.14 (2.7)	0.06 (1.2)	1.44 (27.1)	0.28 (5.2)	5.31
2004	3.29 (63.2)	0.14 (2.8)	0.05 (1.0)	1.44 (27.6)	0.28 (5.3)	5.20
2005	3.19 (62.7)	0.14 (2.8)	0.04 (0.8)	1.44 (28.2)	0.28 (5.5)	5.08
2006	3.09 (61.9)	0.14 (2.9)	0.04 (0.9)	1.44 (28.8)	0.28 (5.6)	4.99
2007	3.01 (61.2)	0.14 (2.9)	0.06 (1.1)	1.44 (29.1)	0.28 (5.6)	4.93

c) Wetland Emission Inventory: JULES

Year	Anthropogenic	Rice	Biomass Burning	Wetlands	Other	Total
1999	3.72 (83.1)	0.14 (3.2)	0.03 (0.7)	0.30 (6.7)	0.28 (6.2)	4.48
2000	3.64 (82.7)	0.14 (3.3)	0.05 (1.0)	0.29 (6.7)	0.28 (6.3)	4.40
2001	3.57 (82.3)	0.14 (3.3)	0.05 (1.1)	0.30 (6.9)	0.28 (6.4)	4.33
2002	3.48 (80.0)	0.14 (3.3)	0.15 (3.4)	0.30 (6.9)	0.28 (6.4)	4.35
2003	3.39 (81.3)	0.14 (3.5)	0.06 (1.5)	0.29 (7.0)	0.28 (6.7)	4.17
2004	3.29 (80.8)	0.14 (3.5)	0.05 (1.3)	0.30 (7.5)	0.28 (6.8)	4.07
2005	3.19 (80.2)	0.14 (3.6)	0.04 (1.0)	0.32 (8.1)	0.28 (7.0)	3.97
2006	3.09 (80.0)	0.14 (3.7)	0.04 (1.1)	0.31 (8.0)	0.28 (7.2)	3.87
2007	3.01 (79.1)	0.14 (3.8)	0.06 (1.5)	0.32 (8.4)	0.28 (7.3)	3.81

d) Wetland Emission Inventory: JULES-GIEMS

Year	Anthropogenic	Rice	Biomass Burning	Wetlands	Other	Total
1999	3.72 (78.1)	0.14 (3.0)	0.03 (0.7)	0.59 (12.3)	0.28 (5.8)	4.76
2000	3.64 (78.0)	0.14 (3.1)	0.05 (1.0)	0.56 (11.9)	0.28 (6.0)	4.67
2001	3.57 (76.8)	0.14 (3.1)	0.05 (1.0)	0.61 (13.1)	0.28 (6.0)	4.64
2002	3.48 (74.5)	0.14 (3.1)	0.15 (3.1)	0.63 (13.4)	0.28 (5.9)	4.68
2003	3.39 (77.6)	0.14 (3.3)	0.06 (1.4)	0.50 (11.4)	0.28 (6.4)	4.37
2004	3.29 (75.9)	0.14 (3.3)	0.05 (1.3)	0.57 (13.2)	0.28 (6.4)	4.34
2005	3.19 (75.7)	0.14 (3.4)	0.04 (0.9)	0.56 (13.3)	0.28 (6.6)	4.21
2006	3.09 (75.4)	0.14 (3.5)	0.04 (1.0)	0.55 (13.3)	0.28 (6.8)	4.10
2007	3.01 (75.5)	0.14 (3.6)	0.06 (1.4)	0.50 (12.5)	0.28 (7.0)	3.99

90

1.2.2 Other emitted species

Table 5: Breakdown of the global annual emissions by sector and year of those non-methane trace gases that have emissions in the UKCA Standard Troposphere chemistry scheme.

(a) Carbon Monoxide (in Tg CO yr^{-1})

Year	Anthropogenic	Biomass Burning	Shipping/Aviation	Other	Total
1997	607.5	736.4	1.1	520.0	1864.9
1998	607.5	594.5	1.1	520.0	1723.1
1999	607.5	378.4	1.2	520.0	1507.0
2000	607.5	328.7	1.2	520.0	1457.3
2001	607.5	311.5	1.1	520.0	1440.1
2002	607.5	463.9	1.2	520.0	1592.6
2003	607.5	449.4	1.2	520.0	1578.1
2004	607.5	411.7	1.3	520.0	1540.5
2005	607.5	442.2	1.3	520.0	1571.0
2006	607.5	476.8	1.4	520.0	1605.7
2007	607.5	417.9	1.5	520.0	1546.9

(b) Oxides of Nitrogen (in Tg NO_x as N yr^{-1})

Year	Anthropogenic	Biomass Burning	Shipping/Aviation	Other	Total
1997	26.1	6.4	6.0	5.9	44.4
1998	26.6	7.1	6.0	5.9	45.6
1999	27.1	4.7	6.4	5.9	44.1
2000	27.7	4.2	6.6	5.9	44.3
2001	28.2	3.9	6.3	5.9	44.2
2002	28.7	5.3	6.5	5.9	46.3
2003	29.4	5.6	6.6	5.9	47.4
2004	29.9	4.9	7.3	5.9	48.0
2005	30.4	5.2	7.3	5.9	48.8
2006	31.0	5.1	7.8	5.9	49.7
2007	31.6	5.0	8.2	5.9	50.7

(c) Formaldehyde (in Tg HCHO yr^{-1})

Year	Anthropogenic	Biomass Burning	Shipping/Aviation	Other	Total
1997	3.2	8.2	-	-	11.3
1998	3.2	7.8	-	-	11.0
1999	3.2	5.1	-	-	8.2
2000	3.2	4.4	-	-	7.6
2001	3.2	4.1	-	-	7.3
2002	3.2	5.8	-	-	9.0
2003	3.2	5.9	-	-	9.1
2004	3.3	5.4	-	-	8.7
2005	3.3	5.9	-	-	9.3
2006	3.4	5.9	-	-	9.3
2007	3.4	5.8	-	-	9.2

(d) Ethane (in Tg C_2H_6 yr^{-1})

Year	Anthropogenic	Biomass Burning	Shipping/Aviation	Other	Total
1997	13.9	16.3	0.4	-	30.6
1998	13.9	15.6	0.4	-	29.9
1999	13.9	10.1	0.4	-	24.4
2000	13.9	8.8	0.4	-	23.1
2001	14.0	8.2	0.4	-	22.6
2002	14.0	11.6	0.4	-	26.0
2003	14.2	11.8	0.4	-	26.4
2004	14.5	10.8	0.5	-	25.8
2005	14.6	11.8	0.5	-	26.9
2006	14.9	11.8	0.5	-	27.2
2007	15.1	11.5	0.6	-	27.2

Table 5 (continued): Breakdown of the global annual emissions by sector and year of those non-methane trace gases that have emissions in the UKCA Standard Troposphere chemistry scheme.

(e) Propane (in Tg C_3H_8 yr^{-1})

Year	Anthropogenic	Biomass Burning	Shipping/Aviation	Other	Total
1997	6.6	8.5	0.7	-	15.7
1998	6.6	8.2	0.7	-	15.4
1999	6.6	5.3	0.7	-	12.5
2000	6.6	4.6	0.7	-	11.9
2001	6.6	4.3	0.7	-	11.6
2002	6.6	6.0	0.7	-	13.3
2003	6.7	6.1	0.7	-	13.6
2004	6.9	5.7	0.8	-	13.3
2005	6.9	6.2	0.8	-	13.9
2006	7.0	6.1	0.9	-	14.0
2007	7.1	6.0	1.0	-	14.1

(f) Acetaldehyde (in Tg CH_3CHO yr^{-1})

Year	Anthropogenic	Biomass Burning	Shipping/Aviation	Other	Total
1997	-	12.4	-	-	12.4
1998	-	11.9	-	-	11.9
1999	-	7.7	-	-	7.7
2000	-	6.6	-	-	6.6
2001	-	6.2	-	-	6.2
2002	-	8.8	-	-	8.8
2003	-	8.9	-	-	8.9
2004	-	8.2	-	-	8.2
2005	-	9.0	-	-	9.0
2006	-	8.9	-	-	8.9
2007	-	8.7	-	-	8.7

(g) Acetone (in Tg CH_3COCH_3 yr^{-1})

Year	Anthropogenic	Biomass Burning	Shipping/Aviation	Other	Total
1997	0.7	7.0	-	40.0	47.6
1998	0.7	6.7	-	40.0	47.3
1999	0.7	4.3	-	40.0	45.0
2000	0.7	3.7	-	40.0	44.4
2001	0.7	3.5	-	40.0	44.2
2002	0.7	4.9	-	40.0	45.6
2003	0.7	5.0	-	40.0	45.7
2004	0.7	4.6	-	40.0	45.3
2005	0.7	5.1	-	40.0	45.8
2006	0.7	5.0	-	40.0	45.7
2007	0.7	4.9	-	40.0	45.6

Notes to Table 5:

1. For CO, the 'Other' category includes emission terms of (a) 475 Tg CO $yr^{-1}$to account for the impact of isoprene emissions from vegetation on atmospheric composition, and (b) 45 Tg yr^{-1} from oceanic sources.

2. For NO_x, the 'Other' category includes 5.9 Tg NO_x yr^{-1} from soils. The emissions of NO_x from lightning are calculated interactively (O'Connor et al., 2013).

3. For acetone, the 'Other' category includes 40 Tg yr^{-1} from vegetation.

1.3 Comparison with Estimates from Inverse Modelling

Maps of the global wetland methane emissions are shown for the JULES-based wetland emissions and are compared, as difference maps, with the emissions derived from the inverse modelling study of Bousquet et al. (2011) in Figs. 8 to 13:

- **Fig. 8**: Maps of the global monthly methane emissions from wetlands in 2000 for the *JULES* wetland emission flux.
- **Fig. 9**: Maps of the difference in the global monthly methane emissions from wetlands in 2000 from the *JULES* run and from the inverse modelling study of Bousquet et al. (2011) using the Fung et al. (1991) dataset as the wetland emission prior.
- **Fig. 10**: Maps of the difference in the global monthly methane emissions from wetlands in 2000 from the *JULES* run and from the inverse modelling study of Bousquet et al. (2011) using the Kaplan dataset as the wetland emission prior.
- **Fig. 11**: Maps of the global monthly methane emissions from wetlands in 2000 for the *JULES–GIEMS* wetland emission flux with the modelled wetland fraction replaced with that derived from the GIEMS EO product.
- **Fig. 12**: Maps of the difference in the global monthly methane emissions from wetlands in 2000 from the *JULES–GIEMS* run and from the inverse modelling study of Bousquet et al. (2011) using the Fung et al. (1991) dataset as the wetland emission prior.
- **Fig. 13**: Maps of the difference in the global monthly methane emissions from wetlands in 2000 from the *JULES* run and from the inverse modelling study of Bousquet et al. (2011) using the Kaplan dataset as the wetland emission prior.

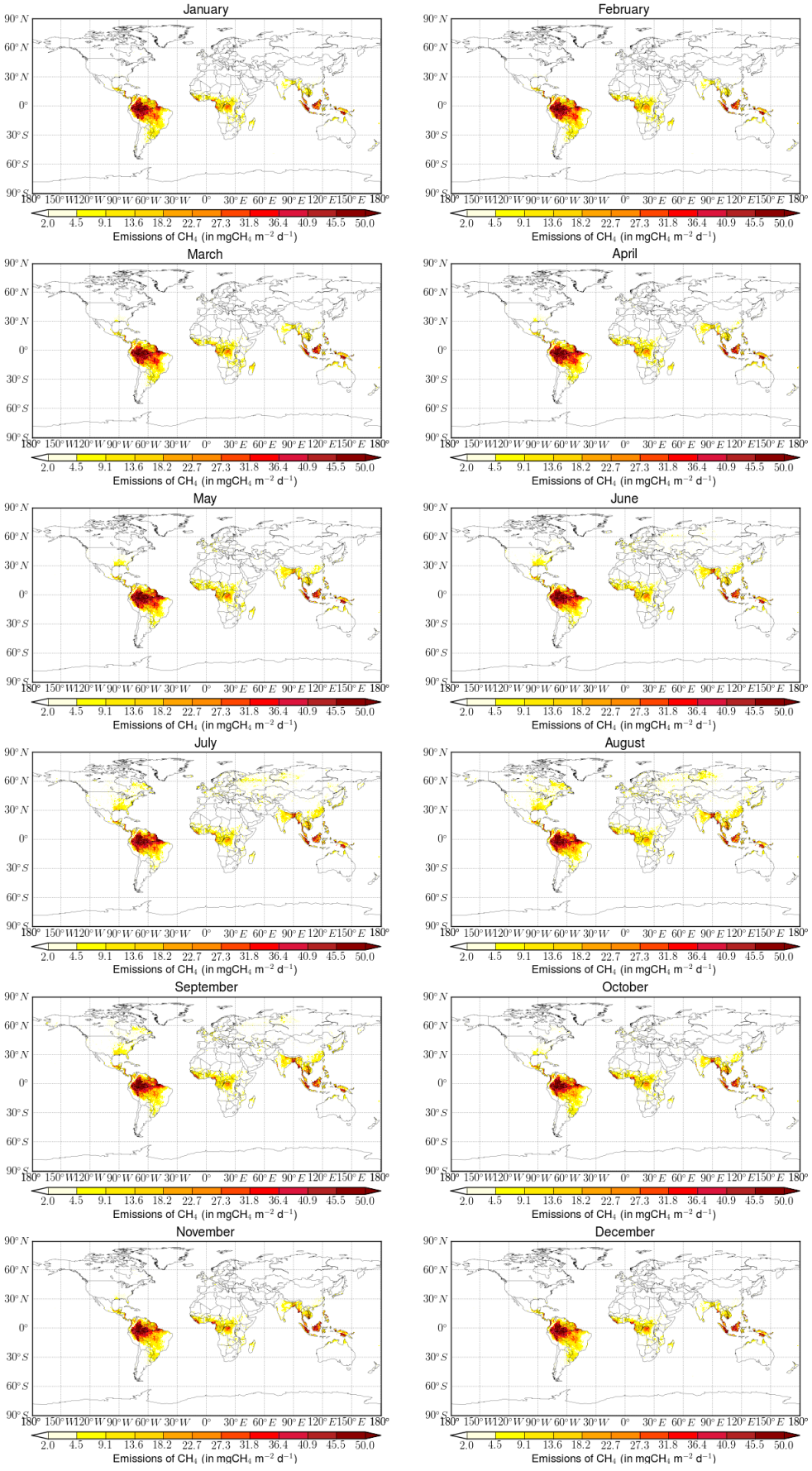

Figure 8: Maps of the global monthly wetland methane emissions for 2000 for the JULES wetland emission flux.

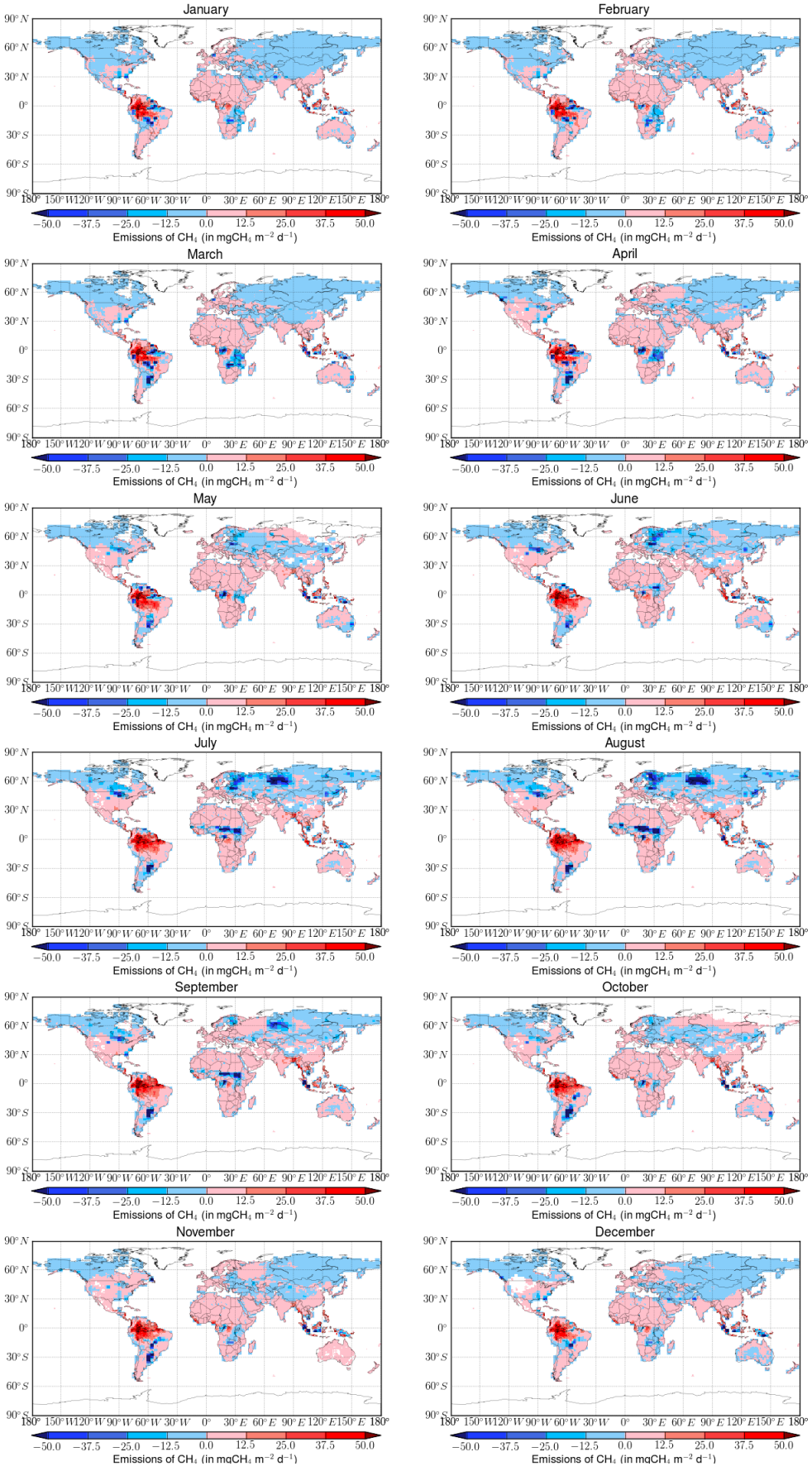

Figure 9: Maps of the differences in the global monthly wetland methane emissions for 2000 between the JULES wetland emission flux and the inverse modelling study of Bousquet et al. (2011) using the Fung et al. (1991) dataset as the wetland emission prior.

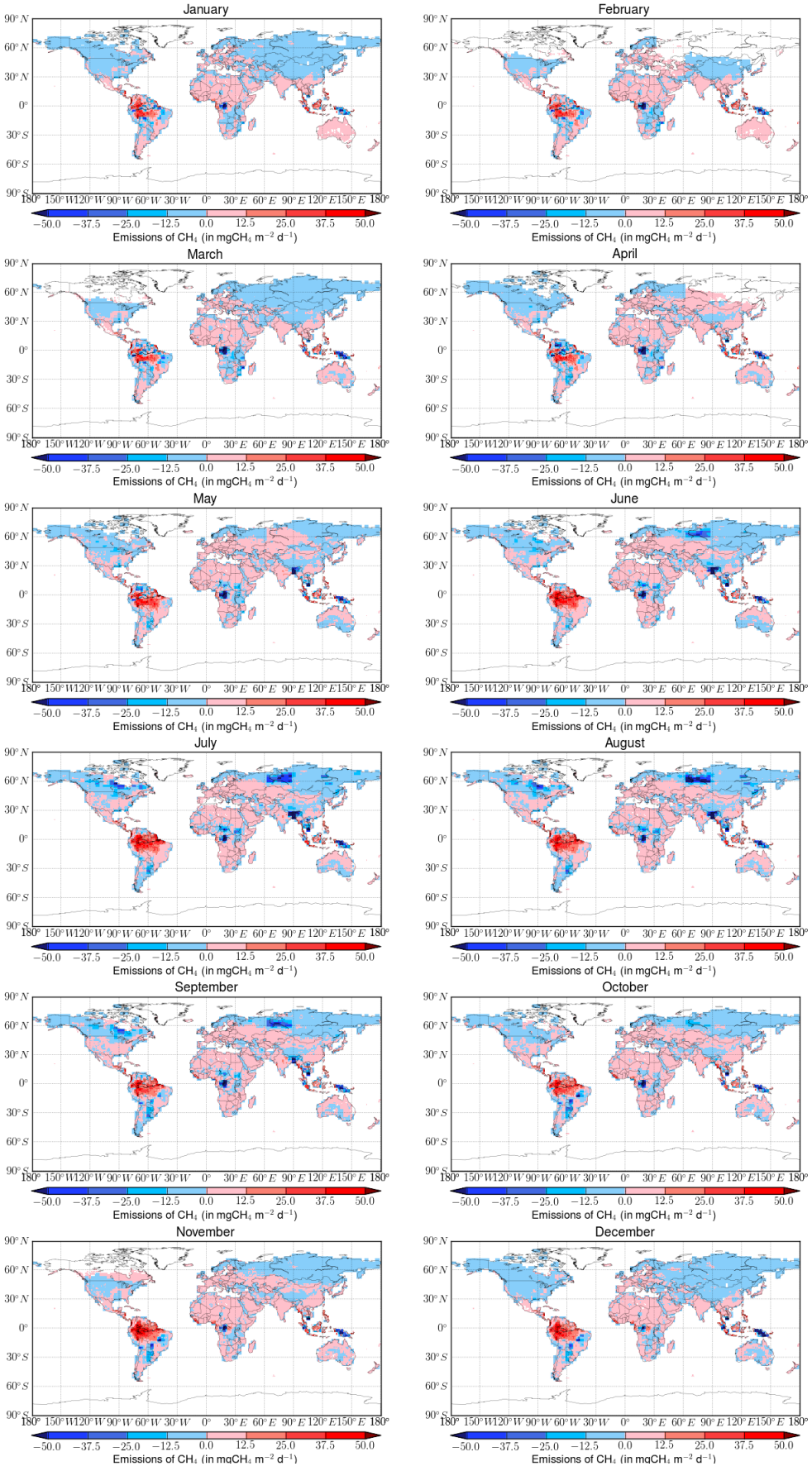

Figure 10: Maps of the differences in the global monthly wetland methane emissions for 2000 between the JULES wetland emission flux and the inverse modelling study of Bousquet et al. (2011) using the Kaplan dataset as the wetland emission prior.

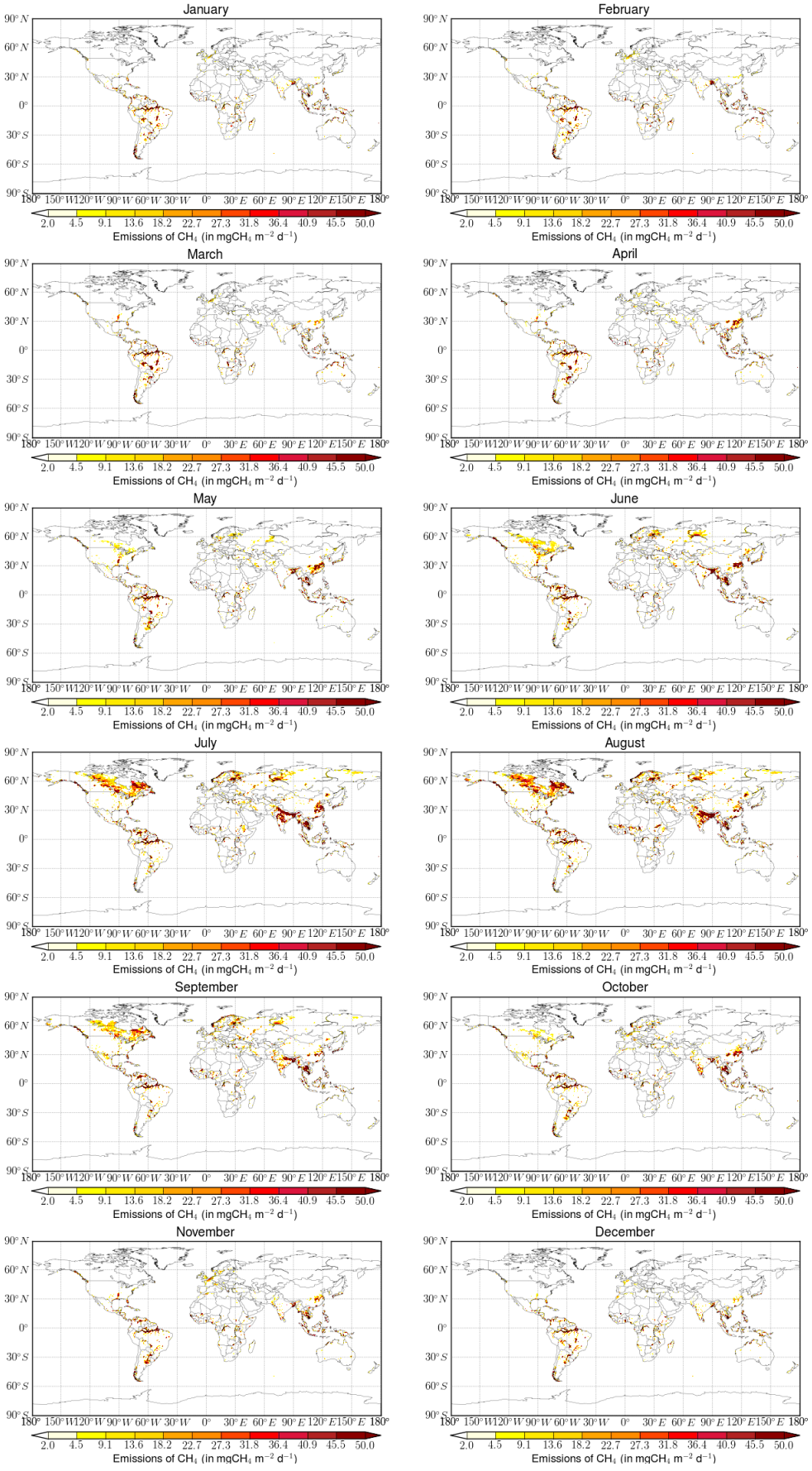

Figure 11: Maps of the global monthly wetland methane emissions for 2000 for the JULES wetland emission flux driven with the GIEMS EO inundation product.

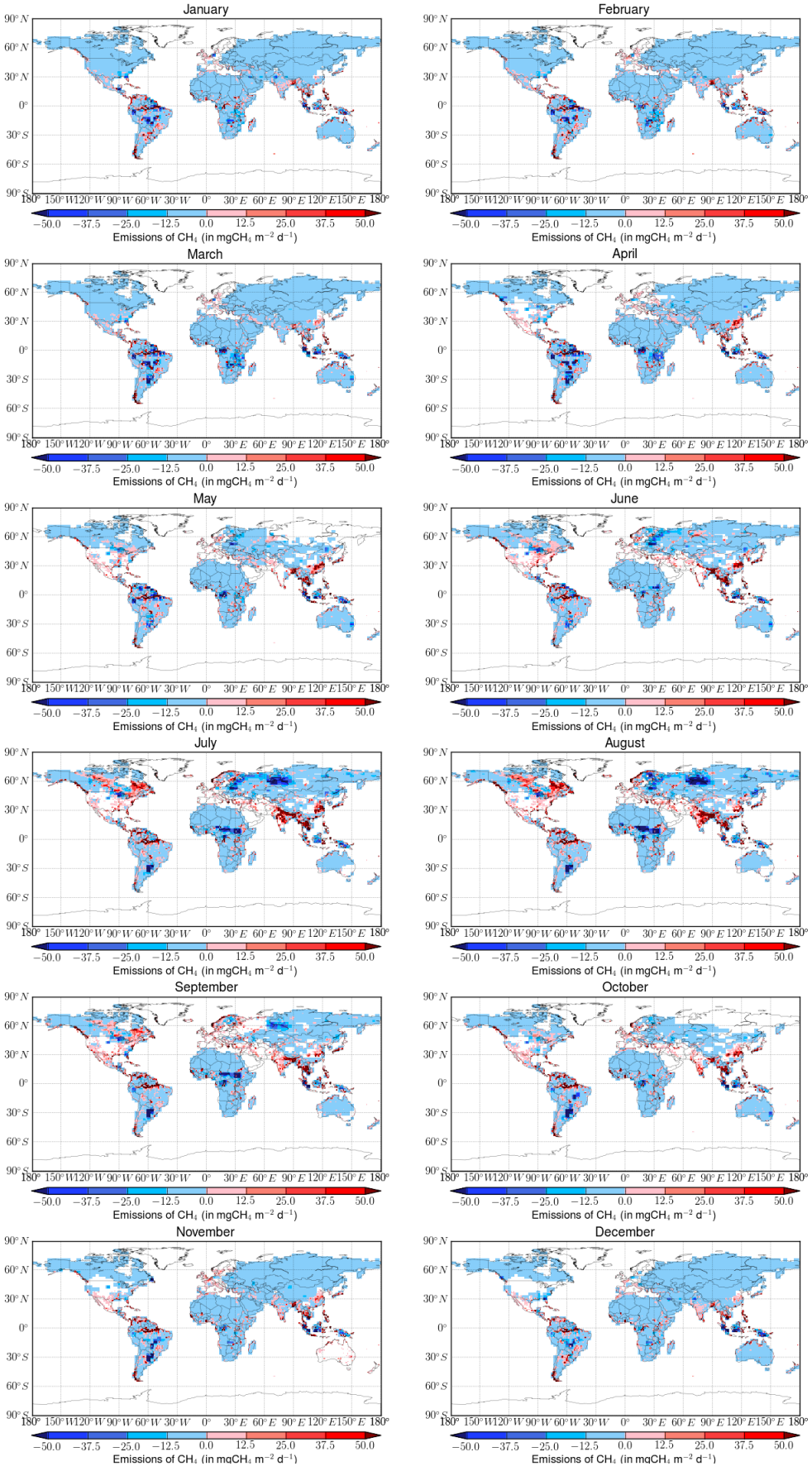

Figure 12: Maps of the differences in the global monthly wetland methane emissions for 2000 between the JULES wetland emission flux driven with the GIEMS product and the inverse modelling study of Bousquet et al. (2011) using the Fung et al. (1991) dataset as the wetland emission prior.

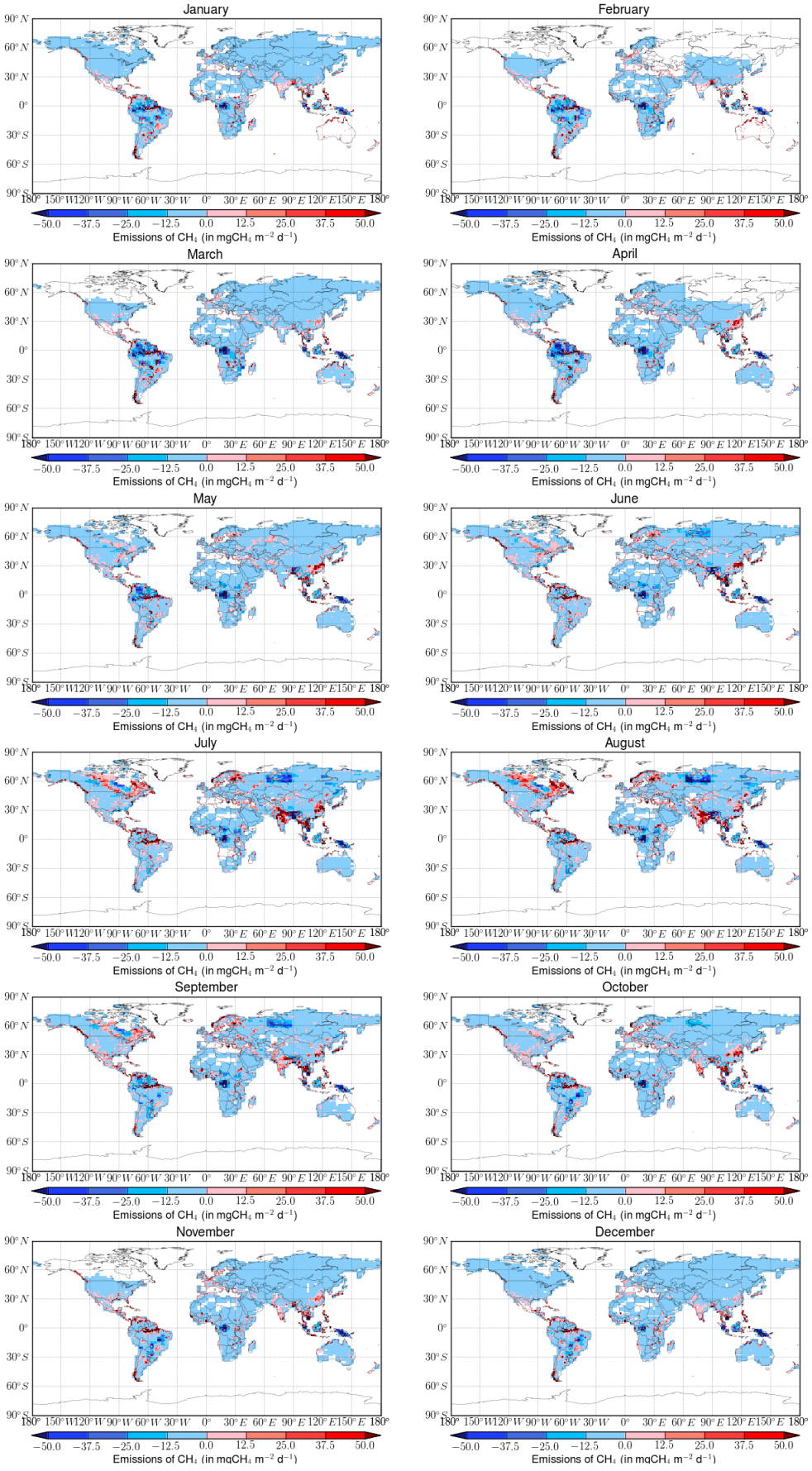

Figure 13: Maps of the differences in the global monthly wetland methane emissions for 2000 between the JULES wetland emission flux driven with the EO inundation product and the inverse modelling study of Bousquet et al. (2011) using the Kaplan dataset as the wetland emission prior.

2 Comparison with surface and satellite observations

2.1 Surface observations

The modelled monthly-averaged surface concentrations of atmospheric methane were compared against the monthly-averaged measurements of atmospheric methane dry air mole fractions from the NOAA ESRL GMD Carbon Cycle Cooperative Global Air Sampling Network (Dlugokencky et al., 2012). Fig. 14 shows a map of the locations of the 64 sites used in this work.

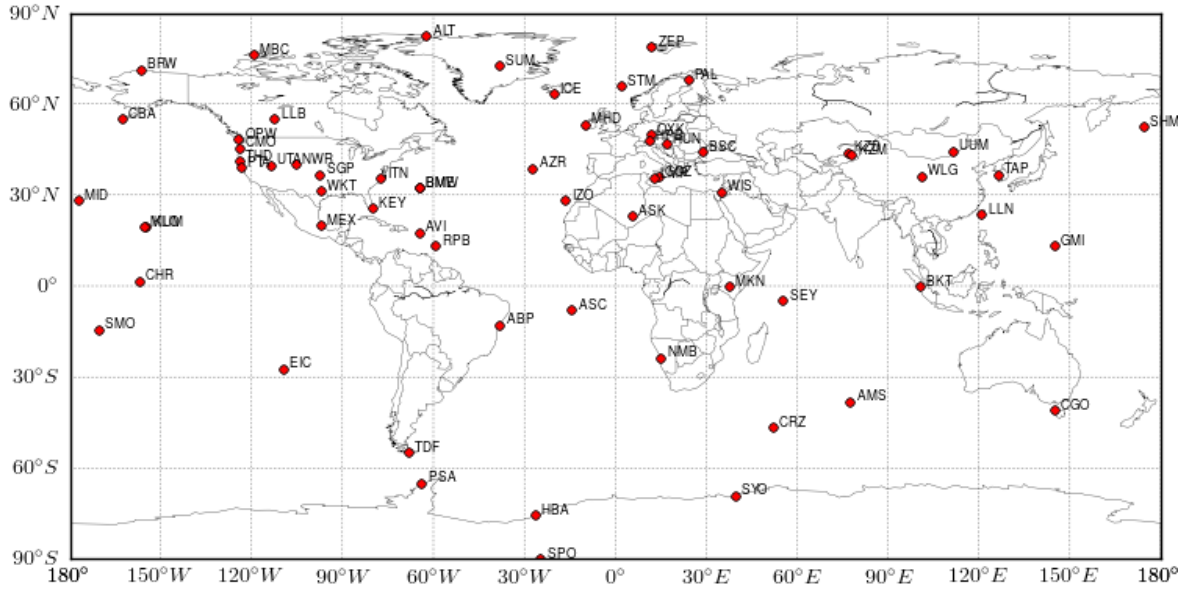

Figure 14: Locations of the surface atmospheric methane sampling sites in the NOAA Global Air Sampling Network: ABP - Arembepe, Bahia; ALT - Alert, Nunavut; AMS - Amsterdam Island; ASC - Ascension Island; ASK - Assekrem; AVI - St. Croix, Virgin Islands; AZR - Terceira Island, Azores; BKT - Bukit Kototabang; BME - St. Davids Head, Bermuda; BMW - Tudor Hill, Bermuda; BRW - Barrow, Alaska; BSC - Black Sea, Constanta; CBA - Cold Bay, Alaska; CGO - Cape Grim, Tasmania; CHR - Christmas Island; CMO - Cape Meares, Oregon; CRZ - Crozet Island; EIC - Easter Island; GMI - Mariana Islands; GOZ - Dwejra Point, Gozo; HBA - Halley Station, Antarctica; HPB - Hohenpeissenberg; HUN - Hegyhatsal; ICE - Storhofdi, Vestmannaeyjar; ITN - Grifton, North Carolina; IZO - Tenerife, Canary Islands; KEY - Key Biscayne, Florida; KUM - Cape Kumukahi, Hawaii; KZD - Sary Taukum; KZM - Plateau Assy; LLB - Lac La Biche, Alberta; LLN - Lulin; LMP - Lampedusa; MBC - Mould Bay, Nunavut; MEX - Mex High Altitude Global; MHD - Mace Head, County Galway; MID - Sand Island, Midway; MKN - Mt. Kenya; MLO - Mauna Loa, Hawaii; NMB - Gobabeb; NWR - Niwot Ridge, Colorado; OPW - Olympic Peninsula, Washington; OXK - Ochsenkopf; PAL - Pallas-Sammaltunturi, GAW; PSA - Palmer Station, Antarctica; PTA - Point Arena, California; RPB - Ragged Point; SEY - Mahe Island; SGP - Southern Great Plains, Oklahoma; SHM - Shemya Island, Alaska; SMO - Tutuila; SPO - South Pole, Antarctica; STM - Ocean Station M; SUM - Summit; SYO - Syowa Station, Antarctica; TAP - Tae-ahn Peninsula; TDF - Tierra Del Fuego, Ushuaia; THD - Trinidad Head, California; UTA - Wendover, Utah; UUM - Ulaan Uul; WIS - WIS Station, Negev Desert; WKT - Moody, Texas; WLG - Mt. Waliguan; ZEP - Ny-Alesund, Svalbard.

In Figs. 15-18, we show plots of the observed and modelled atmospheric methane concentrations between 2000 and 2010 at 16 of these sites, covering both northern and southern hemisphere locations, for the different model runs: *FUNG*, *JULES* and *JULES-GIEMS*. We present the metrics derived from the statistical analysis of the observed and modelled concentrations in Tab. 6.

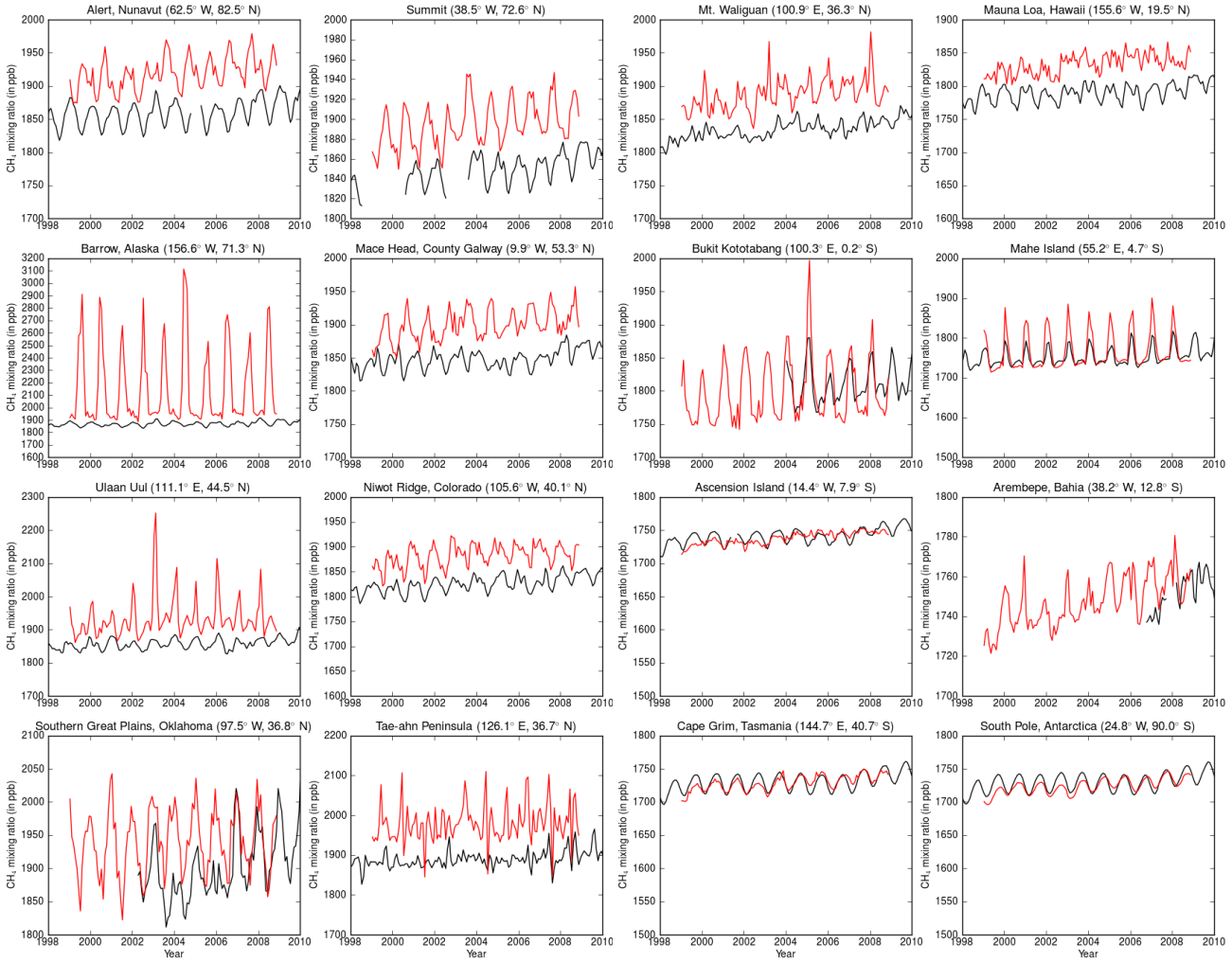

Figure 15: Comparison of the surface atmospheric methane mixing ratio (in ppb) as observed (black) and from the HadGEM2 run using the *FUNG* wetland emission inventory (red) at selected sites between 2000 and 2010.

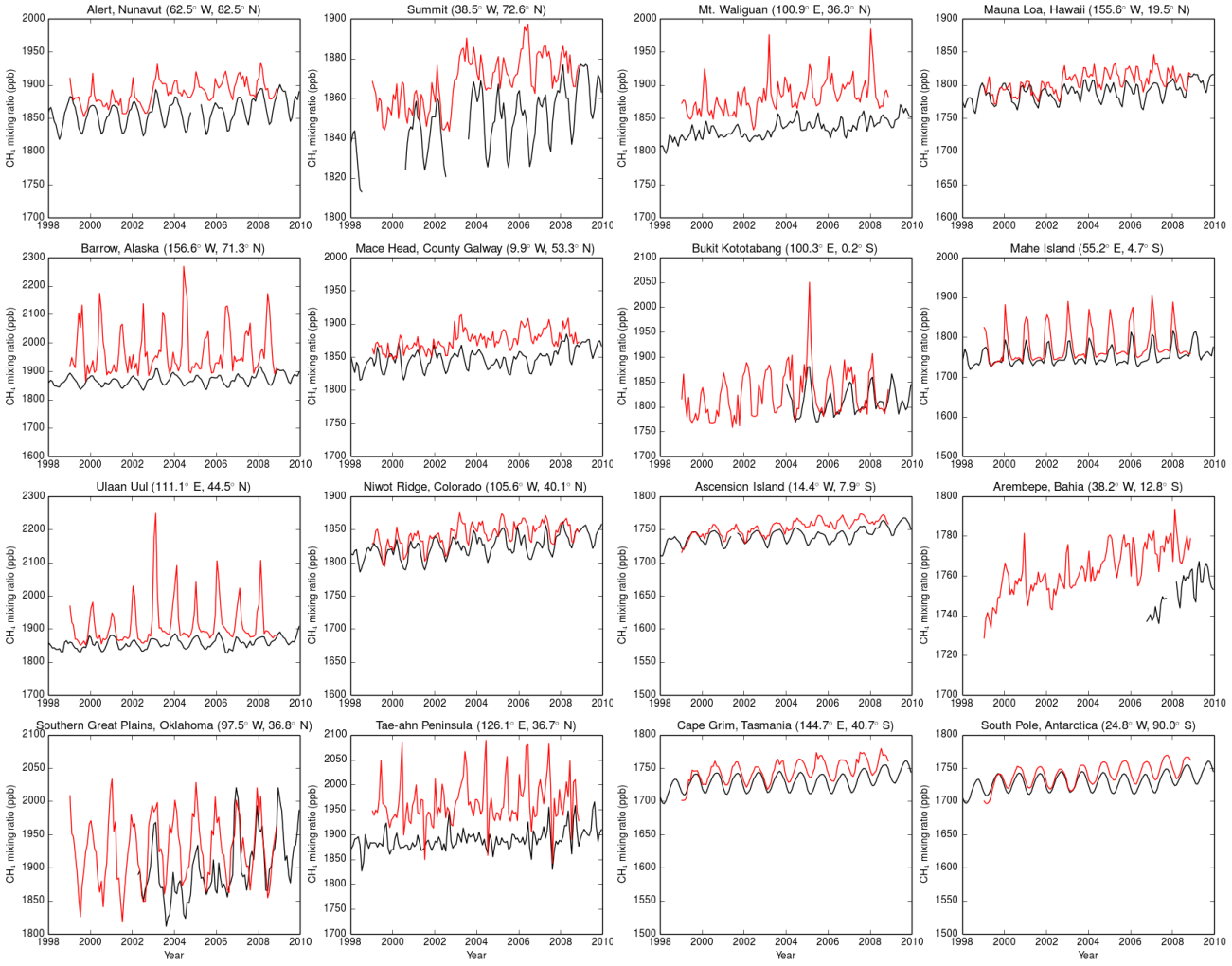

Figure 16: Comparison of the surface atmospheric methane mixing ratio (in ppb) as observed (black) and from the HadGEM2 run using the *FUNG* wetland emission inventory (red) at selected sites between 2000 and 2010.

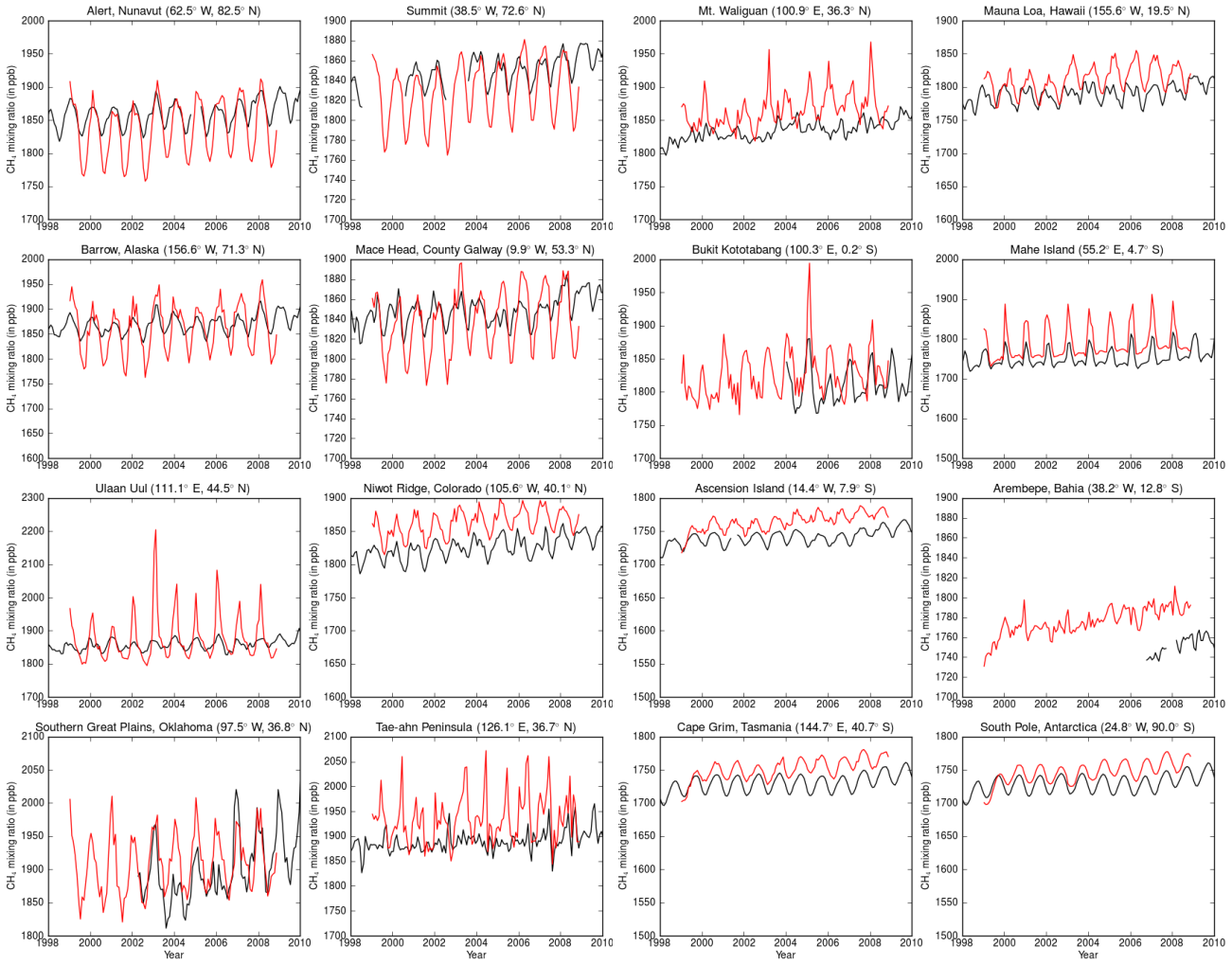

Figure 17: Comparison of the surface atmospheric methane mixing ratio (in ppb) as observed (black) and from the HadGEM2 run using the *JULES* wetland emission inventory (red) at selected sites between 2000 and 2010.

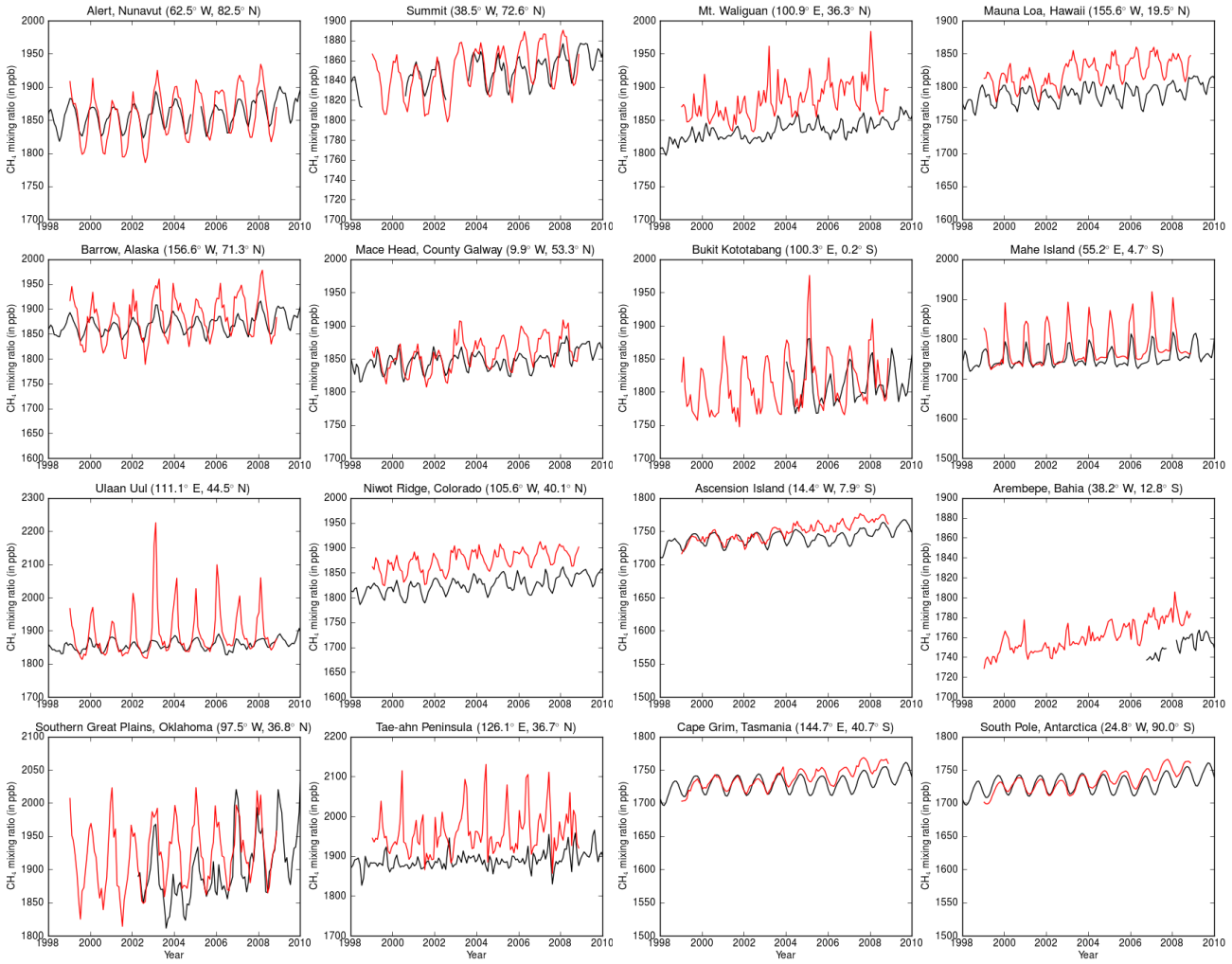

Figure 18: Comparison of the surface atmospheric methane mixing ratio (in ppb) as observed (black) and from the HadGEM2 run using the *JULES-GIEMS* wetland emission inventory (red) at selected sites between 2000 and 2010.

Table 6: Statistical outputs from the analysis of the observed and modelled surface methane concentrations at Barrow and the South Pole for the ~~the three~~ HadGEM2 runs (*FUNG*, *TRANSCOM-FUNG*, *JULES* and *JULES–GIEMS*).

(a) Barrow

Statistic/Metric	*FUNG*	*TRANSCOM-FUNG*	*JULES*	*JULES-GIEMS*
Number of valid data pairs	119	119	119	119
Linear regression – slope	-12.15	-2.53	1.70	1.68
Linear regression – intercept	~~24840.99~~ 24841.0	~~-1308.71~~ 6685.9	~~-1262.04~~ -1308.7	-1262.0
Coefficient of determination (R^2)	0.46	0.29	0.39	0.49
Mean of Observations (in ppb)	~~1867.79~~ 1867.8	~~1867.79~~ 1867.8	~~1867.79~~ 1867.8	1867.8
Mean of Modelled Conc. (in ppb)	~~2147.09~~ 2147.1	~~1861.35~~ 1969.2	~~1882.11~~ 1861.4	1882.1
Mean normalised bias	0.15	0.06	-0.004	0.008
Number of modelled results within a factor of 2 of that observed	~~1.00~~ 1.0	~~1.00~~ 1.0	~~1.00~~ 1.0	1.0
Index of Agreement	0.01	0.09	0.60	0.64
Hit Rate	0.55	0.63	1.00	1.00
Root Mean Square Error (RMSE in ppb)	~~425.82~~ 425.8	~~39.19~~ 136.4	~~34.82~~ 39.2	34.8
Coefficient of Variation in RMSE	0.29	0.07	0.02	0.02

(b) South Pole

Statistic/Metric	*FUNG*	*TRANSCOM-FUNG*	*JULES*	*JULES-GIEMS*
Number of valid data pairs	119	119	119	119
Linear regression – slope	0.72	1.14	1.07	0.96
Linear regression – intercept	~~471.70~~ 471.7	~~-97.51~~ -228.7	~~79.48~~ -97.5	79.5
Coefficient of determination (R^2)	0.60	0.74	0.62	0.59
Mean of Observations (in ppb)	~~1729.16~~ 1729.2	~~1729.16~~ 1729.2	~~1729.16~~ 1729.2	1729.2
Mean of Modelled Conc. (in ppb)	~~1723.82~~ 1723.8	~~1746.40~~ 1740.2	~~1733.13~~ 1746.4	1733.1
Mean normalised bias	-0.003	0.01	0.01	0.002
Number of modelled results within a factor of 2 of that observed	29 ~~1.00~~ 1.0	~~1.00~~ 1.0	~~1.00~~ 1.0	1.0
Index of Agreement	0.84	0.79	0.66	0.85

2.2 Satellite observations

The modelled 4-D methane mass mixing ratio fields (longitude, latitude, altitude, time) were converted into 3-D fields (longitude, latitude, time) of the mean atmospheric column methane mixing ratio, using the SCIAMACHY averaging kernels (equation 4 in Schneising et al., 2009).

$$\mathrm{XCH_4}^{\mathrm{model}} = \frac{1}{\mathrm{p_0}} \sum_l \left[\overline{\mathrm{XCH_4}}^{\,l} + \mathrm{AK}^l \left(\mathrm{XCH_4}^{\mathrm{model}\ l} - \overline{\mathrm{XCH_4}}^{\,l} \right) \right] \Delta \mathrm{p}^l \quad (1)$$

where l is the index of the vertical layer, AK^l the averaging kernel, $\overline{\mathrm{XCH_4}}^{\,l}$ the a-priori mole fraction (1750 ppb below 6km and decreasing above) and $\mathrm{XCH_4}^{\mathrm{model}\ l}$ is the modelled mole fraction of layer l. $\Delta \mathrm{p}^l$ is the pressure difference between the upper and lower boundary of layer l and $\mathrm{p_0}$ denotes the surface pressure.

As discussed in the main paper, the modelled atmospheric methane columns underpredicted the columns in the ~~Sciamachy~~ SCIAMACHY dataset. To overcome this limitation, the methane concentration in the upper model layers were replaced initially using data from the thermal infrared channel of the Tropospheric Emission Spectrometer and subsequently with output from a TOMCAT model run, assimilated with ACE and HALOE data. Fig. ~~??~~ 19 presents contour maps of the annual mean atmospheric column measurements of methane as derived from the unconstrained (panel a) and constrained HadGEM2 (panel b) run and from the monthly regridded ~~Sciamachy~~ SCIAMACHY data (v2.3, panel c). The ~~Sciamachy~~ SCIAMACHY and model atmospheric methane columns have been sampled at common, valid space and time points. A land mask was applied to remove all data over the ocean as the ~~Sciamachy~~ SCIAMACHY data are only available over the oceans for the period between 2003 and 2005.

Figure 10 in the main paper shows time series and annual cycles of the area-weighted mean atmospheric column methane mixing ratios between January 2003 and December 2007 from the SCIAMACHY data and the four constrained HadGEM2 runs for all land surface points and for the 11 terrestrial TRANSCOM regions. In Fig. 20, we show similar time series and annual cycle plots using the unconstrained HadGEM2 model outputs. We discuss these figures further in the Discussion in the main paper.

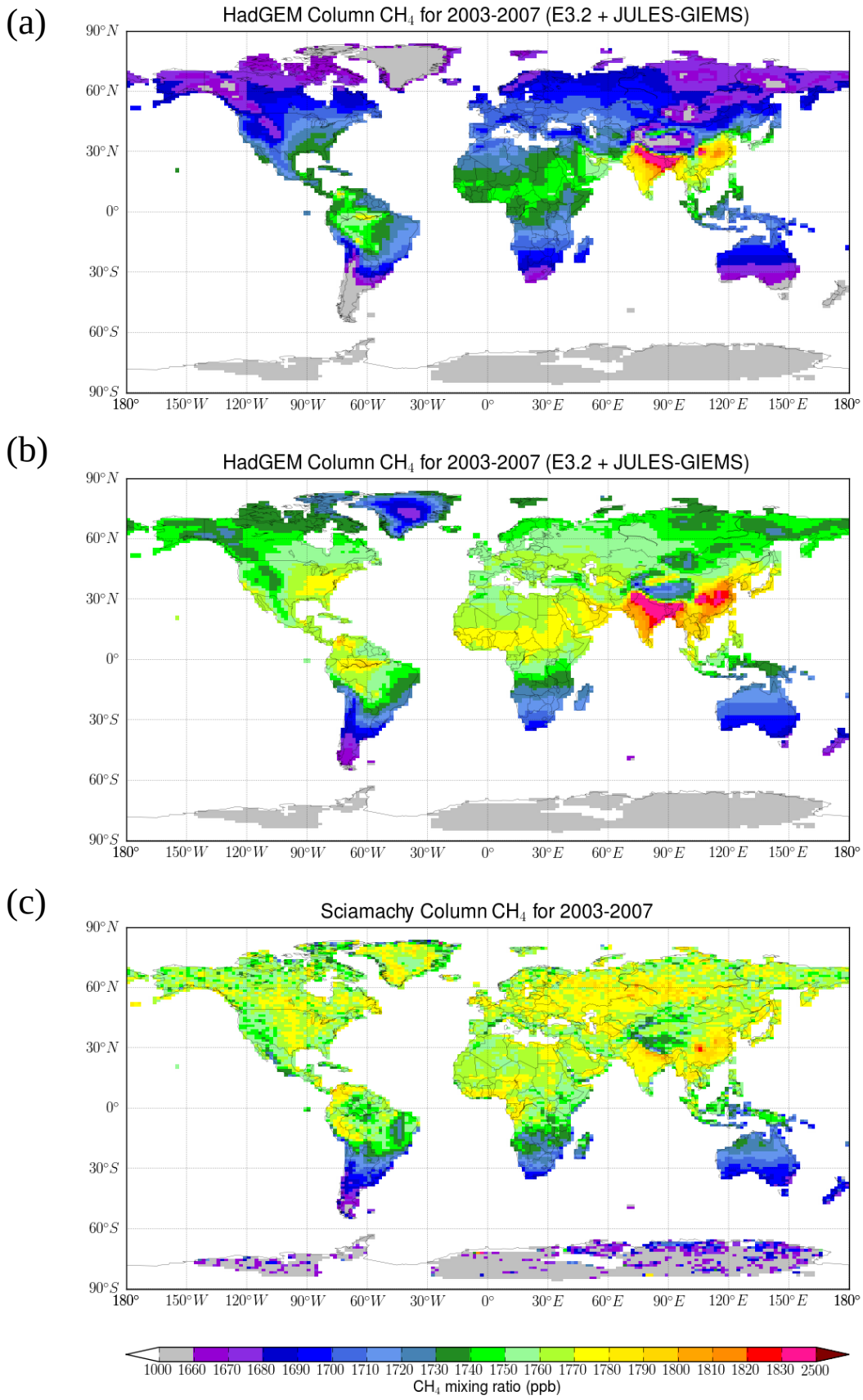

Figure 19: Contour maps of the average atmospheric column methane mixing ratio for 2003-2007 as derived from the unconstrained (panel a) and constrained HadGEM2 (panel b) run and from monthly regridded ~~Sciamachy~~ SCIAMACHY data (v2.3, panel c), sampled at common space and time points.

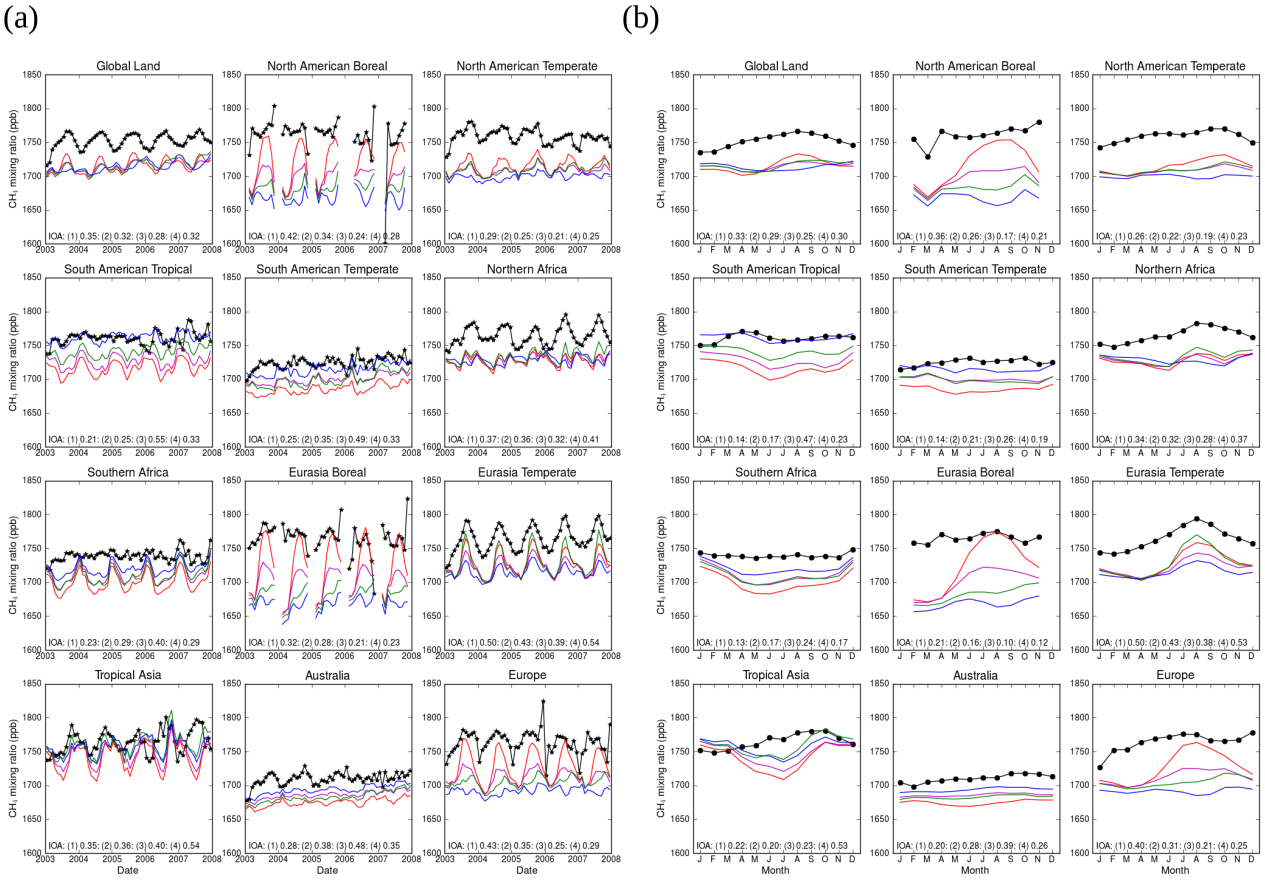

Figure 20: Time series of the area-weighted average atmospheric column methane mixing ratio from January 2003 to December 2007, as derived from monthly regridded SCIAMACHY data (v2.3) and from the unconstrained HadGEM2 runs using (1) the FUNG (red), (2) TRANSCOM FUNG (magenta), (3) the JULES (blue), and (4) the JULES-GIEMS (green) wetland emission inventories and the EDGAR v3.2 (E3.2) anthropogenic methane emission time series, sampled at co-located space and time points for all land surface points and for the 11 terrestrial TRANSCOM regions **(a)**. **(b)** shows the corresponding annual cycles. The index of agreement (IOA) is shown for each run (see Sect.3 of the Supplement for the definition of the IOA).

3 Performance metrics

Evaluation of model performance through statistical metrics focuses on measures that compare a set of N predicted concentrations P_i with their counterpart observed concentrations O_i, where i refers to a given time and/or location. Standard metrics used for air quality model performance evaluation are detailed in numerous papers (e.g., Yu et al., 2006; Dennis et al., 2010) and references therein) and only the ones that are used in our work (main text and Supplement) are reported hereafter. The means of N predictions and observations are defined as

$$P_{mean} = \frac{1}{N}\sum_{i=1}^{N} P_i \quad \text{and} \quad O_{mean} = \frac{1}{N}\sum_{i=1}^{N} O_i \tag{2}$$

respectively. The standard deviations of N predictions and observations are defined as

$$\sigma_P = \sqrt{\frac{1}{N}\sum_{i=1}^{N}(P_i - P_{mean})^2} \quad \text{and} \quad \sigma_O = \sqrt{\frac{1}{N}\sum_{i=1}^{N}(O_i - O_{mean})^2} \tag{3}$$

respectively. The variables a, b, c, and d are used to calculate the categorical statistics A, B, H, and FAR represent:

a - all the exceedances that did not occur

b - all the exceedances that did occur

c - all the exceedances that were not predicted and not observed, and

d - all the exceedances that were not predicted but observed, respectively

The following performance metrics were derived:

1. Accuracy (no unit, in %):

$$\text{Accuracy} = \frac{b+c}{a+b+c+d} \text{ x } 100$$

2. Bias (no unit):

$$\text{Bias} = \frac{a+b}{b+d}$$

3. Correlation coefficient (no units):

$$\text{Correlation coefficient} = \frac{1}{\sigma_P \sigma_O}\sum_{i=1}^{N}(P_i - P_{mean})(O_i - O_{mean})$$

4. Fraction of predictions within a factor of 2 of observations (no unit, %):

$$\text{Fraction of Prediction} = \left[\frac{1}{N}\sum_{i=1}^{N} 1 \mid (0.5 \leq \frac{P_i}{O_i} \leq 2)\right] \text{ x } 100$$

5. Fractional Bias (no unit, range [-2,2]):

$$\text{Fractional Bias} = \sum_{i=1}^{N} (\mathrm{P}_i - \mathrm{O}_i) \ / \ \sum_{i=1}^{N} (\mathrm{P}_i + \mathrm{O}_i)/2$$

6. Hit Rate (no unit, in %):

$$\text{Hit Rate} = \frac{\mathrm{b}}{\mathrm{b+d}} \text{ x } 100$$

7. Index of Agreement (no unit, range [0,1]):

$$\text{Index of Agreement} = 1 - \sum_{i=1}^{N} (\mathrm{P}_i - \mathrm{O}_i)^2 / \sum_{i=1}^{N} (\mid \mathrm{P}_i - \mathrm{O}_{mean} \mid^2 + \mid \mathrm{O}_i - \mathrm{O}_{mean} \mid^2)$$

8. Mean Bias (in unit of concentration):

$$\text{Mean Bias} = \frac{1}{\mathrm{N}} \sum_{i=1}^{N} (\mathrm{P}_i - \mathrm{O}_i)$$

9. Mean Error (in unit of concentration):

$$\text{Mean Error} = \frac{1}{\mathrm{N}} \sum_{i=1}^{N} \mid \mathrm{P}_i - \mathrm{O}_i \mid$$

10. Mean Fractional Bias (no unit, range [-200%, 200%]):

$$\text{Mean Fractional Bias} = \sum_{i=1}^{N} \frac{(\mathrm{P}_i - \mathrm{O}_i)}{(\mathrm{P}_i + \mathrm{O}_i)/2} \text{ x } 100$$

11. Mean Fractional Error (no unit, range [0, 200%]):

$$\text{Mean Fractional Error} = \sum_{i=1}^{N} \frac{\mid \mathrm{P}_i - \mathrm{O}_i \mid}{(\mathrm{P}_i + \mathrm{O}_i)/2} \text{ x } 100$$

12. Mean Normalised Bias (no unit, range [-100%, ∞]):

$$\text{Mean Normalised Bias} = \frac{1}{\mathrm{N}} \sum_{i=1}^{N} \frac{(\mathrm{P}_i - \mathrm{O}_i)}{\mathrm{O}_i} \text{ x } 100$$

13. Mean Normalised Error (no unit, in %):

$$\text{Mean Normalised Error} = \frac{1}{\mathrm{N}} \sum_{i=1}^{N} \frac{\mid \mathrm{P}_i - \mathrm{O}_i \mid}{\mathrm{O}_i} \text{ x } 100$$

14. Normalised Mean Bias (no unit, range [-1, ∞]):

$$\text{Normalised Mean Bias} = \sum_{i=1}^{N} (\mathrm{P}_i - \mathrm{O}_i) \ / \ \sum_{i=1}^{N} \mathrm{O}_i$$

15. Root Mean Square Error (in unit of concentration):

$$\text{Root Mean Square Error} = \sqrt{\frac{1}{\mathrm{N}} \sum_{i=1}^{N} (\mathrm{P}_i - \mathrm{O}_i)^2}$$

16. Skill Variance (no units):

$$\text{Skill variance} = \frac{\sigma_{\mathrm{P}}}{\sigma_{\mathrm{O}}}$$

References

Best, M. J., Pryor, M., Clark, D. B., Rooney, G. G., Essery, R. L. H., Ménard, C. B., Edwards, J. M., Hendry, M. A., Porson, A., Gedney, N., Mercado, L. M., Sitch, S., Blyth, E., Boucher, O., Cox, P. M., Grimmond, C. S. B., and Harding, R. J.: The Joint UK Land Environment Simulator (JULES), model description - Part 1: Energy and water fluxes, Geoscientific Model Development, 4, 677–699, doi:10.5194/gmd-4-677-2011, http://www.geosci-model-dev.net/4/677/2011/, 2011.

Bousquet, P., Ringeval, B., Pison, I., Dlugokencky, E. J., Brunke, E.-G., Carouge, C., Chevallier, F., Fortems-Cheiney, A., Frankenberg, C., Hauglustaine, D. A., Krummel, P. B., Langenfelds, R. L., Ramonet, M., Schmidt, M., Steele, L. P., Szopa, S., Yver, C., Viovy, N., and Ciais, P.: Source attribution of the changes in atmospheric methane for 2006-2008, Atmospheric Chemistry and Physics, 11, 3689–3700, doi:10.5194/acp-11-3689-2011, http://www.atmos-chem-phys.net/11/3689/2011/, 2011.

Clark, D. B., Mercado, L. M., Sitch, S., Jones, C. D., Gedney, N., Best, M. J., Pryor, M., Rooney, G. G., Essery, R. L. H., Blyth, E., Boucher, O., Harding, R. J., Huntingford, C., and Cox, P. M.: The Joint UK Land Environment Simulator (JULES), model description - Part 2: Carbon fluxes and vegetation dynamics, Geoscientific Model Development, 4, 701–722, doi:10.5194/gmd-4-701-2011, http://www.geosci-model-dev.net/4/701/2011/, 2011.

Collins, W. J., Bellouin, N., Doutriaux-Boucher, M., Gedney, N., Halloran, P., Hinton, T., Hughes, J., Jones, C. D., Joshi, M., Liddicoat, S., Martin, G., O'Connor, F., Rae, J., Senior, C., Sitch, S., Totterdell, I., Wiltshire, A., and Woodward, S.: Development and evaluation of an Earth-System model - HadGEM2, Geoscientific Model Development, 4, 1051–1075, doi:10.5194/gmd-4-1051-2011, http://www.geosci-model-dev.net/4/1051/2011/, 2011.

Dennis, R., Fox, T., Fuentes, M., Gilliland, A., Hanna, S., Hogrefe, C., Irwin, J., Rao, S., Scheffe, R., Schere, K., Steyn, D., and Venkatram, A.: A framework for evaluating regional–scale numerical photochemical modeling systems, Environmental Fluid Mechanics, 10, 471–489, doi:10.1007/s10652-009-9163-2, http://dx.doi.org/10.1007/s10652-009-9163-2, 2010.

Dlugokencky, E. J., Lang, P. M., Crotwell, A. M., and Masarie, K. A.: Atmospheric Methane Dry Air Mole Fractions from the NOAA ESRL Carbon Cycle Co-operative Global Air Sampling Network, 1983-2011, Version: 2012-09-24, ftp://ftp.cmdl.noaa.gov/ccg/ch4/flask/event/, 2012.

Fung, I., John, J., Lerner, J., Matthews, E., Prather, M., Steele, L. P., and Fraser, P. J.: Three-dimensional model synthesis of the global methane cycle, Journal of Geophysical Research: Atmospheres, 96, 13 033–13 065, doi:10.1029/91JD01247, http://dx.doi.org/10.1029/91JD01247, 1991.

Gedney, N.: Unpublished results from JULES, 2014.

Gedney, N. and Cox, P. M.: The Sensitivity of Global Climate Model Simulations to the Representation of Soil Moisture Heterogeneity, Journal of Hydrometeorology, 4, 1265–1275, doi:10.1175/1525-7541(2003)004¡1265:TSOGCM¿2.0.CO;2, http://dx.doi.org/10.1175/1525-7541(2003)004<1265:TSOGCM>2.0.CO;2, 2003.

Gedney, N., Cox, P. M., and Huntingford, C.: Climate feedback from wetland methane emissions, Geophysical Research Letters, 31, L20 503, doi:10.1029/2004GL020919, http://dx.doi.org/10.1029/2004GL020919, 2004.

Lamarque, J.-F., Bond, T. C., Eyring, V., Granier, C., Heil, A., Klimont, Z., Lee, D., Liousse, C., Mieville, A., Owen, B., Schultz, M. G., Shindell, D., Smith, S. J., Stehfest, E., Van Aardenne, J., Cooper, O. R., Kainuma, M., Mahowald, N., McConnell, J. R., Naik, V., Riahi, K., and van Vuuren, D. P.: Historical (1850–2000) gridded anthropogenic and biomass burning emissions of reactive gases and aerosols: methodology and application, Atmospheric Chemistry and Physics, 10, 7017–7039, doi:10.5194/acp-10-7017-2010, http://www.atmos-chem-phys.net/10/7017/2010/, 2010.

O'Connor, F. M., Johnson, C. E., Morgenstern, O., Abraham, N. L., Braesicke, P., Dalvi, M., Folberth, G. A., Sanderson, M. G., Telford, P. J., Young, P. J., Zeng, G., Collins, W. J., and Pyle, J. A.: Evaluation of the new UKCA climate-composition model - Part 2: The Troposphere, Geoscientific Model Development Discussions, 6, 1743–1857, doi:10.5194/gmdd-6-1743-2013, http://www.geosci-model-dev-discuss.net/6/1743/2013/, 2013.

Patra, P. K., Houweling, S., Krol, M., Bousquet, P., Belikov, D., Bergmann, D., Bian, H., Cameron-Smith, P., Chipperfield, M. P., Corbin, K., Fortems-Cheiney, A., Fraser, A., Gloor, E., Hess, P., Ito, A., Kawa, S. R., Law, R. M., Loh, Z., Maksyutov, S., Meng, L., Palmer, P. I., Prinn, R. G., Rigby, M., Saito, R., and Wilson, C.: TransCom model simulations of CH_4 and related species: linking transport, surface flux and chemical loss with CH_4 variability in the troposphere and lower stratosphere, Atmospheric Chemistry and Physics, 11, 12 813–12 837, doi:10.5194/acp-11-12813-2011,

http://www.atmos-chem-phys.net/11/12813/2011/, 2011.

Portmann, F. T., Siebert, S., and Döll, P.: MIRCA2000 - Global monthly irrigated and rainfed crop areas around the year 2000: A new high-resolution data set for agricultural and hydrological modeling, Global Biogeochemical Cycles, 24, GB1001, doi:10.1029/2008GB003435, http://dx.doi.org/10.1029/2008GB003435, 2010.

Prigent, C., Papa, F., Aires, F., Jimenez, C., Rossow, W. B., and Matthews, E.: Changes in land surface water dynamics since the 1990s and relation to population pressure, Geophysical Research Letters, 39, L08 403, doi:10.1029/2012GL051276, http://dx.doi.org/10.1029/2012GL051276, 2012.

Schneising, O., Buchwitz, M., Burrows, J. P., Bovensmann, H., Bergamaschi, P., and Peters, W.: Three years of greenhouse gas column-averaged dry air mole fractions retrieved from satellite - Part 2: Methane, Atmospheric Chemistry and Physics, 9, 443–465, doi:10.5194/acp-9-443-2009, http://www.atmos-chem-phys.net/9/443/2009/, 2009.

van der Werf, G. R., Randerson, J. T., Giglio, L., Collatz, G. J., Mu, M., Kasibhatla, P. S., Morton, D. C., DeFries, R. S., Jin, Y., and van Leeuwen, T. T.: Global fire emissions and the contribution of deforestation, savanna, forest, agricultural, and peat fires (1997-2009), Atmospheric Chemistry and Physics, 10, 11 707–11 735, doi:10.5194/acp-10-11707-2010, http://www.atmos-chem-phys.net/10/11707/2010/, 2010.

Viovy, N. and Ciais, P.: A combined dataset for ecosystem modelling, available at: http://dods.extra.cea.fr/data/p529viov/cruncep/readme.htm (last access: 10 July 2013), 2009.

Yu, S., Eder, B., Dennis, R., Chu, S.-H., and Schwartz, S. E.: New unbiased symmetric metrics for evaluation of air quality models, Atmospheric Science Letters, 7, 26–34, doi:10.1002/asl.125, http://dx.doi.org/10.1002/asl.125, 2006.